ECG Noise Filtering Using Online Model-Based Bayesian Filtering Techniques

by

Aron Su

A thesis
presented to the University of Waterloo
in fulfillment of the
thesis requirement for the degree of
Master of Applied Science
in
Electrical and Computer Engineering

Waterloo, Ontario, Canada, 2013

I hereby declare that I am the sole author of this thesis. This is a true copy of the thesis, including any required final revisions, as accepted by my examiners.

I understand that my thesis may be made electronically available to the public.

Abstract

The electrocardiogram (ECG) is a time-varying electrical signal that interprets the electrical activity of the heart. It is obtained by a non-invasive technique known as surface electromyography (EMG), used widely in hospitals. There are many clinical contexts in which ECGs are used, such as medical diagnosis, physiological therapy and arrhythmia monitoring. In medical diagnosis, medical conditions are interpreted by examining information and features in ECGs. Physiological therapy involves the control of some aspect of the physiological effort of a patient, such as the use of a pacemaker to regulate the beating of the heart. Moreover, arrhythmia monitoring involves observing and detecting life-threatening conditions, such as myocardial infarction or heart attacks, in a patient. ECG signals are usually corrupted with various types of unwanted interference such as muscle artifacts, electrode artifacts, power line noise and respiration interference, and are distorted in such a way that it can be difficult to perform medical diagnosis, physiological therapy or arrhythmia monitoring. Consequently signal processing on ECGs is required to remove noise and interference signals for successful clinical applications.

Existing signal processing techniques can remove some of the noise in an ECG signal, but are typically inadequate for extraction of the weak ECG components contaminated with background noise and for retention of various subtle features in the ECG. For example, the noise from the EMG usually overlaps the fundamental ECG cardiac components in the frequency domain, in the range of 0.01 Hz to 100 Hz. Simple filters are inadequate to remove noise which overlaps with ECG cardiac components.

Sameni *et al.* have proposed a Bayesian filtering framework to resolve these problems, and this gives results which are clearly superior to the results obtained from application of conventional signal processing methods to ECG. However, a drawback of this Bayesian filtering framework is that it must run offline, and this of course is not desirable for clinical applications such as arrhythmia monitoring and physiological therapy, both of which require online operation in near real-time. To resolve this problem, in this thesis we propose a dynamical model which permits the Bayesian filtering framework to function online. The framework with the proposed dynamical model has less than 4% loss in performance compared to the previous (offline) version of the framework. The proposed dynamical model is based on theory from fixed-lag smoothing.

Acknowledgements

I would like to give thanks to my supervising professor, Professor Andrew Heunis for his dedication, encouragement and guidance during my graduate studies here at the University of Waterloo. This research would not have been accomplished without his constant support.

I sincerely thank my committee members Professor Dan Miller and Professor Dan Davison for reviewing this thesis and for their valuable comments.

I would like to thank my parents and my sisters for all their support and encouragement through my life. I would not be here without them.

I would like to thank the University of Waterloo Writing Centre for providing supports on English writing developments.

Dedication

This is dedicated to the one I love.

Table of Contents

List of Tables

List of Figures

Chapter 1

Introduction

The electrocardiogram (ECG) signal represents the electrical activity of the heart. This is the most commonly used cardiovascular signal in clinical practice since it involves a noninvasive and low-cost procedure which provides an abundance of diagnostic information. Doctors routinely use ECGs to guide clinical decision making, and these days it remains the standard tool for clinical diagnosis despite advances in many other diagnostic techniques [36]. However, the recorded ECG signal is typically contaminated by several different sources of noise and interference, such as respiration baseline wander, power-line interference, electrode motion artifacts, and muscle artifacts, and the resulting distortion of the recorded ECG signal usually makes it difficult to perform automatic diagnosis for clinical purposes without prior noise reduction.

Noise reduction of ECGs is in fact essential in many applications. To mention but a few, these include arrhythmia detection [33], detection of QRS complexes [3], ECG data compression [4], extraction of a fetal ECG signal from the maternal abdominal ECG [28], and diagnosis of myocardial ischemia [33]. All of these applications require the contaminated ECG signals to be preprocessed to extract essential ECG components. One particularly common and important application is that of cardiac arrhythmia detection, in which the ECG signal of a patient is monitored in real-time to detect life-threatening cardiac arrhythmias. For this to be possible all noise and interference must be removed. Despite the rich literature in the field of signal denoising, for clinical applications such as cardiac arrhythmia detection there is still a genuine need for reliable methods to remove such noise and interference while extracting the subtle features of an ECG signal. For example, electrode motion artifacts are generally regarded as one of the most troublesome sources of interference since the resulting contamination overlaps with the ECG cardiac components in the frequency domain. Simple filters like the bandpass filter cannot remove such

contamination. [8]

Several techniques have been proposed to extract useful information from ECG signals while removing signal noise. These include statistical techniques such as principle component analysis [2], independent component analysis [12], neural networks [25], and wavelet denoising (WD) [1, 34] for signals with multi-resolution characteristics. A particularly common approach is based on adaptive filtering. This has been used in [31, 18, 35] for noise reduction in ECGs contaminated by baseline wander, electrode motion artifacts, and motion artifacts, and involves mean-square error minimization. The goal of this thesis is to study the application of Bayesian filtering methods, which belong to the general class of adaptive filtering methods, to the problem of screening out contamination in ECG signals.

1.1 Contribution

McSharry *et al.* [19] have proposed a simple and practical dynamical model for the ECG signal, and a series of studies of ECG denoising methods based on their dynamical model report improved performance compared with model-free approaches such as the wavelet denoising method. Sameni *et al.* [30] modified the dynamical model of McSharry *et al.* from Cartesian coordinates to a much more natural set of polar coordinates, resulting in a significantly simpler two-state dynamical model, and used this modified dynamical model on Bayesian filters to remove noise in ECGs [31]. Subsequently, they then applied the Bayesian filtering model to extract fetal cardiac signals from an array of maternal abdominal recordings [28]. Their studies indicate that fixed-interval smoothing gives the best overall denoising performance compared to other Bayesian techniques, but the main drawback of their procedure is that the analysis is offline rather than online.

In the present thesis, we propose two modifications to the two-dimensional state space model of Sameni *et al.* [30]. In the first modification, the model is extended from two states to seventeen states to allow for more flexibility to adapt to different patients. This extended-state model is used in conjunction with several nonlinear Bayesian filtering approaches, such as the extended Kalman Filter, the unscented Kalman Filter, fixed-lag smoother, and fixed-interval smoother. In order to compare the results of the proposed seventeen-state dynamical model with McSharry's dynamical model, we add white noise, coloured noise and muscle artifacts to clean ECG signals to simulate various noisy ECG signals. Results with the proposed seventeen-state model showed only slight improvement for the extended Kalman Filter and the unscented Kalman Filter, and displayed even a slight performance degradation compared to the two-state model when fixed-interval smoothing and fixed-lag smoothing were used. A fixed-lag smoother with a lag window of thirty steps

resulted in denoising performance close to that of fixed-interval smoothing, which is the best possible filtering obtainable but is implementable only offline. In other words, with fixed-lag smoothing one gets online ECG signal denoising comparable to the offline ECG denoising obtainable from fixed-interval smoothing. However, a possible drawback of this fixed-lag smoothing is that the size of the state vector increases with each increment in the length of the lag window. For very long lag windows this means that online signal denoising may become impractical. This leads to the second modification proposed in this thesis, namely a suboptimal fixed-lag smoother the performance of which is very comparable to that of the original fixed lag smoother, but now with significantly reduced state dimension which makes online implementation much more feasible.

1.2 Thesis Overview

This thesis is organized as follows. Background information regarding electrocardiograms and common sources of noise and signal interference are reviewed in Chapter 2. Then, in Chapter 3, some necessary mathematical background on Bayesian filters is presented. In Chapter 4 we introduce the dynamical models of McSharry *et al.* [19] and Semani *et al.* [30] and discuss the advantages of the latter model over the former model. Then we propose an extension of the model of Semani *et al.* [30] from two states to seventeen states, the motivation for this increase in state dimension being to improve the flexibility of the model. Chapter 5 provides the Bayesian filtering framework needed for the online filtering algorithm, as well as the simulation results. These simulation results compare the performance of the two-dimensional state space model of Sameni *et al.* [30] with the seventeen-dimensional state space model of this thesis. Then Chapter 6 introduces the second modification along with its simulation results. These results show that a fixed-lag smoother which is implementable online gives results which are very comparable to those from a fixed-interval smoother, which gives best possible performance but at the expense of being implementable only offline. Lastly, conclusions and future work are discussed in Chapter 7.

Chapter 2

Biomedical Background

This chapter reviews some necessary background on electrocardiograms. First, the electrical phenomena aspects of the heart are presented in order to understand how the familiar "waves" observed in an ECG arise. Then the main sources of noise and other interference in ECGs are examined and their features are identified.

2.1 Electrocardiogram

The electrocardiogram (ECG) is a time-varying electro-cardiac signal that represents the electrical activity of the human heart. It is obtained using surface electromyography (EMG), where electrodes are attached to the surface of the skin in close proximity to the human heart. It is a non-invasive procedure that is widely used in hospital settings to measure and diagnose abnormal rhythms of the heart. The ECG signal measured from the patient results in a periodic waveform with multiple apexes called the **PQRST-complex**. Figure 2.1 shows an ideal PQRST-complex waveform.

The apexes in the PQRST-complex are labelled with P, Q, R, S and T, which are commonly used in medical ECG terminology. Each apex results from ionic current exchanges in the heart causing muscle contractions and relaxations. All the muscle contractions and relaxations in the heart begin at the sinoatrial (SA) node, which is a specialized cell that regulates the heart beat. (see Figure 2.2). The SA node produces electrical impulses, which spread radially throughout the whole heart. As the electrical impulses traverse through the heart, different muscle groups in the heart contract in a sequential manner to produce the PQRST-complex waveform. The order of muscle contractions is shown in Figure 2.3.

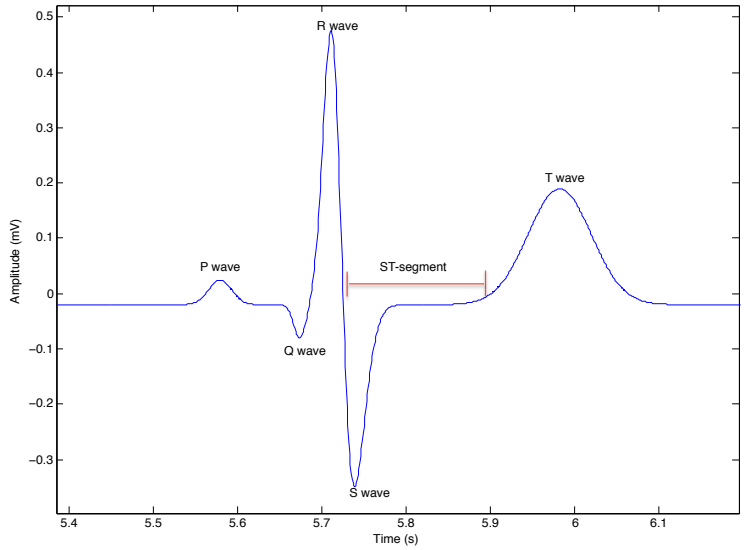

Figure 2.1: The waveform of an ideal, normal ECG waveform with peaks labelled by P, Q, R, S and T. The ST segment defines the interval from the beginning of the S wave to the beginning of the T wave.

In Figure 2.3, the atria contraction produces the P wave and the ventricle contraction produces the QRS complex and the T wave.

2.1.1 P wave

The electrical impulses produced by the SA node first propagate to the right atrium then the left atrium (see Figure 2.2). Depolarization of the right atrium produces a small-voltage deflection away from the baseline. The plateau of the P wave represents the completion of the right atrial contraction and beginning of the left atrial contraction; the left atrium contraction finishes at the end of the P wave. In other words, the P wave is produced by the contraction of the right and left atria (see Figure 2.3).

The P wave is a small, smooth, rounded deflection that precedes the spiky-looking QRS-complex. The duration from the end of the P wave to the beginning of the Q wave represents the necessary physiologic delay to allow the left and the right ventricles to prepare for contraction.To achieve this necessary delay, the electrical impulses pass through multiple parts of the heart: the AV node, the bundle branch, and the Purkinje network (see Figure 2.3). This delay is a natural delay mechanism to allow the ventricles to be

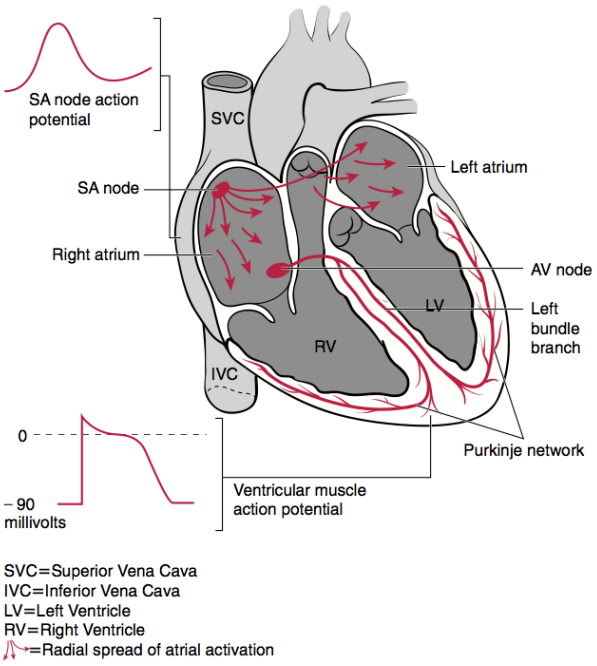

Figure 2.2: Electrical activities of the heart are controlled by the sinoatrial (SA) node. The electrical impulses fired by the SA node spread radially outward to the atria and the atrioventricular (AV) node. The AV node relegates the current from the SA node down the left bundle branch to the ventricular muscles and Purkinje network [13].

filled with blood.

2.1.2 QRS complex

The QRS-complex reflects the rapid depolarization of the right and left ventricles, and marks the beginning of the ventricle contraction. The ventricles have a large muscle mass compared to the atria, so the QRS complex has a much larger deflection than the P wave. The wave is composed of the Q wave, R wave and S wave, and is used as a landmark to estimate the heart rate of a patient by tracking the RR interval. The RR interval is the interval from the R peak of one ECG waveform to the R peak of the next ECG waveform. The RR interval indicates the interval between successive heart beats and determines the heart rate. The RR interval often contains other valuable information, such as the types of arrhythmia that might be present in a patient [13].

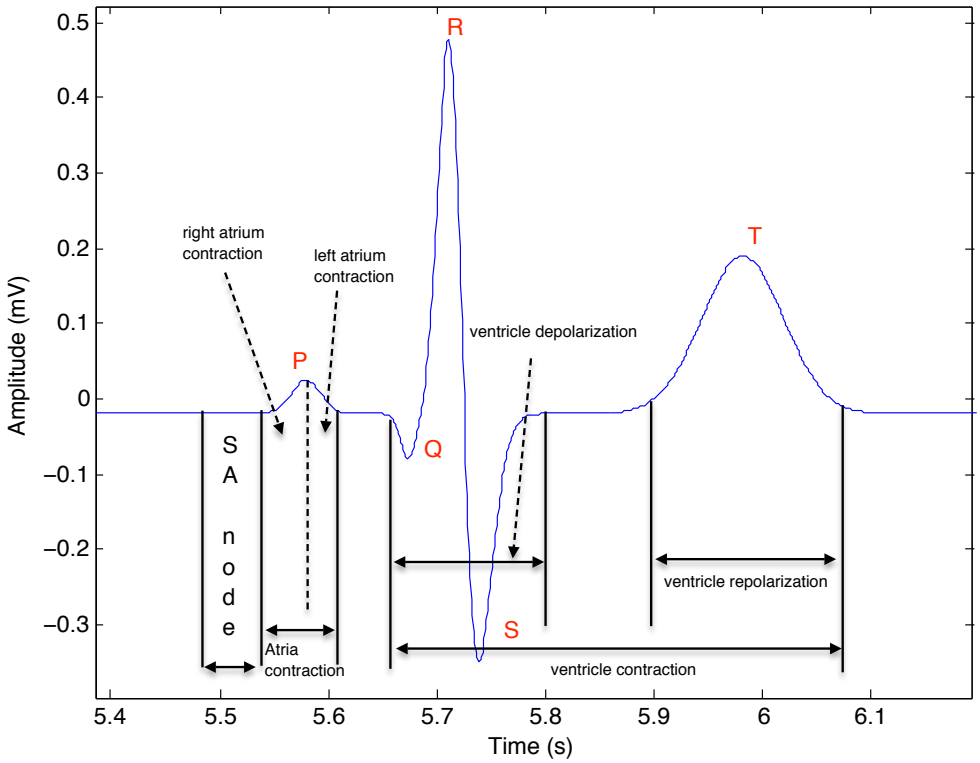

Figure 2.3: The sequence of muslce contractions follows after the firing of the electrical impulses from the sinoatrial (SA) node.

2.1.3 T wave

The T wave depicts the electrical recovery and repolarization of the ventricles, and marks the end of the contraction of the ventricles. It is typically a round, approximately semi-circular shaped wave, which deflects slightly above the baseline. The T wave follows each QRS complex. The time-separation between the QRS complex and the T wave is typically constant for normal ECG traces and is also known as the ST segment.

Using the five basic waves as landmarks, the ECG tracing is divided into various segments and intervals. An ECG segment is defined as the period between the end of one wave to the start of the next wave (see Figure 2.4). For example, the PR-segment begins at the end of the P wave and ends at the beginning of the Q wave. An ECG interval (not to be confused with an ECG segment) includes one segment and one or more waves (see Figure 2.6). Thus, the PR-interval starts at the beginning of the P wave and ends at the

onset of the QRS-complex. Each segment and interval displayed in Figure 2.4 and Figure 2.6 has its own characteristics and clinical significance, which are discussed in the following subsections.

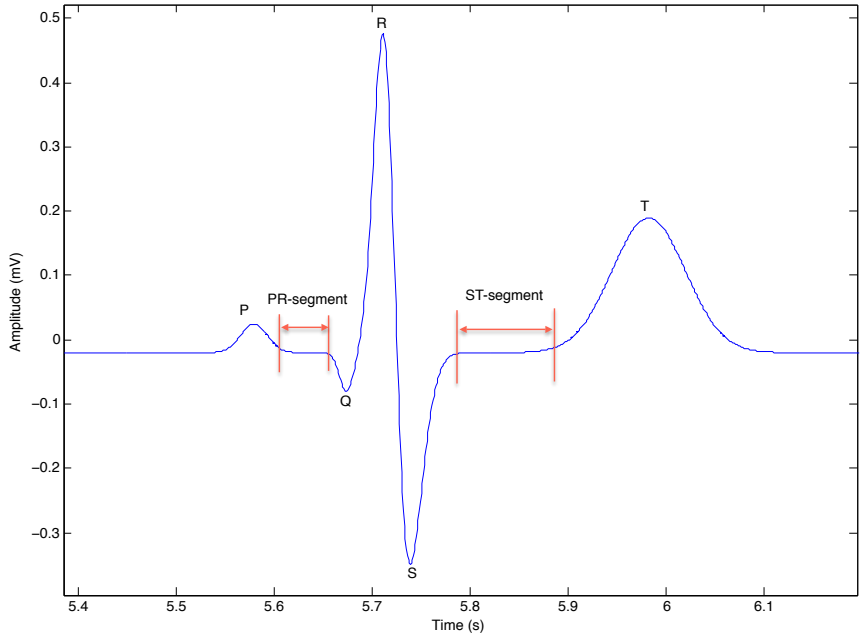

Figure 2.4: The ECG tracing is divided into two segments: PR segment and ST segment.

2.1.4 PR-segment

The PR-segment starts from the end of the P wave to the beginning of the successive Q wave. It appears as a flat, horizontal tracing on the ECG tracing. The duration of the segment represents the delay of the electrical impulse at the AV node where the electrical current traverses down the bundle of branches to the ventricles. Under both normal and abnormal ECG activities, the baseline of the PR segment remains constant and is approximately the same amplitude level as the isoelectric line. The isoelectric line is equivalent to the baseline of the entire ECG wave, which is typically at $0mV$. The amplitude of the PR segment is used to measure the amplitude of the isoelectric line. The portion of the ECG tracing following the T wave and preceding the next P wave could also be used to measure the isoelectric line.

2.1.5 ST-segment

The ST-segment starts from the end of the QRS-complex to the beginning of the succeeding T wave. This is the period of slow depolarization of the ventricles after the contractions of the left and right ventricles. In normal individuals, the baseline of the ST-segment typically remains close to the isoelectric line. The baseline of the ST-segment also curves rapidly into the ascending limb of the T wave from the end of the S wave as in Figure 2.5(a); it should not form a horizontal line nor a sharp angle with the start of the T wave like Figure 2.4. In abnormal cardiac activities, the baseline of the ST-segment is abnormally elevated or depressed from the isoelectric line as shown in Figure 2.5(b) and 2.5(c). For cardiac arrhythmia analysis, elevation of the ST-segment indicates myocardial infraction, while depression of the ST-segment is typically associated with hypokalemia or digitalis toxicity.

2.1.6 QT-interval

The QT-interval (see Figure 2.6) is the time from the beginning of the Q wave to the end of the T wave. The interval reflects the amount of time for ventricle depolarization and repolarization. If the interval is abnormally prolonged or shortened, there is a risk of developing ventricular arrhythmia. In certain cases, a prolonged QT-interval could lead to a life-threatening cardiac arrhythmia known as ventricular tachycardia, which in turn can lead to death of the patient.

2.1.7 RR-interval

The RR-interval (see Figure 2.6) is measured from one peak of the R wave to the next peak of the R wave. The RR-interval reflects the heart rate of a patient. The RR-interval varies over time as a consequence of the general physiological and psychological condition of the patient. The variations in the RR-interval is also known as heart rate variability (HRV). Both research and clinical studies have indicated the HRV contains valuable information about the various types of arrhythmia that might be present in a patent [15]. For instance, the HRV can be used to predict the survivability of a patient after a heart attack [15].

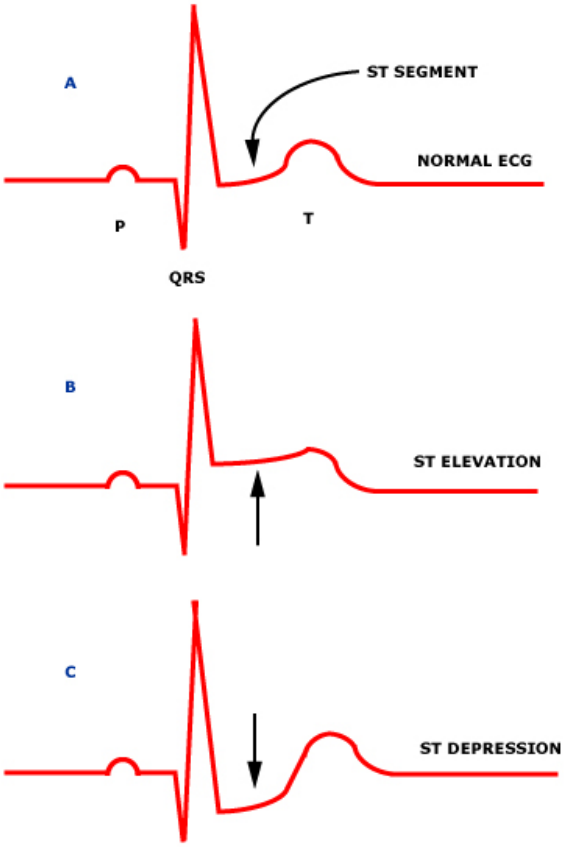

Figure 2.5: (a) A normal ST-segment in a normal ECG showing the base of the ST-segment remains relatively close to the isoelectric line. In normal ECG, the ST-segment moves into the beginning of the T wave. (b) ST-segment is elevated above the isoelectric line, (c)and the ST-segment is depressed below the isoelectric line. Figure taken from [20]

2.1.8 PR-interval

The PR-interval (see Figure 2.6) is measured from the beginning of the P-wave to the beginning of QRS-complex. This is the amount of time that is required by the electrical impulse to travel from the atria to permit the ventricular muscle to begin to depolarize. The variations in the PR-interval can be associated with certain medical conditions. For instance, a prolonged PR-interval indicates a first degree heart block.

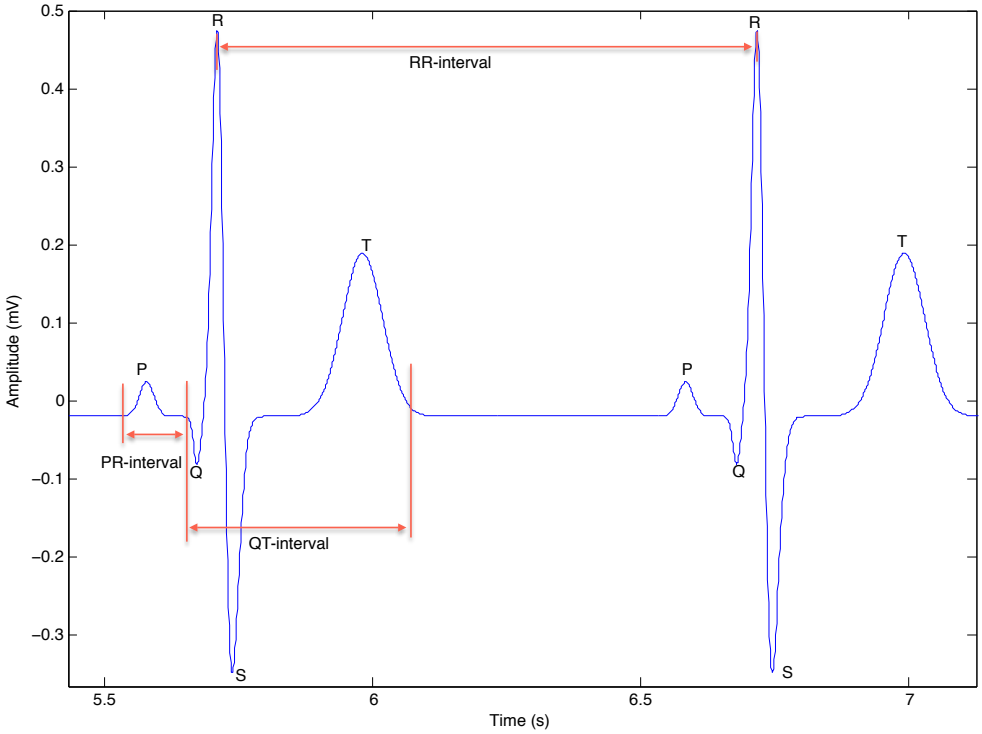

Figure 2.6: The ECG tracing is divided into various intervals: PR-interval, RR-interval, and QT-interval.

2.2 Types of ECG Noise

ECG signals obtained from EMG measurements are often corrupted by several kinds of noise. These noise signals can be within the frequency band of interest and can display characteristics quite similar to those of the ECG signal itself. Preprocessing is needed in order to extract useful information from a noisy ECG signal, and this will be discussed in Section 5.2.1.

The present section focuses on the four primary sources of noise in ECG signals:

1. Power Line Interference (PL)
2. Respiration Baseline Wandering (BW)
3. Muscle Artifacts (MA)

4. Electrode Motion Artifacts (EM)

2.2.1 Power Line Interference

Power line interference is a stationary noise that derives from capacitive and inductive coupling in the ECG signal acquisition circuitry. Typically, capacitive coupling is responsible for a narrow-band noise centred at 50 Hz or 60 Hz with a bandwidth of less than 1 Hz. In contrast, the inductive coupling induces a low frequency noise which interferences with the fundamental cardiac frequency components of the ECG. In Figure 2.7, the Fourier power spectrum of a typical ECG signal with a 60 Hz power line interference is displayed with high frequency component at 60 Hz in yellow circle. Since the low frequency components in the power line interference signal overlap with the ECG cardiac frequencies, the inductive coupling which causes these low frequency components is the main problem arising from power line interference.

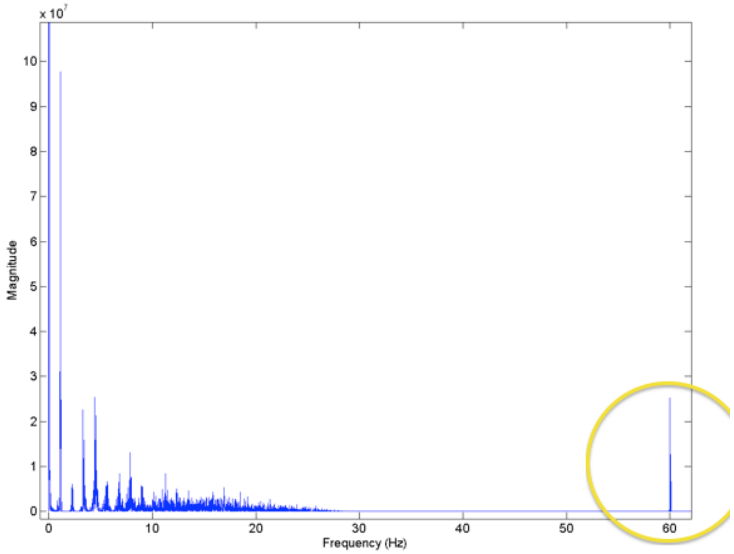

Figure 2.7: Fourier power spectrum of a normal ECG trace with 60 Hz power line interference

The high-frequency part of power line interference is easily modelled by the following sinusoid [38]:

$$y(t) = A(t)sin(2\pi f_0 t + \phi_0). \tag{2.1}$$

Here $A(t)$ is the time-varying peak value of the interference; f_0 is the fundamental frequency, which could be 50 Hz or 60 Hz; ϕ_0 is the phase of the sinusoid, which is a random variable with a uniform distribution in the range from $-\pi$ to π. Since, the high frequency component is generally well separated from the cardiac frequency components, it can be removed using a notch filter or a comb filter. Removal of low frequency components on the other hand requires more complex filters such Baysian filters.

2.2.2 Respiration Baseline Wandering

Respiration baseline wandering is a low-frequency, baseline-changing noise that is generated by the breathing of the subject. The expansion and contraction of the lung causes the electrode-skin impedance to vary, which, in turn, causes the baseline of the ECG to change. The frequency spectrum of the respiration baseline wandering ranges between 0.05Hz and 1Hz during relaxation. In most cases, the frequencies are in the range of 0.15 and 0.3 Hz. During strenuous exercise, the breathing rate increases and causes the frequency of the baseline wandering to increase. For the reduction of respiration baseline wandering, a low pass filter at 1 Hz could be applied to remove the low frequency variations in the baseline. However, this can be problematic because baseline wandering can be difficult to distinguish from muscle artifacts and electrode motion artifacts (see Figure 2.9).

2.2.3 Electrode Motion Artifact

Electrode motion artifacts are induced by the vibration, movement, or respiration of the subject. These movements produce sudden changes in the amplitude of the ECG traces, as well as baseline drifting. The baseline drifts are transient changes that can cause a significant shift in the baseline of the ECG signal. Because the resulting noise is non-stationary, it is difficult to filter out electrode motion artifacts. This noise is generally considered to be particularly troublesome because it cannot be removed easily by linear filters [22].

2.2.4 Muscle Artifact

Muscle artifacts, often known as EMG noise, originate in the contraction of muscles adjacent to the heart. The contraction of these muscles can generate polarization and depolarization waves that could be picked up by the surface electrode and mixed in with the ECG signal. The artifacts from other muscles produce a noise-like waveform that varies

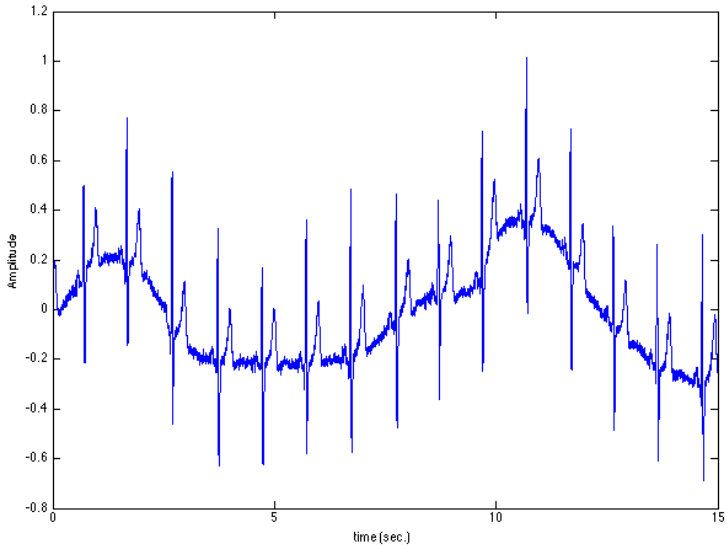

Figure 2.8: Baseline wandering of the ECG baseline due to patient breathing.

in amplitude with the amount of muscular activity and the quality of the probes. Studies have revealed that the peak amplitude of the noise is typically 10% of the peak-to-peak amplitude of the ECG [5], and vary in range from $25\mu V$ to approximately $5mV$ [16]. Similar to electrode motion artifacts, muscle artifacts are a non-stationary random noise that depends on the physical movement of the subject during EMG measurement.

2.3 Summary

The noise sources briefly discussed in this chapter are the ones which are of greatest concern for accurate real-time analysis of ECGs. Power line interference results in a harmonic noise artifact, which comprises a high frequency component and a low frequency component. Interference caused by electrode motion artifacts, muscle artifacts and respiration baseline wander, results in random drifting of the isoelectric line, all of which are difficult to remove. Reducing the effect of these noise sources is the main objective of this thesis. Understanding the characteristics of these noise processes is important to modelling parameters for Bayesian filters, such as the measurement noise covariance matrix and the process noise covariance matrix, since these covariance matrices can have a significant effect

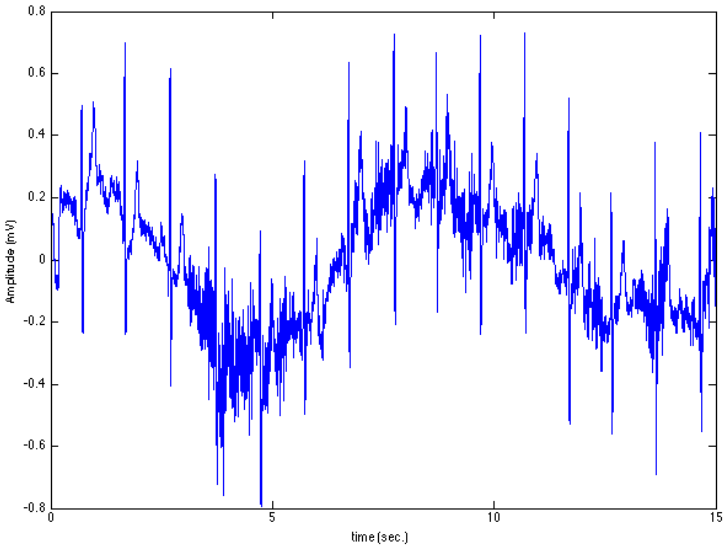

Figure 2.9: Baseline changing of ECG traces due to respiration baseline wander, muscle artifacts and electrode motion artifact.

on the performance of Bayesian filters.

Chapter 3

Optimal Filtering Theory

3.1 Introduction

Noise sources for ECG signals have been discussed in Chapter 2. These are: power line interference, respiration baseline wandering, electrode motion artifacts and muscle artifacts. To-date, many approaches have been developed to remove these noise sources. Some contributions propose the use of linear and nonlinear filters, such as the elliptic filter, the median filter, the Wiener filter and the wavelet transform. One drawback to these approaches is that not only noise is removed but some cardiac components of the ECG may also be removed. These cardiac components may contain important characteristic features, which are crucial for feature extraction and signal analysis. This is especially true for abnormal heart beats where the morphologies of signals change fast and significantly. Since the establishment of dynamical models for the ECG by McSharry [19], nonlinear filters based on these dynamics have shown improved performance over other methods. Two components must be involved in any model-based filtering problem: the filtering algorithm and the system dynamical model. Various nonlinear filters and smoothers are adapted and compared in this thesis with the system dynamical model. This chapter focuses on background information for the filtering algorithms.

3.2 Optimal Filters

3.2.1 The Extended Kalman Filter

The Extended Kalman Filter (EKF) is an extension of the conventional Kalman Filter (KF), and is a nonlinear version of the KF that linearizes about a state estimation at a reference point. Consider a discrete-time nonlinear dynamical system with the underlying unobserved system state vector $\mathbf{x}_k$, which contains n states. A measurement vector $\mathbf{z_k}$ is a set of m measurements at instant k. Mathematically, a nonlinear dynamical system is modelled as:

$$\mathbf{x}_{k+1} = f(\mathbf{x}_k, \mathbf{w}_k, k) \tag{3.1}$$

$$\mathbf{z}_k = g(\mathbf{x}_k, \mathbf{v}_k, k). \tag{3.2}$$

Here $\mathbf{x}_k \in \mathbb{R}^n$, $\mathbf{z}_k \in \mathbb{R}^m$.

Equation (3.1) is known as the state difference function and equation (3.2) is identified as the observation function. The $\mathbf{w}_k$ and the $\mathbf{v}_k$ are the process error and the measurement error, respectively. Both errors, $\mathbf{w}_k$ and $\mathbf{v}_k$, are assumed to be independent zero-mean white Gaussian random noise processes with the following statistics:

$$\bar{\mathbf{w}}_k \doteq \mathrm{E}[\mathbf{w}_k] = 0, \mathrm{E}[\mathbf{w}_k \mathbf{w}_k^T] = \mathbf{Q}_k, \mathrm{E}[\mathbf{w}_k \mathbf{w}_j] = 0 \text{ for } k \neq j, \tag{3.3}$$

$$\bar{\mathbf{v}}_k \doteq \mathrm{E}[\mathbf{v}_k] = 0, \mathrm{E}[\mathbf{v}_k \mathbf{v}_k^T] = \mathbf{R}_k, \mathrm{E}[\mathbf{v}_k \mathbf{v}_j] = 0 \text{ for } k \neq j, \tag{3.4}$$

Also, the two random noise vectors $\mathbf{w}_k$ and $\mathbf{v}_k$ are uncorrelated:

$$\mathrm{E}[\mathbf{w}_k \mathbf{v}_j^T] = 0, \text{for all} \quad k,\, j \geq 0. \tag{3.5}$$

In (3.3) and (3.4), $\mathbf{R}_k$ is the process noise covariance matrix and $\mathbf{Q}_k$ is the measurement noise covariance matrix. Both matrices are assumed to be symmetric, positive definite matrices.

The state differential function (3.1) propagates forward from the initial state $\mathbf{x}_0$. However, the precise value of $\mathbf{x}_0$ is not known *a priori*; thus, $\mathbf{x}_0$ is assumed to be a random vector which is normally distributed about a mean value $\hat{\mathbf{x}}_0$ with :

$$\hat{\mathbf{x}}_0 \doteq \mathrm{E}[\mathbf{x}_0] \tag{3.6}$$

$$\mathbf{P}_0 \doteq \mathrm{E}[(\mathbf{x}_0 - \hat{\mathbf{x}}_0)(\mathbf{x}_0 - \hat{\mathbf{x}}_0)^T] \tag{3.7}$$

We will begin this section with a broad overview, covering the "high-level" operation of the extended Kalman filter recursive algorithm. After presenting the high-level view, we will present the summary of the recursive algorithm. To start, we define $\hat{\mathbf{x}}_k^-$ and $\hat{\mathbf{x}}_k^+$ as

$$\hat{\mathbf{x}}_k^- \doteq \mathrm{E}[\mathbf{x}_k|\mathbf{Z}_{k-1} = \{\mathbf{z}_{k-1}, \mathbf{z}_{k-2}, ..., \mathbf{z}_1\}] \tag{3.8}$$
$$\hat{\mathbf{x}}_k^+ \doteq \mathrm{E}[\mathbf{x}_k|\mathbf{Z}_k = \{\mathbf{z}_k, \mathbf{z}_{k-1}, ..., \mathbf{z}_1\}] \tag{3.9}$$

with conditional covariance matrix

$$\mathbf{P}_k^- \doteq \mathrm{E}[(\mathbf{x}_k - \hat{\mathbf{x}}_k^-)(\mathbf{x}_k - \hat{\mathbf{x}}_k^-)^T|\mathbf{Z}_{k-1}] \tag{3.10}$$
$$\mathbf{P}_k^+ \doteq \mathrm{E}[(\mathbf{x}_k - \hat{\mathbf{x}}_k^+)(\mathbf{x}_k - \hat{\mathbf{x}}_k^+)^T|\mathbf{Z}_k] \tag{3.11}$$

for all $k \geq 1$. $\hat{\mathbf{x}}_k^+$ is the estimation of the state vector $\mathbf{x}_k$ projected from all the measurements up to instant k in the Hilbert space and $\hat{\mathbf{x}}_k^-$ is the estimation of the state vector $\mathbf{x}_k$ projected from all the measurements up to instant $k-1$ in the Hilbert space.

Suppose $\hat{\mathbf{x}}_k^-$ and its covariance matrix $\mathbf{P}_k^-$ are known; a new measurement is observed at instant k. With the new observed measurement, the estimate $\hat{\mathbf{x}}_k^-$ is updated by incorporating the new information to obtain an improved *a posteriori* estimate $\hat{\mathbf{x}}_k^+$. It can be shown that the conditional expectation in (3.8) given the newly arrived observed measurement is computable from the following equations [6, 17, 27]:

$$\mathbf{K}_k \doteq \mathbf{P}_k^- - \mathbf{C}_k^T \left[\mathbf{C}_k \mathbf{P}_k^- \mathbf{C}_k^T + \mathbf{R}_k\right]^{-1} \tag{3.12}$$
$$\mathbf{r}_k \doteq \mathbf{z}_k - g(\hat{\mathbf{x}}_k^-, \bar{\mathbf{v}}_k, k) \tag{3.13}$$
$$\hat{\mathbf{x}}_k^+ = \hat{\mathbf{x}}_k^- + \mathbf{K}_k \mathbf{r}_k \tag{3.14}$$
$$\mathbf{P}_k^+ = \mathbf{P}_k^- - \mathbf{K_k} \mathbf{C}_k \mathbf{P}_k^- \tag{3.15}$$

in which

$$\mathbf{C}_k = \left.\frac{\partial g(\mathbf{x}, \bar{\mathbf{v}}_k, k)}{\partial \mathbf{x}}\right|_{\mathbf{x}=\hat{\mathbf{x}}_k^-}, \tag{3.16}$$

$$\mathbf{G}_k = \left.\frac{\partial g(\hat{\mathbf{x}}_k^-, \mathbf{v}_k, k)}{\partial \mathbf{v}}\right|_{\mathbf{v}=\bar{\mathbf{v}}_k}. \tag{3.17}$$

$\mathbf{K}_k$ in (3.12) denotes the Kalman gain which is the optimal weighted matrix in the minimum mean square error sense to generate a corrective term to be added to $\hat{\mathbf{x}}_k^k$. $\mathbf{r}_k$ in (3.13) is known as the measurement residual or the innovation signal, which measures the difference between the true measurement value $\mathbf{z}_k$ and the estimated value $g(\hat{\mathbf{x}}_k^-, \bar{\mathbf{v}}_k, k)$. The residuals reflect the degree to which the KF correctly models the underlying system[6]. By

monitoring the residuals, the effectiveness of the KF can be determined. Residuals can also be used for adaptive purposes[17] and fault-identification purposes [9].

After obtaining the *a posteriori* estimate $\hat{\mathbf{x}}_k^+$, the estimate is projected forward in time to obtain the next *a priori* estimate $\hat{\mathbf{x}}_{k-1}^-$. From (3.8), we know that $\hat{\mathbf{x}}_{k-1}^-$ is a conditional expectation given all past measurement:

$$\hat{\mathbf{x}}_{k+1}^- \doteq \mathrm{E}[\mathbf{x}_{k+1}|\mathbf{Z}_k] \tag{3.18}$$

The conditional expectation in the above equation can be shown to be the projection of the previous *a posteriori* estimate using the state difference equation (3.1) [6, 17, 27]:

$$\mathrm{E}[\mathbf{x}_{k+1}|\mathbf{Z}_k] = f(\hat{\mathbf{x}}_k^+, \bar{\mathbf{w}}_k, k) \tag{3.19}$$

Therefore,

$$\hat{\mathbf{x}}_{k+1}^- = f(\hat{\mathbf{x}}_k^+, \bar{\mathbf{w}}_k, k) \tag{3.20}$$

Similarly, if we define $\mathbf{P}_k^-$ to be the conditional covariance of $\hat{\mathbf{x}}_{k+1}^-$ as

$$\mathbf{P}_{k+1}^- \doteq \mathrm{E}[(\mathbf{x}_{k+1} - \hat{\mathbf{x}}_{k+1}^-)(\mathbf{x}_{k+1} - \hat{\mathbf{x}}_{k+1}^-)^T|\mathbf{Z}_k]. \tag{3.21}$$

It can be shown that the covariance matrix is estimated by [6, 17, 27]

$$\mathbf{P}_{k+1}^- = \mathbf{A}_k \mathbf{P}_k^+ \mathbf{A}_k^T + \mathbf{F}_k \mathbf{Q}_k \mathbf{F}_k^T \tag{3.22}$$

where

$$\mathbf{A}_k = \left.\frac{\partial f(\mathbf{x}, \bar{\mathbf{w}}_k, k)}{\partial \mathbf{x}}\right|_{\mathbf{x}=\hat{\mathbf{x}}_k^+} \tag{3.23}$$

$$\mathbf{F}_k = \left.\frac{\partial f(\hat{\mathbf{x}}_k^+, \mathbf{w}, k)}{\partial \mathbf{w}}\right|_{\mathbf{w}=\bar{\mathbf{w}}_k} \tag{3.24}$$

One iteration of the recursive algorithm has been defined with the following estimate transitions:

$$\left\{\begin{matrix}\hat{\mathbf{x}}_k^- \\ \mathbf{P}_k^-\end{matrix}\right\} \Rightarrow \left\{\begin{matrix}\hat{\mathbf{x}}_k^+ \\ \mathbf{P}_k^+\end{matrix}\right\} \Rightarrow \left\{\begin{matrix}\hat{\mathbf{x}}_{k+1}^- \\ \mathbf{P}_{k+1}^-\end{matrix}\right\} \text{ for all } k \geq 1$$

We still need to determine $\hat{\mathbf{x}}_1^-$ and the conditional covariance $\mathbf{P}_1^-$ in order to begin the above recursion. The extended Kalman filter begins the recursive algorithm from an estimated initial condition $\hat{\mathbf{x}}_0$ with the covariance matrix $\mathbf{P}_0$ which are known. The initial

condition is propagated forward in time to obtain the *a priori* estimate $\hat{\mathbf{x}}_1^-$ at instant $k = 1$ with covariance matrix $\mathbf{P}_1^-$ which follows the equations in (3.20) and (3.22):

$$\hat{\mathbf{x}}_1^- \doteq f(\hat{\mathbf{x}}_0, \bar{\mathbf{w}}_0) \tag{3.25}$$

with covariance matrix

$$\mathbf{P}_1^- = \mathbf{A}_0 \mathbf{P}_0 \mathbf{A}_0 + \mathbf{F}_0 \mathbf{Q}_0 \mathbf{F}_0^T \tag{3.26}$$

where

$$\mathbf{A}_0 = \left. \frac{\partial f(\mathbf{x}, \bar{\mathbf{w}}_0, 0)}{\partial \mathbf{x}} \right|_{\mathbf{x}=\hat{\mathbf{x}}_0} \tag{3.27}$$

$$\mathbf{F}_0 = \left. \frac{\partial f(\hat{\mathbf{x}}_0, \mathbf{w}, 0)}{\partial \mathbf{w}} \right|_{\mathbf{w}=\bar{\mathbf{w}}_0} \tag{3.28}$$

Since the initial $\hat{\mathbf{x}}_0$ and $\mathbf{P}_0$ are known, $\mathbf{x}_1^-$ and $\mathbf{P}_1^-$ are deterministic. By applying the equations in (3.12) - (3.15) on $\mathbf{x}_1^-$ and $\mathbf{P}_1^-$, the posteriori estimate $\hat{\mathbf{x}}_1^+$ with $\mathbf{P}_1^+$ can be determined. Similarly, (3.20) and (3.22) are applied on the posteriori estimate $\hat{\mathbf{x}}_1^+$ to predict the next *a priori* estimate $\hat{\mathbf{x}}_2^-$. This completes the induction of the extended Kalman Filter algorithm which follows the estimate transitions:

$$\begin{Bmatrix} \hat{\mathbf{x}}_0 \\ \mathbf{P}_0 \end{Bmatrix} \Rightarrow \begin{Bmatrix} \hat{\mathbf{x}}_1^- \\ \mathbf{P}_1^- \end{Bmatrix} \Rightarrow \begin{Bmatrix} \hat{\mathbf{x}}_1^+ \\ \mathbf{P}_1^+ \end{Bmatrix} \Rightarrow \begin{Bmatrix} \hat{\mathbf{x}}_2^- \\ \mathbf{P}_2^- \end{Bmatrix} \Rightarrow \ldots \Rightarrow \begin{Bmatrix} \hat{\mathbf{x}}_k^- \\ \mathbf{P}_k^- \end{Bmatrix} \Rightarrow \begin{Bmatrix} \hat{\mathbf{x}}_k^+ \\ \mathbf{P}_k^+ \end{Bmatrix} \Rightarrow \begin{Bmatrix} \hat{\mathbf{x}}_{k+1}^- \\ \mathbf{P}_{k+1}^- \end{Bmatrix} \Rightarrow \ldots$$

for all $k \geq 1$.

In summary, the extended Kalman filter is an ongoing recursive algorithm which follows a two step procedure: the measurement step and the the time update step. The measurement step is responsible for incorporating a new measurement into the *a priori* estimate as shown by the estimate transition from $\hat{\mathbf{x}}_k^-$ to $\hat{\mathbf{x}}_k^+$. The time update time is responsible for projecting forward in time the *a posteriori* estimate $\hat{\mathbf{x}}_k^+$ to obtain the *a priori* estimate for the next time step as shown by the transition from $\hat{\mathbf{x}}_k^+$ to $\hat{\mathbf{x}}_{k+1}^-$. The recursive algorithm is shown in Figure 3.1. The specific equations for the time and measurement updates are summarized below:

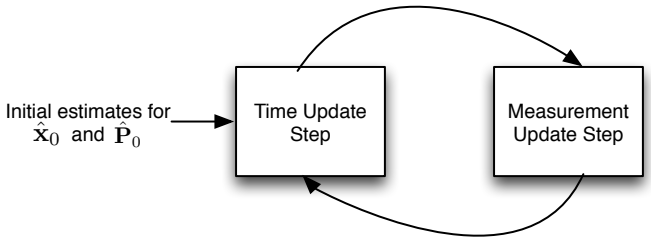

Figure 3.1: The ongoing discrete Kalman filter cycle. The time update step projects the current state estimate ahead in time. The measurement update step adjusts the projected estimate by an actual measurement at that time.

Initial Conditions

$$\mathbf{x}_0 \sim \mathrm{N}(\hat{\mathbf{x}}_0, \mathbf{P}_0) \tag{3.29}$$

The Time Update Step

$$\hat{\mathbf{x}}_{k+1}^- = f(\hat{\mathbf{x}}_k^+, \bar{\mathbf{w}}_k, k) \tag{3.30}$$

$$\mathbf{P}_{k+1}^- = \mathbf{A}_k \mathbf{P}_k^+ \mathbf{A}_k^T + \mathbf{F}_k \mathbf{Q}_k \mathbf{F}_k^T \tag{3.31}$$

The Measurement Update Step

$$\mathbf{K}_k = \mathbf{P}_k^- - \mathbf{C}_k^T \left[\mathbf{C}_k \mathbf{P}_k^- \mathbf{C}_k^T + \mathbf{R}_k \right]^{-1} \tag{3.32}$$

$$\mathbf{r}_k = \mathbf{z}_k - g(\hat{\mathbf{x}}_k^-, \bar{\mathbf{v}}_k, k) \tag{3.33}$$

$$\hat{\mathbf{x}}_k^+ = \hat{\mathbf{x}}_k^- + \mathbf{K}_k \mathbf{r}_k \tag{3.34}$$

$$\mathbf{P}_k^+ = \mathbf{P}_k^- - \mathbf{K_k} \mathbf{C}_k \mathbf{P}_k^- \tag{3.35}$$

where

$$\mathbf{A}_k = \left.\frac{\partial f(\mathbf{x}, \bar{\mathbf{w}}_k, k)}{\partial \mathbf{x}}\right|_{\mathbf{x}=\hat{\mathbf{x}}_k^+} \tag{3.36}$$

$$\mathbf{C}_k = \left.\frac{\partial g(\mathbf{x}, \bar{\mathbf{v}}_k, k)}{\partial \mathbf{x}}\right|_{\mathbf{x}=\hat{\mathbf{x}}_k^-} \tag{3.37}$$

$$\mathbf{F}_k = \left.\frac{\partial f(\hat{\mathbf{x}}_k^+, \mathbf{w}, k)}{\partial \mathbf{w}}\right|_{\mathbf{w}=\bar{\mathbf{w}}_k} \tag{3.38}$$

$$\mathbf{G}_k = \left.\frac{\partial g(\hat{\mathbf{x}}_k^-, \mathbf{v}_k, k)}{\partial \mathbf{v}}\right|_{\mathbf{v}=\bar{\mathbf{v}}_k} \tag{3.39}$$

The derivation of the Kalman recursive algorithm is based on the assumption that $\mathbf{P}_k^-$ and $\mathbf{P}_k^+$ are positive definite matrices[17]. $\mathbf{P}_k^-$ and $\mathbf{P}_k^+$ become positive definite matrices under two sufficient conditions. First, $\mathbf{P}_0$ must be a positive definite matrix. Second, $\mathbf{Q}_k$ must remain positive definite for all time k. Thus, both $\mathbf{P}_0$ and $\mathbf{Q}_k$ must be positive definite[17]. Failure to attain these conditions will lead to numerical ill-conditioning when the EKF is implemented. In order to overcome ill-conditioning the inverse-covariance form and the Joseph-form are applied (See Section 3.2.2 and Section 3.2.3).

3.2.2 The Inverse-Covariance Form

In this section, the two-step optimal recursive algorithm of EKF is expressed in another form called the inverse-covariance form. Both the inverse-covariance form and the original form are algebraically equivalent. However, the inverse-covariance form possesses some very desirable characteristics. First, the inverse-covariance form includes the case where $\mathbf{P}_0^{-1}$ is singular. Second, it allows the dynamical systems to propagate backward in time, which is used in fixed-interval smoothing discussed in Section 3.3. The inverse-covariance form re-defines the *a priori* estimate $\mathbf{x}_k^+$ and the *a posteriori* $\mathbf{x}_k^-$ as [17]:

$$\hat{\mathbf{y}}_k^- \doteq (\mathbf{P}_k^-)^{-1}\hat{\mathbf{x}}_k^- \tag{3.40}$$

$$\hat{\mathbf{y}}_k^+ \doteq (\mathbf{P}_k^+)^{-1}\hat{\mathbf{x}}_k^+ \tag{3.41}$$

Here, $\hat{\mathbf{y}}_k^-$ and $\hat{\mathbf{y}}_k^+$ allow a proper startup procedure when $\mathbf{P}_0^{-1}$ is singular[17]. The time update equations in the inverse-covariance form become [17]:

$$(\mathbf{P}_{k+1}^-)^{-1} = \mathbf{M}_{k+1} - \mathbf{L}_k \mathbf{F}_k^T \mathbf{M}_{k+1} \tag{3.42}$$

$$\mathbf{M}_{k+1} = \mathbf{A}_k^T \mathbf{P}_k^{+^{-1}} \mathbf{A}_k \tag{3.43}$$

$$\hat{\mathbf{y}}_k^- = \left[\mathbf{I} - \mathbf{L}_k \mathbf{F}_k\right] \mathbf{A}_k^T \hat{\mathbf{y}}_k^+ \tag{3.44}$$

$$\mathbf{L}_k = \mathbf{M}_{k+1} \mathbf{F}_k \left[\mathbf{F}_k^T \mathbf{M}_{k+1} \mathbf{F}_k + \mathbf{Q}_k^{-1}\right]^{-1} \tag{3.45}$$

Additionally, the measurement update equations in the inverse-covariance form are [17]:

$$\hat{\mathbf{y}}_k^+ = \hat{\mathbf{y}}_k^- + \mathbf{C}_k^T \mathbf{R}_k^{-1} \mathbf{z}_k \tag{3.46}$$

$$(\mathbf{P}_k^+)^{-1} = (\mathbf{P}_k^-)^{-1} + \mathbf{F}_k^T \mathbf{R}_k{}^{-1} \mathbf{F}_K \tag{3.47}$$

The inverse-form recursive algorithm begins with $\hat{\mathbf{y}}_0 = \mathbf{P}_0^{-1} \hat{\mathbf{x}}_0$. As previously mentioned, $\mathbf{P}_0^{-1}$ can be singular. In other words, certain eigenvalues of $\mathbf{P}_0$ go to infinity. By allowing $\mathbf{P}_0^{-1}$ to be singular, one can model the case when some or all initial states of the system are unknown. To revert $\hat{\mathbf{y}}_k$ back to $\hat{\mathbf{x}}_k$ the following equation can simply be used:

$$\hat{\mathbf{x}}_k^+ = \mathbf{P}_k^+ \hat{\mathbf{y}}_k^+ \tag{3.48}$$

$$\hat{\mathbf{x}}_k^- = \mathbf{P}_k^- \hat{\mathbf{y}}_k^- \tag{3.49}$$

3.2.3 The Joseph-Form

The covariance update in the EKF and its inverse-covariance form involve subtraction, which can result in a loss of symmetry and positive definiteness due to numerical rounding errors[17]. These errors pose serious numerical problems which can result in numerical instability. For online applications, these numerical problems are an important consideration because long duration of normal operations is required. The Joseph-form is a modification to the equations (3.35) and (3.47) to avoid loss of symmetry and positive definiteness, although at some extra computational expense (greater number of computations in multiplications and additions). The covariance update equation in the EKF recursive algorithm in equation (3.35) is reproduced here:

$$\mathbf{P}_k^+ = \mathbf{P}_k^- - \mathbf{K_k} \mathbf{C}_k \mathbf{P}_k^- \tag{3.50}$$

(3.50) involves m-by-m matrix inversions due to the Kalman gain $\mathbf{K}_k$ in (3.32), where m is the dimension of the measurement vector. If $\mathbf{K_k} \mathbf{C}_k \mathbf{P}_k^-$ becomes very close to 0, the

matrix subtractions between $\mathbf{P}_k^-$ and $\mathbf{K_k C}_k\mathbf{P}_k^-$ can result in a very small number. This outcome occurs when the measurements are very accurate. When storing a small numerical value on a finite word length computer, the positive definiteness of $\mathbf{P}_k^+$ sometimes cannot be guaranteed, because $\mathbf{P}_k^+$ might become a semi-definite matrix; thus, the condition on $\mathbf{P}_k^+$ is violated (discussed in Page 22). Once the condition is violated, the computations of the covariance eigenvalues may give negative eigenvalues. Once a negative eigenvalue is obtained, subsequent computations of the Kalman Filter become erroneous [17]. To resolve this numerical computation problem, the covariance update equation in (3.50) can be rewritten into the Joseph-form [17]:

$$\mathbf{P}_k^+ = [\mathbf{I} - \mathbf{K}_k\mathbf{F}_k]\,\mathbf{P}_k^-\,[\mathbf{I} - \mathbf{K}_k\mathbf{F}_k]^T + \mathbf{K}_k\mathbf{R}_k\mathbf{K}_k^T \tag{3.51}$$

The Joseph-form in (3.51) involves matrix summations between two symmetric matrices: $[\mathbf{I} - \mathbf{K}_k\mathbf{F}_k]\,\mathbf{P}_k^-\,[\mathbf{I} - \mathbf{K}_k\mathbf{F}_k]^T$ and $\mathbf{K}_k\mathbf{R}_k\mathbf{K}_k^T$, where the former matrix is a positive-definite matrix and the latter is a positive semi-definite matrix. As a result, the computation of $\mathbf{P}_k^+$ becomes better conditioned than the previous form in (3.50). Nevertheless, the Joseph-form involves greater computational effort to secure better conditioned numerical computations. To reduce the computational burden for online applications the symmetry of the matrices is exploited by updating only the lower triangular forms of the covariance matrices [17].

The Joseph-form can also be applied to the inverse-covariance update equation in (3.42). For the inverse-covariance update equation:

$$(\mathbf{P}_{k+1}^-)^{-1} = \mathbf{M}_{k+1} - \mathbf{L}_k\mathbf{F}_k^T\mathbf{M}_{k+1} \tag{3.52}$$

or, in the analog of the Joseph-form,

$$(\mathbf{P}_{k+1}^-)^{-1} = [\mathbf{I} - \mathbf{L}_k\mathbf{F}_k^T]\mathbf{M}_{k+1}[\mathbf{I} - \mathbf{L}_k\mathbf{F}_k^T]^T + \mathbf{L}_k\mathbf{Q}_k^{-1}\mathbf{L}_k^T \tag{3.53}$$

3.2.4 The Unscented Kalman Filter

The EKF has been used successfully in many applications, but nevertheless has several flaws. First, the EKF linearizes the dynamical system at an operating point by approximating the state distribution through the first order Taylor series approximation. By linearizing higher-order terms using the first-order Taylor series approximation, the posterior mean and covariance estimations becomes suboptimal and unmodeled errors are introduced. The suboptimal estimations due to linearization can lead to instability and divergence particularly when the system dynamics are very nonlinear [17]. Many proposed

revisions to the EKF were researched and one of the more successful is known as the Unscented Kalman Filter (UKF). The UKF attempts to remove some of the flaws associated with the EKF. It is a derivative-free alternative that uses the unscented transformation to determine the *a priori* mean and covariance of the states. The unscented transformation uses a set of sample points, the sigma points, which determine the *a priori* mean and covariance of the states. It is a method for calculating the statistics of a random variable when it undergoes a nonlinear transformation [11]. For nonlinear systems, the UKF can provide better stability and better accuracy than the EKF [11]. Since the dynamics of the electrocardiogram are highly nonlinear, the UKF is used to achieve higher accuracy in estimations. Note in particular that no explicit calculations of Jacobian matrices or Hessian matrices are necessary to implement this algorithm (unlike the EKF), and this is one of its great advantages. Just like the EKF, the UKF has a two-step recursive algorithm, which is displayed in Appendix A.

3.3 Optimal Linear Smoothers

In order to evaluate the effectiveness of noise reduction it is important to compare the performance of the optimal linear filters (for example, EKF and UKF) with optimal linear smoothers. The reason is that optimal linear smoothers are generally believed to produce better estimates in most cases than optimal linear filters [6]. Optimal filters provide the best estimates based on all measurements, present and past. In contrast, linear smoothers use the information of future observations to obtain more accurate estimates of the current state. Because smoothers use more information than optimal linear filters, it is usually the case that smoothers are more effective estimators. Most applications of smoothing are based on three distinct types of smoothers: the fixed-interval smoother, the fixed-lag smoother and the fixed-point smoother. In this thesis, the fixed-interval smoother and the fixed-lag smoother are studied. Fixed-point smoothers are not considered here because these do not suit our particular estimation problem (such smoothers are useful for estimation problems in which the system state is of interest only at some fixed instant rather than for all instants). The following subsections describe the constraints on the times at which measurements are made relative to the times when the value of the state vector is to be estimated

3.3.1 Fixed-Interval Smoothing

To describe the fixed-interval smoother (FIS), suppose that ECG measurement data is collected over an interval $0 < k \leq N$, assuming N is fixed. After all this data has been collected, it is desired to obtain the optimal smoothed estimate of $\hat{\mathbf{x}}_{k,FIS}$ of FIS for all $k \in (0, N]$ using all the available data, past and future. Because all the data must be collected beforehand, this smoothing process is carried out offline for post-experiment data analysis. We define the optimal smoothed estimate as

$$\hat{\mathbf{x}}_{k,FIS} = \mathrm{E}[\mathbf{x}_k | \mathbf{Z}_{1:N} = \{\mathbf{z}_1, \mathbf{z}_2, ..., \mathbf{z}_N\}] \quad \text{for all } k,\ 0 < k \leq N \tag{3.54}$$

Essentially, a three-part procedure can be employed to determine the optimal estimate $\hat{\mathbf{x}}_{k,FIS}$: forward filtering, backward filtering and smoothing.

The forward filter runs forward in time to determine the optimal estimates by accounting for all past measurement. Mathematically, the forward filter calculates

$$\hat{\mathbf{x}}_k^+ = \mathrm{E}[\mathbf{x}_k | \mathbf{Z}_{1:k}] \quad \text{for all } k,\ 0 < k \leq N \tag{3.55}$$

where $\hat{\mathbf{x}}_k^+$ is the *a posteriori* state estimates presented in Section 3.2.1. For simplicity, let $\hat{\mathbf{x}}_k^f$ denote the state estimates obtained from the forward filter with covariance matrix $\mathbf{P}_k^f$ (i.e., $\hat{\mathbf{x}}_k^f = \hat{\mathbf{x}}_k^+$ and $\mathbf{P}_k^f = \mathbf{P}_k^+$). Essentially, the forward filter runs the EKF to determine the *a posteriori* state estimates.

The backward filter deals with the issue of state estimates pertaining to the future measurements, where the filter begins at the final time state N and runs the filter in reverse time. The backward filter calculates:

$$\hat{\mathbf{x}}_k^b = \mathrm{E}[\mathbf{x}_k | \mathbf{Z}_{k+1:N}] \quad \text{for all } k,\ 0 < k \leq N \tag{3.56}$$

The initial state for the backward filter is established by assuming $\mathbf{x}_N^b$ is a random vector with no *a priori* statistical information. Thus, the covariance matrix $\mathbf{P}_N^b$ for the state estimate $\mathbf{x}_N^b$ is assumed to have "infinite" covariance (see [17]) that is:

$$(\mathbf{P}_N^b)^{-1} = 0 \tag{3.57}$$

Since the backward filter runs backward in time, the inverse-covariance formulation for the EKF is appropriate for the computations of $\mathbf{x}_N^b$, which is previous mentioned in Section 3.2.2.

The last step involves smoothing the state estimates obtained from the forward and backward filters to generate the smoothed estimate $\hat{\mathbf{x}}_{k,FIS}$. Smoothed estimates are computed by viewing $\hat{\mathbf{x}}_k^f$ and $\hat{\mathbf{x}}_k^f$ as two independent state estimates and assigning weights to

$\hat{\mathbf{x}}_k^f$ and $\hat{\mathbf{x}}_k^f$ according to the confidence on each estimate, which can be determined from $\mathbf{P}_k^f$ and $\mathbf{P}_k^b$, respectively. Subsequently, the smoothed estimates are determined by [17]:

$$\hat{\mathbf{x}}_{k,FIS} = \mathbf{P}_{k,FIS}[(\mathbf{P}_k^f)^{-1}\hat{\mathbf{x}}_k^f + (\mathbf{P}_k^b)^{-1}\hat{\mathbf{x}}_k^b] \tag{3.58}$$

$$(\mathbf{P}_{k,FIS})^{-1} = (\mathbf{P}_k^f)^{-1} + (\mathbf{P}_k^b)^{-1} \tag{3.59}$$

where $\mathbf{P}_{k,FIS}$ is the covariance matrix of $\hat{\mathbf{x}}_{k,FIS}$.

For the implementation of fixed-interval smoothing, the Rauch-Tung-Striebel Two-Pass smoother is implemented. This fixed-interval two-pass implementation is the fastest fixed-interval smoother and has been used quite successfully for decades [9]. In Appendix B, a summary of the Rauch-Tung-Striebel algorithm is shown.

3.3.2 Fixed-Lag Smoothing

To describe the fixed-lag smoother, suppose ECG measurement data is available over an interval $0 < k \leq N$, where N is fixed. The optimal estimate at $\mathbf{x}_k$ for all $0 < k \leq N$ uses all the past measurements, and l additional future measurements to obtain the optimal estimate. The optimal estimate is defined as

$$\hat{\mathbf{x}}_{k,FLS} = \mathrm{E}[\mathbf{x}_k|\mathbf{Z}_{1:j}], \quad \text{for all } k,\ 0 < k \leq N \tag{3.60}$$

where $j = min\{k + l + 1, N - 1\}$ and $\mathbf{Z}_{1:j} = \{\mathbf{z}_1, \mathbf{z}_2, ...\mathbf{z}_{j-1}, \mathbf{z}_j\}$.

In other words, the fixed-lag smoother delays the computation of the estimate $\hat{\mathbf{x}}_{k,FLS}$ until the time instant $j = k+l+1$ to take advantage of the additional information in these l measurements. Fundamentally, two filters are running simultaneously to obtain $\hat{\mathbf{x}}_{k,FLS}$: a forward filter and the smoothing filter. The forward filter is an EKF, mentioned in Section 3.2.1, which determines the optimal estimates pertaining to all past measurement. The smoother filter refines the optimal estimates from the EKF by incorporating future available measurements in the window of length l. Therefore, a fixed-lag smoother with an l-step time lag generates the smoothed estimates from the relationship [17]

$$\hat{\mathbf{x}}_{k+1} = \mathbf{A}_k\hat{\mathbf{x}}_k + \mathbf{B}_j\mathbf{K}_j\mathbf{r}_j + \mathbf{U}_k[\hat{\mathbf{x}}_{k,FLS} - \hat{\mathbf{x}}_k^+] \tag{3.61}$$

$\mathbf{K}_j$ and $\mathbf{r}_j$ are the Kalman gain and the measurement residual of the EKF at time instant j in (3.32) and (3.33), which is available from the the EKF. $\mathbf{B}_j$ is a n-by-n gain matrix given by [17]

$$\mathbf{B}_j = \mathbf{B}_{k+l+1} = \prod_{i=k+1}^{k+l} \mathbf{W}_i = \mathbf{W}_k^{-1}\mathbf{B}_{k+l}\mathbf{W}_{k+l} \tag{3.62}$$

where $\mathbf{W}_k$ is the "smoothing estimator gain matrix" [17] given by

$$\mathbf{W}_k = \mathbf{P}_k^+ \mathbf{A}_k^T \mathbf{P}_k^{-1}. \tag{3.63}$$

$\mathbf{P}_k^+$ and $\mathbf{P}_k^-$ are also obtainable from the EKF in (3.30) and (3.35), respectively. Lastly, $\mathbf{U}_k$ is given by

$$\mathbf{U}_k = \mathbf{F}_k \mathbf{Q}_k \mathbf{F}_k^T \mathbf{A}_k^T (\mathbf{P}_k^+)^{-1} \tag{3.64}$$

In (3.62), the first term $\mathbf{A}_k \hat{\mathbf{x}}_k$ propagates the previous smoothed estimate $\hat{\mathbf{x}}_{k,FLS}$ forward by one step. The second term $\mathbf{B}_j \mathbf{K}_j \mathbf{r}_j$ is a corrective term by incorporating all the measurements $\mathbf{Z}_{1:j}$ up to time instant j. The last term $\mathbf{U}_k[\hat{\mathbf{x}}_{k,FLS} - \hat{\mathbf{x}}_k^+]$ further refines the estimate by using information from the noise terms.

The covariance matrix $\mathbf{P}_k$ of $\hat{\mathbf{x}}_{k,FLS}$ is computed by [17]

$$\mathbf{P}_k = \mathbf{P}_k^- - \mathbf{B}_j \mathbf{K}_j \mathbf{C}_j \mathbf{P}_j^- \mathbf{B}_j^T - \mathbf{W}_k^{-1}[\mathbf{P}_k^+ - \mathbf{P}_k](\mathbf{A}_k^{-1})^T \tag{3.65}$$

for $j = min\{k + l + 1, N - 1\}$

Equations (3.62)-(3.63) above are historically important, being the very earliest implementation of a fixed-lag smoother by Rauch (c1963) [26], but this was later shown to be numerically unstable [9]. These days the Biswas-Mahalanabis fixed-lag smoother (BMFLS) is usually implemented since this has guaranteed stability properties, and BMFLS is now the standard implementation for fixed-lag smoothing[9] (further discussed in detail in Chapter 6).

3.4 Summary

Two components must be involved in any model-based filtering problem, the filtering algorithm and the system dynamical model. The system dynamical model describes the behaviour of the quasi-periodic ECG signal and is discussed in Chapter 4. Since the dynamical model of ECG is nonlinear, the filtering algorithm adopts nonlinear Bayesian filters such as EKF and UKF. The EKF is a derivative of the well-known Kalman Filter that optimally estimates in the minimum mean square error sense. The UKF is a derivative-free alternative to the EKF, which results in better estimates than EKF if the dynamical model is highly nonlinear. Since the dynamical model considered in this thesis is highly nonlinear, the UKF is expected to exceed the EKF in denoising performance. Fixed-interval smoothers and fixed-lag smoothers are two types of Bayesian smoothers that are expected to generate better estimates than EKF and UKF, because these incorporate future measurements. From the previous two sections we have seen that the fixed-interval smoother

can only be implemented offline, whereas the fixed-lag smoother can be implemented online.

Chapter 4

ECG Dynamical Model

The seventeen-state dynamical model proposed in this thesis is a modification of the synthetic ECG model originally due to McSharry *et al* [19] and Semani *et al* [31]. McSharry *et al* proposed a dynamical model which is capable of generating a realistic ECG. According to both McSharry *et al* and Semani *et al*, the model has various free parameters for the operator to set to generate normal and abnormal ECGs. This model was then reformulated by Semani *et al.* in terms of polar coordinates, which are much more natural model coordinates than the Cartesian coordinates used by McSharry *et al.* To help with understanding the dynamical model proposed in this thesis we first summarize the dynamical models of McSharry *et al.* and Sameni *et al.* in Section 4.1.

4.1 Dynamical Modeling

The dynamical model proposed by McSharry *et al* [19] is described by three coupled, ordinary differential equations as follows

$$\begin{cases} \dot{x} = \rho\omega - \omega y \\ \dot{y} = \rho y + \omega x \\ \dot{z} = -\sum_{i\in\{P,Q,R,S,T\}} a_i \Delta\theta_i \exp(-\frac{\Delta\theta_i^2}{2b_i^2}) - (z - z_0) \end{cases} \tag{4.1}$$

in which x, y and z are the states that represent position in a three-dimensional (3-D) coordinate system. Here $\rho = 1 - \sqrt{x^2 - y^2}$, $\Delta\theta_i = (\theta - \theta_i) \mod 2\pi$, and $\theta = atan2(y, x)$ is the four quadrant arctangent of the elements of x and y that is bounded between $-\pi \leq$

Table 4.1: ECG Gaussian parameters proposed in [31]

Landmarks	P	Q	R	S	T
θ_i	$-\frac{\pi}{3}$	$-\frac{\pi}{12}$	0	$\frac{\pi}{12}$	$\frac{\pi}{2}$
a_i	1.2	5.0	30	-7.5	0.75
b_i	0.25	0.1	0.1	0.1	0.4

$atan2(y, x) \leq \pi$. The model generates a 3-D trajectory of the quasi-periodic ECG signal in a circular limit cycle. The parameter ω determines the angular velocity of the trajectory around the limit cycle. The dynamics of the state variable z are modelled using the sum of five Gaussian functions denoted by P, Q, R, S and T (Figure 4.1). Each Gaussian profile is located at a specific angular position, θ_i. The a_i and b_i correspond to the peak and variance of the Gaussian function. Typical values for these parameters are listed in Table 4.1 [31].

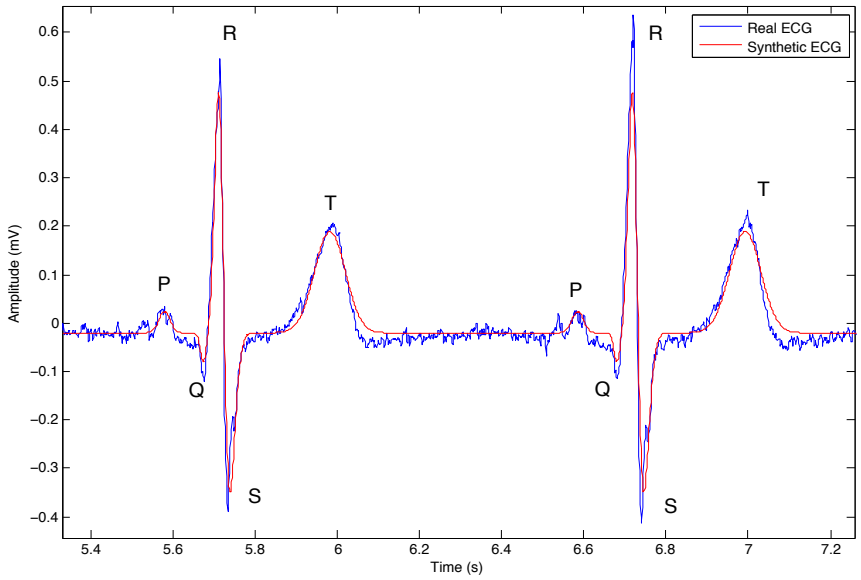

Figure 4.1: ECG signal portion from a normal sinus ECG record (blue) and the synthetic ECG generated by the dynamical model (red) [19].

The dynamics of this model can be imaged to be a 3-D trajectory that circles around a limit cycle illustrated in Figure 4.2, which deflects up and down as it approaches one

of the Gaussian functions. The initial value z_0 is a parameter which models the baseline wander phenomenon, which is a low amplitude frequency component. It can be removed by a low pass filter.

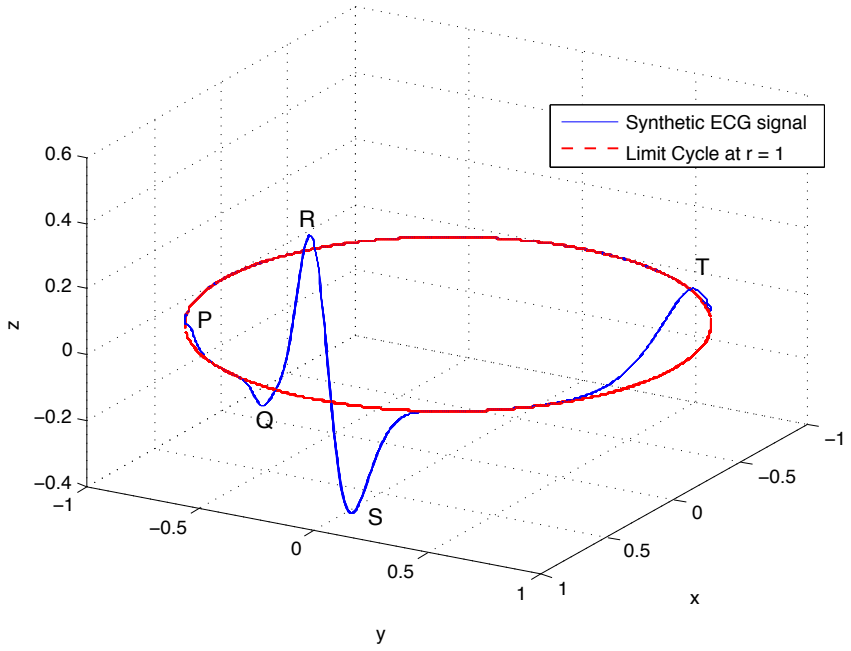

Figure 4.2: Illustrating circling synthetic ECG around the limit cycle.

Sameni *et al* [31] later proposed a slightly modified version of the preceding dynamical model, in which the states are transformed from the 3-D coordinate system (x, y, z) into polar form. In addition, Sameni *et al* replaced the a_i terms with

$$a_i = \frac{\alpha_i \omega}{b_i^2}, i \in \{P, Q, R, S, T\} \tag{4.2}$$

to better relate the model parameters with actual ECG recordings. Here the α_i are the peak amplitudes of each Gaussian function in millivolts. The b_i give the variance of each Gaussian function in radians and ω is the sampling frequency in Hz. These parameters are readily obtained from clinical ECG recordings.

The polar form representation due to Sameni [31] of McSharry's dynamical model is

then

$$\begin{cases} \dot{r} = r(1-r) \\ \dot{\theta} = \omega \\ \dot{z} = -\sum_{i\in\{P,Q,R,S,T\}} \frac{\alpha_i \omega}{b_i^2} \Delta\theta_i \exp(-\frac{\Delta\theta_i^2}{2b_i^2}) - (z - z_0) \end{cases} \tag{4.3}$$

The first equation in (4.3), which is the dynamics of r, represents the radial behaviour of the generated trajectory. The dynamics of r generates a stable limit cycle of $r = 1$ and an unstable limit cycle of $r = 0$; thus, for any initial value of r, the trajectory converges to $r = 1$. The r state, however, can be eliminated by realizing that the dynamics of r are not coupled with the other two states to become

$$\begin{cases} \dot{\theta} = \omega \\ \dot{z} = -\sum_{i\in\{P,Q,R,S,T\}} \frac{\alpha_i \omega}{b_i^2} \Delta\theta_i \exp(-\frac{\Delta\theta_i^2}{2b_i^2}) - (z - z_0) \end{cases} \tag{4.4}$$

Since the dynamical model is applied to the Kalman Filter, the discrete-form of (4.4) needs to be determined and is found by discretizing (4.4):

$$\begin{cases} \frac{\theta_{k+1}-\theta_k}{\delta} = \omega \\ \frac{z_{k+1}-z_k}{\delta} = -\sum_{i\in\{P,Q,R,S,T\}} \frac{\alpha_i \omega}{b_i^2} \Delta\theta_i \exp(-\frac{\Delta\theta_i^2}{2b_i^2}) - (z_k - z_0) \end{cases} \tag{4.5}$$

where δ is the sampling period of the ECG measurements, which is assumed to be small because the sampling frequency is usually high. By bringing δ over to the right-hand side and re-arranging terms, (4.5) becomes

$$\begin{cases} \theta_{k+1} = (\theta_k + \omega\delta) \mod (2\pi) \\ z_{k+1} = -\sum_{i\in\{P,Q,R,S,T\}} \delta\frac{\alpha_i \omega}{b_i^2} \Delta\theta_i \exp(-\frac{\Delta\theta_i^2}{2b_i^2}) + \underbrace{(1-\delta)z_k + \delta z_0}_{\approx z_k + \eta} \end{cases} \tag{4.6}$$

The modular operation is added to the dynamics of θ to limit the angular position of the trajectory between 0 and 2π. $(1-\delta)z_k + \delta z_0$ is approximated as $z_k + \eta$, where η is an additive noise which represents any inaccuracies in the model from the approximation. This approximation can be justified when the sampling period is small ($\delta << 1$). Therefore, the discrete-form of (4.4) turns out to be

$$\begin{cases} \theta_{k+1} = (\theta_k + \omega\delta) \mod (2\pi) \\ z_{k+1} = -\sum_{i\in\{P,Q,R,S,T\}} \delta\frac{\alpha_i \omega}{b_i^2} \Delta\theta_i \exp(-\frac{\Delta\theta_i^2}{2b_i^2}) + z_k + \eta \end{cases} \tag{4.7}$$

which is the same as equation (7) in Sameni *et al.* [31]. In (4.7), ω, α_i, θ_i and η are random variables and consider to be process noises.

4.2 Dynamical ECG Model Proposed in this Thesis

The dynamical equations proposed by Sameni *et al* in [31] have two states, θ and z. The parameters α_i, b_i and θ_i for each Gaussian function are fixed, where $i \in \{P, Q, R, S, T\}$. However, in clinical applications, the Gaussian parameters vary due to psychological and physiological effects in a patient. To better model the fluctuations in the Gaussian functions, we propose a first-order autoregression process to model α_i, b_i and θ_i with a mean nonlinearity $\bar{\alpha_i}$, $\bar{\theta_i}$ and $\bar{b_i}$ to limit the fluctuations. The fluctuations need to be limited because the fluctuations are known to be within physiologic limits. Outside the known physiologic limits indicate abnormalities in patients. The proposed dynamical ECG model in discrete-form is

$$\begin{cases} \theta_{k+1} = (\theta_k + \omega\delta) \mod (2\pi) \\ z_{k+1} = -\sum_{i\in\{P,Q,R,S,T\}} \delta \frac{\alpha_i \omega}{b_i^2} \Delta\theta_i \exp(-\frac{\Delta\theta_i^2}{2b_i^2}) + z_k + \eta \\ \alpha_{i_{k+1}} = \bar{\alpha_i} + \beta\{\alpha_{i_k} - \bar{\alpha_i}\}, i \in \{P, Q, R, S, T\} \\ b_{i_{k+1}} = \bar{b_i} + \kappa\{b_{i_k} - \bar{b_i}\}, i \in \{P, Q, R, S, T\} \\ \theta_{i_{k+1}} = \bar{\theta_i} + \phi\{\theta_{i_k} - \bar{\theta_i}\}, i \in \{P, Q, R, S, T\} \end{cases} \tag{4.8}$$

where $\bar{\alpha_i}$, $\bar{\theta_i}$ and $\bar{b_i}$ are the known mean values for α_i, θ_i and b_i, respectively. These are the *a priori* estimates of the expected Gaussian functions for the ECG signal, which can be set specifically for each patient to optimize the filter performance. As mentioned in Section 4.1, the dynamics of state z is modelled using the sum of five Gaussian functions. Therefore, α_i, b_i and θ_i comprise fifteen states, where $i \in \{P, Q, R, S, T\}$. In total, the proposed model has seventeen states. The auto-regression equations at (4.8) have three variables, β, ϕ and κ, to control the variation fluctuation. Having parameters β, κ and ϕ allows the model to better adjust to a patient's constantly changing waveforms.

4.3 Linearization of the Nonlinear Dynamic ECG Model

The dynamical model introduced by Sameni *et al* has two states, and, for the purpose of this thesis, is known as ECG2. The model proposed in the previous section is extended to seventeen states, which is known as ECG17. In both cases, when the models are applied on Bayesian filters it is necessary to derive the linearized equations involving Jacobian matrices.

4.3.1 Linearization of the ECG2 Model

ECG2 has the following states and process noise vectors:

$$\begin{aligned}\mathbf{x}_k &= \begin{bmatrix}\theta_k & z_k\end{bmatrix}^T \\ \mathbf{w}_k &= \begin{bmatrix}\alpha_P, ..., \alpha_T, b_P, ..., b_T, \theta_P, ..., \theta_T, \omega, \eta\end{bmatrix}^T\end{aligned}$$

Define the dynamics for θ_{k+1} and z_{k+1} from (4.7) as:

$$\begin{cases}\theta_{k+1} = F_1(\theta_k, \omega, k) = (\theta_k + \omega\delta) \mod (2\pi) \\ z_{k+1} = F_2(\theta_k, z_k, \omega, \alpha_i, \theta_i, b_i, \eta, k) = -\sum_{i\in\{P,Q,R,S,T\}} \delta \frac{\alpha_i\omega}{b_i^2}\Delta\theta_i \exp(-\frac{\Delta\theta_i^2}{2b_i^2}) + z_k + \eta\end{cases} \tag{4.9}$$

The linearized model of ECG2 with respect to the state variables x_k and z_k then involves the Jacobian matrices

$$\begin{aligned}\frac{\partial F_1}{\partial z_k} &= 0, \frac{\partial F_1}{\partial \theta_k} = \frac{\partial F_2}{\partial z_k} = 1 \\ \frac{\partial F_2}{\partial \theta_k} &= -\sum_{i\in\{P,Q,R,S,T\}} \delta\frac{\alpha_i\omega}{b_i^2}\left[1 - \frac{\Delta\theta_i^2}{b_i^2}\right]\exp\left(-\frac{\Delta\theta_i^2}{2b_i^2}\right)\end{aligned}$$

The linearized model with respect to the process noise states involves the further Jacobian matrices:

$$\begin{aligned}\frac{\partial F_1}{\partial \omega} &= \delta, \frac{\partial F_2}{\partial \eta} = 1 \\ \frac{\partial F_1}{\partial \alpha_i} &= \frac{\partial F_1}{\partial b_i} = \frac{\partial F_1}{\partial \theta_i} = \frac{\partial F_1}{\partial \eta} = 0 \\ \frac{\partial F_2}{\partial \alpha_i} &= -\delta\frac{\omega\Delta\theta_i}{b_i^2}\exp\left(-\frac{\Delta\theta_i^2}{2b_i^2}\right) \\ \frac{\partial F_2}{\partial b_i} &= 2\delta\frac{\alpha_i\omega\Delta\theta_i}{b_i^3}\left[1 - \frac{\Delta\theta_i^2}{2b_i^2}\right]\exp\left(-\frac{\Delta\theta_i^2}{2b_i^2}\right) \\ \frac{\partial F_2}{\partial \theta_i} &= \delta\frac{\alpha_i\omega}{b_i^2}\left[1 - \frac{\Delta\theta_i^2}{b_i^2}\right]\exp\left(-\frac{\Delta\theta_i^2}{2b_i^2}\right) \\ \frac{\partial F_2}{\partial \omega} &= -\sum_i \delta\frac{\alpha_i\omega}{b_i^2}\exp\left(-\frac{\Delta\theta_i^2}{2b_i^2}\right)\end{aligned}$$

4.3.2 Linearization of the ECG17 Model

The nonlinear dynamical model of the ECG with seventeen states proposed in this thesis has the following state vector and process noise vector:

$$\begin{aligned} \mathbf{x}_k &= \left[\theta_k, z_k, \alpha_P, ..., \alpha_T, b_P, ..., b_T, \theta_P, ..., \theta_T\right]^T \\ \mathbf{w}_k &= \left[\omega, \eta, \bar{\alpha_P}, ..., \bar{\alpha_T}, \bar{b_P}, ..., \bar{b_T}, \bar{\theta_P}, ..., \bar{\theta_T}\right] \end{aligned}$$

The dynamical equations for the seventeen states are define from (4.8) as:

$$\begin{cases} \theta_{k+1} = G_1\left(\theta_k, \omega, k\right) = \left(\theta_k + \omega\delta\right) \mod (2\pi) \\ z_{k+1} = G_2\left(\theta_k, z_k, \alpha_{i_k}, b_{i_k}, \theta_{i_k}, \eta, k\right) = -\sum_{i\in\{P,Q,R,S,T\}} \delta \frac{\alpha_i \omega}{b_i^2} \Delta\theta_i \exp(-\frac{\Delta\theta_i^2}{2b_i^2}) + z_k + \eta \\ \alpha_{P_{k+1}} = G_3\left(\alpha_{P_k}, \bar{\alpha_P}, k\right) = \bar{\alpha_P} + \beta\{\alpha_{P_k} - \bar{\alpha_P}\} \\ \vdots \\ \alpha_{T_{k+1}} = G_8\left(\alpha_{T_k}, \bar{\alpha_T}, k\right) = \bar{\alpha_T} + \beta\{\alpha_{T_k} - \bar{\alpha_T}\} \\ b_{P_{k+1}} = G_9\left(b_{P_k}, \bar{b_P}, k\right) = \bar{b_i} + \kappa\{b_{P_k} - \bar{b_P}\} \\ \vdots \\ b_{T_{k+1}} = G_{13}\left(b_{T_k}, \bar{b_T}, k\right) = \bar{b_i} + \kappa\{b_{T_k} - \bar{b_T}\} \\ \theta_{P_{k+1}} = G_{14}\left(\theta_{P_k}, \bar{\theta_P}, k\right) = \bar{\theta_P} + \phi\{\theta_{P_k} - \bar{\theta_P}\} \\ \vdots \\ \theta_{T_{k+1}} = G_{17}\left(\theta_{T_k}, \bar{\theta_T}, k\right) = \bar{\theta_T} + \phi\{\theta_{T_k} - \bar{\theta_T}\} \end{cases} \tag{4.10}$$

The linearized state-space model with respect to the states involves the following Jacobian

matrices (all the Jacobian matrices that are equal to zero are omitted):

$$
\begin{aligned}
\frac{\partial G_1}{\partial \theta_k} &= 1, \frac{\partial G_2}{\partial z_k} = 1 \\
\frac{\partial G_2}{\partial \theta_k} &= -\sum_{i \in \{P,Q,R,S,T\}} \delta \frac{\alpha_i \omega}{b_i^2} \left[1 - \frac{\Delta\theta_i^2}{2b_i^2}\right] \exp\left(-\frac{\Delta\theta_i^2}{2b_i^2}\right) \\
\frac{\partial G_2}{\partial \alpha_{i_k}} &= -\delta \frac{\omega}{b_i^2} \Delta\theta_i \exp\left(-\frac{\Delta\theta_i^2}{2b_i^2}\right) \\
\frac{\partial G_2}{\partial b_{i_k}} &= -2\delta \frac{\alpha_i \omega}{b_i^3} \Delta\theta_i \left[1 - \frac{\Delta\theta_i^2}{2b_i^2}\right] \exp\left(-\frac{\Delta\theta_i^2}{2b_i^2}\right) \\
\frac{\partial G_2}{\partial \theta_{i_k}} &= \delta \frac{\alpha_i \omega}{b_i^2} \left[1 - \frac{\Delta\theta_i^2}{2b_i^2}\right] \exp\left(-\frac{\Delta\theta_i^2}{2b_i^2}\right) \\
\frac{\partial G_3}{\partial \alpha_{P_k}} &= \frac{\partial G_4}{\partial \alpha_{Q_k}} = \frac{\partial G_5}{\partial \alpha_{R_k}} = \frac{\partial G_6}{\partial \alpha_{S_k}} = \frac{\partial G_7}{\partial \alpha_{T_k}} = 1 \\
\frac{\partial G_8}{\partial b_{P_k}} &= \frac{\partial G_9}{\partial b_{Q_k}} = \frac{\partial G_{10}}{\partial b_{R_k}} = \frac{\partial G_{11}}{\partial b_{S_k}} = \frac{\partial G_{12}}{\partial b_{T_k}} = 1 \\
\frac{\partial G_{13}}{\partial \theta_{P_k}} &= \frac{\partial G_{14}}{\partial \theta_{Q_k}} = \frac{\partial G_{15}}{\partial \theta_{R_k}} = \frac{\partial G_{16}}{\partial \theta_{S_k}} = \frac{\partial G_{17}}{\partial \theta_{T_k}} = 1
\end{aligned}
$$

In the same manner, the linearized equations with respect to the process noise states involves the following Jacobian matrices:

$$
\begin{aligned}
\frac{\partial G_1}{\partial \omega} &= \delta, \frac{\partial G_2}{\partial \eta} = 1 \\
\frac{\partial G_2}{\partial \omega} &= -\sum_i \delta \frac{\alpha_i \Delta\theta_i}{b_i^2} \exp\left(-\frac{\Delta\theta_i^2}{2b_i^2}\right) \\
\frac{\partial G_3}{\partial \bar{\alpha_P}} &= \frac{\partial G_4}{\partial \bar{\alpha_Q}} = \frac{\partial G_5}{\partial \bar{\alpha_R}} = \frac{\partial G_6}{\partial \bar{\alpha_S}} = \frac{\partial G_7}{\partial \bar{\alpha_T}} = (1 - \beta) \\
\frac{\partial G_8}{\partial \bar{b_P}} &= \frac{\partial G_9}{\partial \bar{b_Q}} = \frac{\partial G_{10}}{\partial \bar{b_R}} = \frac{\partial G_{11}}{\partial \bar{b_S}} = \frac{\partial G_{12}}{\partial \bar{b_T}} = (1 - \kappa) \\
\frac{\partial G_{13}}{\partial \bar{\theta_P}} &= \frac{\partial G_{14}}{\partial \bar{\theta_Q}} = \frac{\partial G_{15}}{\partial \bar{\theta_R}} = \frac{\partial G_{16}}{\partial \bar{\theta_S}} = \frac{\partial G_{17}}{\partial \bar{\theta_T}} = (1 - \phi)
\end{aligned}
$$

4.4 Observation Matrix

Having derived the state-space model of the ECG signal for ECG2 and ECG17, the measurements must be related to the states. One obvious measurement is the noisy signal in the ECG measurement. Before the noisy signal is used for the Kalman filter, it must undergo a pre-processing stage to remove any baseline wander to improve the overall denoising performance. The characteristics of typical noise processes have been discussed in Section 2.2 and the filtering framework will be discussed in Chapter 5. For all the results in this thesis, we assumed the measurement noise to be additive Gaussian noise. In most applications, assuming measurement noise to be white Gaussian is sufficient.

In addition to the noisy ECG measurement, a phase assignment technique is used to add phase θ into the measurement vector. The phase assignment technique assigns all the R peaks to $\theta = 0$. Thus the ECG measurements between two consecutive R peaks then correspond to values of θ in the range between $-\pi$ and π [31]. Figure 4.3 illustrates the phase assignment approach. The main purpose of the phase assignment is to allow the KF to synchronize the trajectory with the reference noisy signal. The heart rate varies from one patient to another, and therefore the dynamic of the ECG circles around the limit cycle at various angular speeds which depend on the particular patient. Allowing phase assignment permits fast adaptation to the heart rate of the subject. This phase assignment approach has been previously used for the synchronization of adaptive filters for event-related signals [14].

Thus, the noisy ECG measurements, y_k, and assigned phases, ψ_k, are the observable measurements. The observation matrix is constructed for ECG2 and ECG17 [31]:

$$\begin{aligned} \psi_k &= \theta_k + u_k \\ y_k &= z_k + v_k \end{aligned}$$

where v_k and u_k represent the (white Gaussian) measurement noise. There are many states in ECG17 that have no impact on the measurement and are considered as hidden states in (4.11). The states in the observation matrix are modelled as a random walk where the variance is controlled by the variance of the corresponding process noise term, v_k and u_k. The process noise terms are collectively represented in the observation noise covariance matrix R_k. The variance of process noise represents the degree of reliability of a single observation. If the noise variance for a parameter is small, the observed measurement is assumed to be a precise measurement, and the KF relies heavily on this measurement. If the noise variance for a parameter is large, the KF tends to follow the model's dynamics rather than using the observation. That is, a large variance indicates a small signal-to-noise

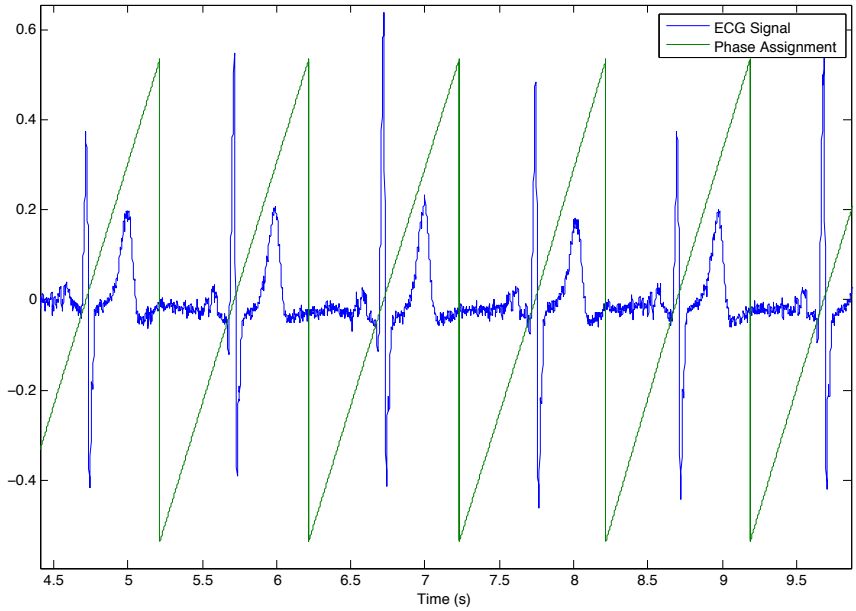

Figure 4.3: Demonstrating the idea of phase assignment. The phase assignment assignments values between $-\pi$ and π. The R peaks are assigned 0 as the reset points.

ratio. The tradeoff between these two extremes must be made by a careful selection of the noise variance by the operator.

Chapter 5

Model-Based Denoising Framework

5.1 Introduction

This chapter focuses on the denoising framework that allows raw ECG signals to be processed online. This framework consists of two phases: the initialization phase and the filtering phase. The initialization phase processes raw ECG traces for a fixed duration to properly initialize parameters for the Bayesian filter. The most important parameters, such as the process noise covariance matrix $\mathbf{Q}_k$ and the measurement covariance matrix $\mathbf{R}_k$, are initialized during this phase. As previously mentioned, the initialization of these matrices $\mathbf{Q}_k$ and $\mathbf{R}_k$ can have a significant effect on the performance of the Bayesian filter. Once all the parameters in the Bayesian filter are initialized, the framework goes into the filtering phase where raw ECG signals are presented to the framework to screen out any noise. The experimental results are discussed in Section 5.4.

5.2 Initialization Phase

The initialization phase systematically estimates all user-specified model parameters for the Bayesian filter, such as $\mathbf{R}_k$, $\mathbf{Q}_k$, $\mathbf{x}_0$ and $\mathbf{P}_0$ by using information gathered from the ECGs. In essence, the procedure is divided into three sequential stages by their functionalities: the preprocessing stage, the feature extraction stage and the filter parameter estimation stage. The preprocessing stage focuses on the reduction of the baseline drift in raw ECG signals for accurate feature extraction in the feature extraction stage. After baseline drift is removed, the parameters of the five Gaussian kernels, α_i, b_i and θ_i, are optimally selected to

fit the subject's ECG waveform by using curve fitting optimization methods in the feature extraction stage. Once the Gaussian parameters are defined, these parameters are used to estimate filter parameters to initialize the Bayesian filter. The model parameter selection procedure to be described in this chapter is similar to the approach of Sameni *et al* [31].

5.2.1 Preprocessing

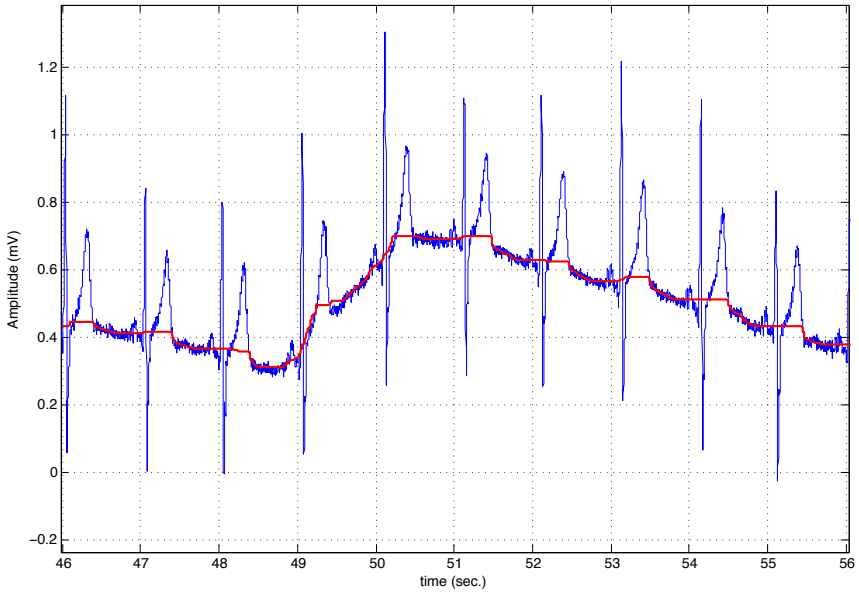

Figure 5.1: ECG traces with baseline drifting (blue) where the isoelectric line drifts randomly up and down. The two-stage moving window median filter determines and tracks the isoelectric line (red).

Preprocessing is the first stage of the procedure proposed in this thesis. This stage removes any noise interference that could impact performance at the feature-extraction stage. As discussed in Section 2.2, there are four major sources of interference which contaminate a clean ECG signal. Among these four sources of interference it is typically the case that respiration baseline wandering, electrode motion artifacts, and muscle artifacts are the most problematic because each of them can cause baseline drift in the isoelectric line. The remaining source of interference is power line interference, which induces low frequency white Gaussian noise. The ECG traces in Figure 5.1 illustrate the upward drift and downward drift of the isoelectric line due to baseline drift. For a typical clean

and normal ECG signal, the isoelectric line remains constant to represent the periods in the cardiac cycle when there are no currents flowing towards either the positive or negative ends of the the ECG lead. If baseline drift is not reduced prior to the feature extraction stage then erroneous detection of R-peaks is possible due to sudden upward or downward changes in the amplitudes of the R-peaks. Proper R-peak detection is critical for the phase assignment technique, which permits the Bayesian filter to synchronize the dynamical model trajectory with the noisy signal. As a result, it is necessary to suppress baseline wandering in the preprocessing stage.

In order to reduce baseline drift, a two-stage moving window median (MWM) filter with 300 ms and 600 ms in window lengths is adopted. The MWM filter uses a smoothing window that replaces each data point with the median of the neighbouring data points defined within a fixed window length. The idea used in the MWM filter is rather similar to the moving average filter that replaces the data point with the average of the neighbouring data points. In terms of performance, the MWM filter outperforms the moving average filter because it preserves the outliers, such as the R-peaks, which are more likely to pass through the MWM filter without being distorted. The two-stage MWM filter has two moving window median filters. The first MWM filter has a narrow window length which focuses removing baseline drifting on the QRS complex. The second MWM filter has a wider window length which removes baseline drifting in the P and T waves. In Figure 5.1, the two-stage MWM filter estimates the baseline drift in the ECG. Once the baseline drift is estimated, it is subtracted from the input ECG dataset to correct the isoelectric line. Figure 5.2 demonstrates the result of baseline drift removal, where the isoelectric line is corrected and centered at $0mV$. The source code of the implementation for the two-stage MWM is derived from the OSET (Open-Source Electrophysiological Toolbox) [29].

Among the four main types of interference, the two-stage MWM filter does not reduce the sinusoidal power line interference, because the baseline drift removal only shifts the baseline of the ECG signal. The power line interference contains the high frequency components and the low frequency components. The high frequency component can be removed easily, because it does not interfere with any cardiac frequency components. A high pass filter at 50Hz is applied after the baseline drift removal to eliminate the high frequency noise component. The lower frequency noise components of the power line interference are mixed with the cardiac frequency components; the removal of these low frequency components is left to the Bayesian filter. Once the raw ECG signal has been subject to baseline drift removal and high pass filtering, the resulting signal is ready for feature extraction. We discuss this in the next section.

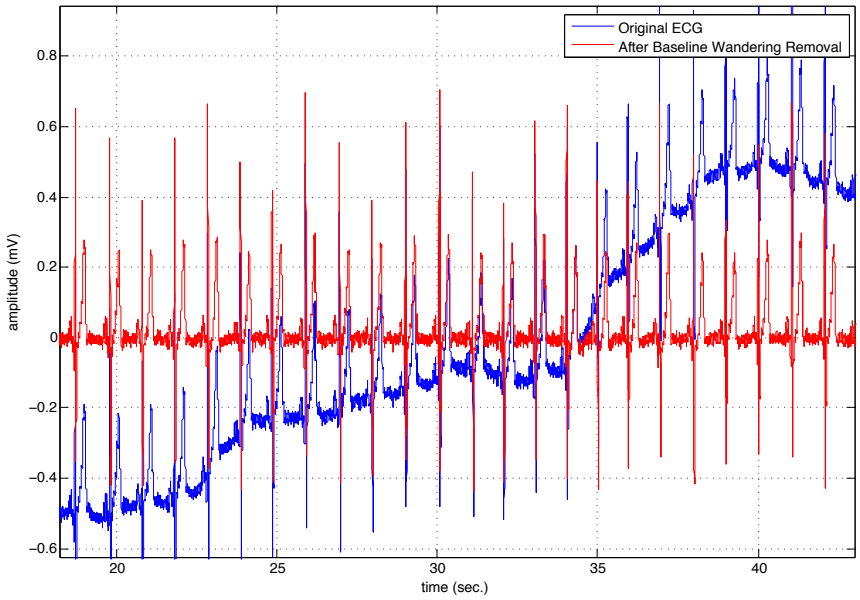

Figure 5.2: Use of the two-stage MWM filter to remove baseline drift from ECGs in blue. The resulting ECGs after the two-stage MWM filter in red, where the isoelectric line centres at 0mV.

5.2.2 Feature Extraction

The goal of the feature extraction stage is to extract information and features from the ECGs to initialize the parameters for the Bayesian filter, such as the five Gaussian functions, the process noise covariance matrix and the measurement noise covariance matrix. The ECG feature extractor first detects all R-peaks in the signal, which are required for constructing phase values θ for the measurement vector. The Bayesian filter uses the phase θ measurements to synchronize the trajectory of the model with the reference signal. Phase synchronization permits fast adaptation of the model to the slow-changing heart rate of the subject. In other words, the phase measurements act as a guide for the dynamical model to follow through the limit cycle. Thus, an accurate detection of the R-peaks is critical for successful synchronization between the measurement and the model. For the detection of the R-peak, a classic Pan-Tompkins R-peak detector algorithm is applied [24]. This is a real-time R-peak detector algorithm based on an analysis of the slope, amplitude, and width of the QRS complexes. The algorithm includes a series of filters and calculations which perform lowpass, high pass, derivative, squaring, integration , adaptive thresholding, and search procedure to successfully find the R-peaks (Figure 5.3). Once all the R-peaks

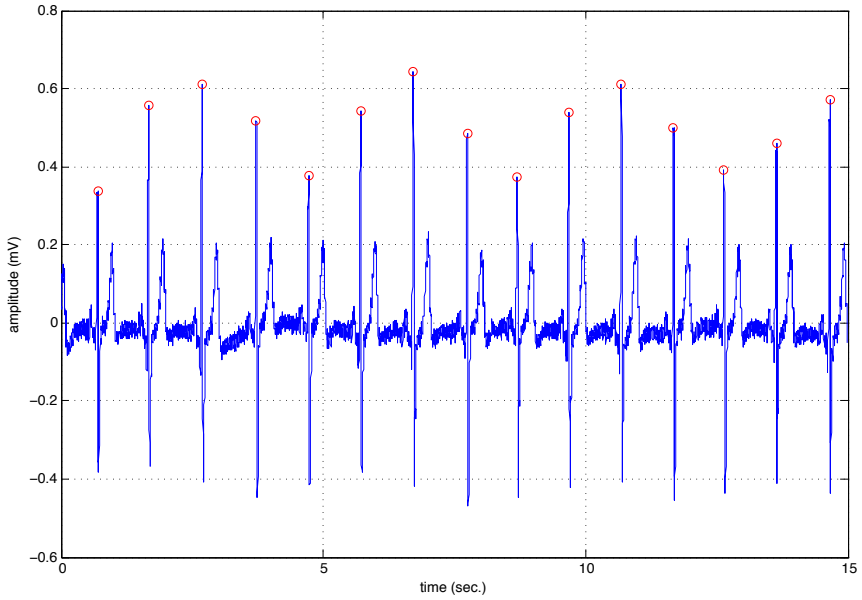

Figure 5.3: Pan-Tompkins R-peak detector used to extract all R-peaks (red dots) in the ECG signal

are detected, the phase assignment technique is applied to assign all the R-peaks to have $\theta = 0$ and measurements lying between two consecutive R-peaks are assign values between $-\pi$ and π. Figure 4.3 illustrates the phase assignment approach.

Plotting the noisy ECG trace versus the periodic phase assigned to each sample in polar coordinates creates a phase-wrapped ECG waveform (Figure 5.4). Once the phase-wrapped waveform is created, it is possible to calculate the mean and variance of the phase-wrapped ECG waveform. The mean and variance waveform are denoted by $\overline{ECG}\,(\theta)$ and $\sigma_{ECG}(\theta)$, respectively. To calculate $\overline{ECG}\,(\theta)$ and $\sigma_{ECG}(\theta)$, the mean and variance value at each sample index is calculated for the whole waveform (Figure 5.5). Once $\overline{ECG}\,(\theta)$ and $\sigma_{ECG}(\theta)$ have been determined, the optimal estimates of the model parameters, α_i, b_i and θ_i, in the minimum mean squared error (MMSE) sense are determined by a least-squares approach, which finds all of the model parameters to optimally fit $\overline{ECG}\,(\theta)$.

5.2.3 Bayesian Filter Parameter Estimation

Prior to running the Bayesian filter, the initial values of the model parameters $\mathbf{x}_o$, the process noise covariance matrix $\mathbf{Q}_k$, the measurement noise covariance matrix $\mathbf{R}_k$, and the

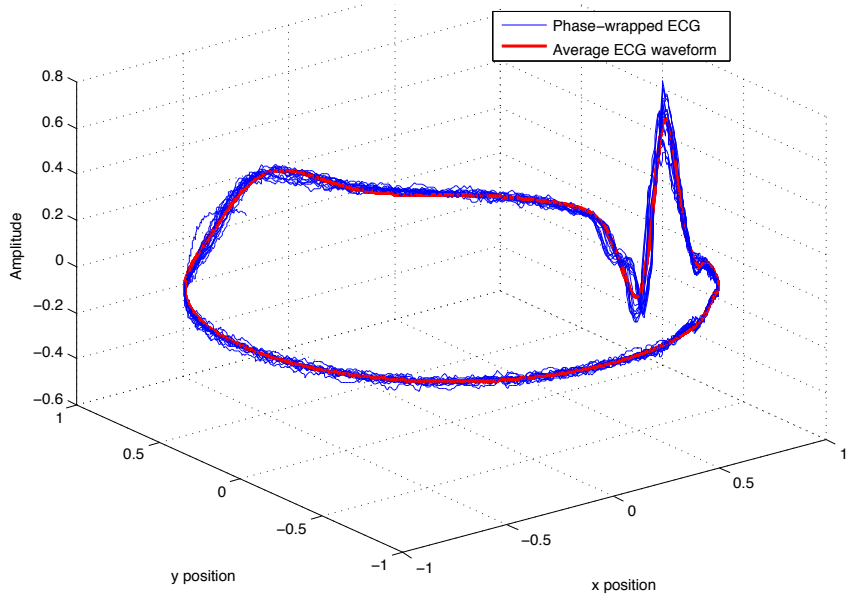

Figure 5.4: After phase values are assigned to each ECG measurement, ECG measurements traverse along the limit cycle in blue to create the phase-wrapped ECG. Using the phase-wrapped ECG to approximate the mean ECG waveform in red.

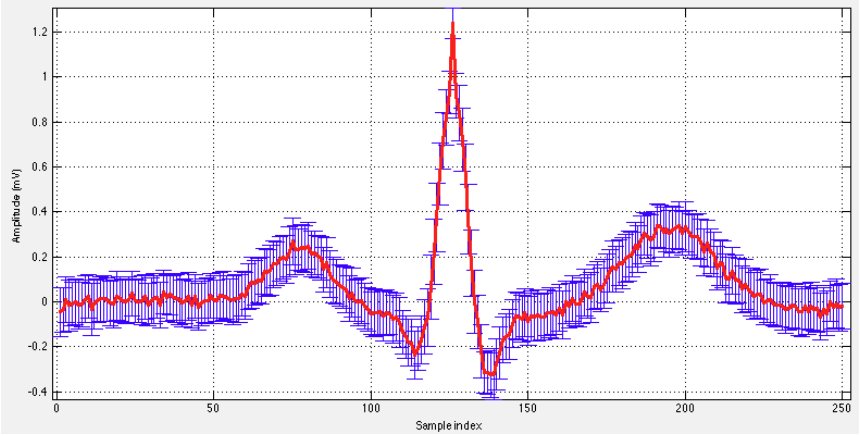

Figure 5.5: Calculating the mean and variance at each sample index to determine the mean ECG waveform, $\overline{ECG}\,(\theta)$, in red and the variance ECG waveform, $\sigma_{ECG}(\theta)$, in blue.

estimation covariance matrix $\mathbf{P}_0$ need to be determined.

Determining Process Noise Covariance Matrix

The process noise covariance matrix for ECG2 is defined as a diagonal matrix

$$\begin{aligned} \mathbf{Q}_{k,ECG2} &= E\left[\mathbf{w}_k \mathbf{w}_k^T\right] \\ &= diag\left(\sigma_{\alpha_P}^2, ..., \sigma_{\alpha_T}^2, \sigma_{b_P}^2, ..., \sigma_{b_T}^2, \sigma_{\theta_P}^2, ..., \sigma_{\theta_T}^2, \sigma_{\omega}^2, \sigma_{\eta}^2\right) \end{aligned} \tag{5.1}$$

where each of the elements in the diagonal matrix is the variance of a process noise variable. The elements are in a diagonal matrix because the noise sources are assumed to be uncorrelated with each other.

The initial values of α_i, b_i and θ_i are set to the five Gaussian kernels in $\overline{ECG}(\theta)$. The variances for the parameters of the five Gaussian functions, σ_{α_i}, σ_{b_i} and σ_{θ_i}, are estimated by finding the amount of deviation from the mean to stay within the upper and lower bounds of $\overline{ECG}(\theta) + \sigma_{ECG}(\theta)$ and $\overline{ECG}(\theta) - \sigma_{ECG}(\theta)$ [31]. This problem reduces to a nonlinear least-squares problem which involves finding the maximum and minimum values for each parameter to stay within the bounds. In a more straightforward case, the variances for the parameters of the five Gaussian functions are estimated between 10% to 20% away from the expected value [31].

The angular frequency of the model, ω, is assigned the mean value $\overline{\omega} = 2\pi/T_{RR}$, where T_{RR} is the expected RR interval between heart beats. T_{RR} is determined during the feature extraction stage. The variance of ω is the standard deviation of the RR-interval between heart beats $\sigma_{\overline{\omega}}$. It is important to find T_{RR} using a set of ECG waveforms without any abnormalities. Sometimes, the PR-interval and QT-interval are known to change under varying autonomic tone and heart rate, which can cause ω to vary with time [31]. In real situations, ω is expected to vary slowly over time. In the proposed dynamical model, we did not incorporate the dynamics of ω into the model and used phase assignment technique to synchronize the trajectory of the model with the time-varying heart rate of the patient. The dynamics of ω can be further studied to be incorporated into the proposed dynamical model.

Lastly, η is used to represent the imperfections of the dynamic model that might influence the estimates. From now on η is assumed to be a zero-mean Gaussian random variable with the variance set to $\sigma_\eta = E\left[\sigma_{ECG}(\theta)\right]$ between the end of the T wave to the beginning of the next P wave. It could also be set to the $E\left[\sigma_{ECG}(\theta)\right]$ between the end of the P wave and the Q point [31]. These two segments are selected because few abnormalities and baseline drift occur during these segments [31].

The process noise covariance matrix $\mathbf{Q}_k$ for ECG17 is initialized in the same manner

as the process noise covariance matrix for ECG2; it is defined as

$$\begin{aligned} \mathbf{Q}_{k,ECG17} &= E\left[\mathbf{w}_k \mathbf{w}_k^T\right] \\ &= diag\left(\sigma^2_{\overline{\alpha}_P}, ..., \sigma^2_{\overline{\alpha}_T}, \sigma^2_{\overline{b}_P}, ..., \sigma^2_{\overline{b}_T}, \sigma^2_{\overline{\theta}_P}, ..., \sigma^2_{\overline{\theta}_T}, \sigma^2_{\omega}, \sigma^2_{\eta}\right) \end{aligned} \tag{5.2}$$

The variances of $\overline{\alpha_i}$, $\overline{b_i}$ and $\overline{\theta_i}$ are denoted by $\sigma_{\overline{\alpha}_i}$, $\sigma_{\overline{b}_i}$ and $\sigma_{\overline{\theta}_i}$ which account for the error in the estimation of the mean phase-wrapped ECG waveform $\overline{ECG}(\theta)$ from beat-to-beat, since $\overline{ECG}(\theta)$ is an estimated function using the least-squares approach. For simplicity, the error in estimation is assumed to be small; thus, $\sigma_{\overline{\alpha}_i}$, $\sigma_{\overline{b}_i}$ and $\sigma_{\overline{\theta}_i}$ are initialized to 5% of the nominal values. The variance of η and ω are the same as ECG2.

Determining the Measurement Noise Covariance Matrix

The measurement noise covariance matrices for ECG2 and ECG17 are identical, and involve two kinds of measurement noise: σ_{u_k} and σ_{v_k}, where u_k is the phase assignment noise and v_k is ECG measurement noise. Finding the possible sources of error associated with the phase assignment technique is required to determine σ_{u_k} and σ_{v_k}. Two possibilities exist. The first possibility is sampling error, which arises when the location of the actual R-peak is not detected precisely. The second possibility is the measurement noise that arises from additive measurement noise, which causes false detection of R-peaks. The first possibility is a noise which is included in the covariance matrix, whereas the second possibility is a definite challenge to model accurately. A precise study of this second possibility requires the amplitude noise to be related to the phase error. For simplicity, the phase assignment error is the only one considered in this thesis, and a reliable R-peak detector with zero R-peak mis-detection is assumed. To model the imprecision of the sampling time, the detection of R-peaks is modelled by a random variable that is uniformly distributed between two consecutive samples. Since one ECG cycle is equivalent to 2π, the angular range of one sample is $\omega\delta$, where δ is the sampling period and ω is the angular frequency. Therefore, u_k is uniformly distributed between $-\omega\delta/2$ and $+\omega\delta/2$. Then, $E[u_k^2] = (\omega\delta)^2/12 = \sigma^2_{u_k}$ [31].

The variance of measurement noise is estimated from the power of the deviations of the phase-wrapped ECG waveform, $\sigma^2_{ECG}(\theta)$. It can also be estimated from the partial segment of $\sigma^2_{ECG}(\theta)$ from the end of a T wave to the beginning of the next P-wave. This follows because the segment from the end of the T wave to the beginning of the next P wave has no late potentials or baseline wander.

Table 5.1: Parameters of the Initial Estimate Covariance Matrix $\mathbf{P}_0$ for ECG2 and ECG17

Parameter	Value
θ_k	2π
z_k	10% of the maximum ECG peak
α_i	10% of the Gaussian kernel peaks
b_i	10% of the Gaussian kernel width
θ_i	10% of Gaussian kernel center

Determining Initial State Values and Estimate Covariance Matrix

For ECG2, the initial estimate of $\hat{\mathbf{x}}_0$ is set to the first measurement from the ECG recording and the associated phase assigned value. Since ECG17 has fifteen more states than ECG2, the initial estimates of α_i, b_i and θ_i use the initial value from the Gaussian kernels obtained from $\overline{ECG}(\theta)$. The initial estimate of the covariance matrix $\mathbf{P}_0$ is a diagonal matrix and is assigned the values in Table 5.1. The initial estimates of $\hat{\mathbf{x}}_0$ and $\mathbf{P}_0$ have no effect on the performance of the Bayesian filter because the estimate of state $\hat{\mathbf{x}}_k$ becomes independent of the initial estimates for $\hat{\mathbf{x}_0}$ and $\mathbf{P}_0$ as k increases [9]. There is no effect because the state vector update, the Kalman gain, and error covariance equations for the extended Kalman filter form an asymptotically stable system. When given an inaccurate selection of $\hat{\mathbf{x}_0}$ and $\mathbf{P}_0$, the the system requires more k steps to reach the asymptotically stable state, which affects the denoising performance during these steps. Thus, a proper and accurate selection of $\mathbf{x}_0$ and $\mathbf{P}_0$ can provide effective denoising performance even at the start of the filtering stage. If the filtering stage is expected to run for long duration however, which is expected in hospital settings, then inaccurate selection of $\hat{\mathbf{x}_0}$ and $\mathbf{P}_0$ have little or no effect on the performance of the denoising system over the long term.

5.3 Signal Denoising Phase

Once the user-specified parameters are initialized for the Bayesian filter, the framework starts processing the noisy ECG recordings by going through the stages that we have already discussed. First, any baseline drift and power line noise are removed in the preprocessing stage, similar to the preprocessing stage discussed in Section 5.2.1. In the feature extraction stage, R-peaks are determined and phase values are assigned in real-time by the Pan-Tompkins algorithm and the phase assignment technique. Once the phase value is assigned to the ECG measurement, the noise is filtered by the Bayesian filter.

5.4 Experimental Setup

To study the performance of the proposed ECG17 model, the model is tested with two standard data sets obtained from PhysioBank [8]: MIT-BIH normal sinus rhythm database (DB1) [23] and the MIT-BIH noise stress test database(DB2) [22] used in the experiment. DB1 is composed of eighteen different subjects with no significant sign of arrhythmia and the data are recorded at a sampling frequency of 128 Hz. DB2 has a set noise data of an electrode motion artifact, respiration baseline wander, and muscle artifacts that can be added to clean signals to generate noisy signals with baseline drift. The noise data are sampled at a sampling frequency of 360 Hz.

In the experimental setup, one minute of low-noise segments is manually selected from each of the subjects . Segments from DB1 are injected with various types of noise, such as white noise, coloured noise and muscle artifacts with various SNRs. White noise and coloured noise are manually generated using a noise generation method discussed in Section 5.4.1. The non-stationary noise from muscle artifacts is taken from real muscle artifacts recorded in DB2. Note: the noise data in DB1 are resampled to 128 Hz in order to match the sampling frequency of the patient data in DB1.

To ensure consistency of the results, the entire procedure is repeated over 200 ECG segments for each subject in the DB1. Since there are eighteen different subjects in DB1, a different set of noise is generated each time. The notion of SNR improvement is used to measure the filtering performance. This is defined as the output SNR of the filter minus the input SNR, in decibels, that is

$$SNR_{impr} = SNR_{output} - SNR_{input} = 10log\left(\frac{\sum_i |x_n(i) - x(i)|^2}{\sum_i |x_d(i) - x(i)|^2}\right) \tag{5.3}$$

Here x denotes the clean ECG, x_d is the de-noised signal and x_n represents the noisy ECG. The SNRs are calculated over the whole filtered segment.

Bayesian filters, such as the EKF, UKF, fixed-lag smoother and fixed-interval smoother are tested and compared in terms of SNR improvement. The implementations of the EKF and UKF use the EKF/UKF Toolbox[10]. The parameters are initialized to $\beta = 0$, $\alpha = 1$ and $\kappa = 0$ for the UKF, which are the optimal selections for the system with a Gaussian input noise [30]. The implementations of the fixed-lag smoother uses the Biswas-Mahalanabis Fixed-Lag Smoother (BMFLS) [9]. BMFLS is essentially a conventional Kalman filter using an augmented state vector, which remembers the successive values of the system state vector over a discrete time window of fixed width. The fixed width of the window determines the amount of lag in the filter. Figure 5.6 from [9] illustrates the idea of BMFLS.

Through the experiment, the fixed-lag smoother sets the width of the lag window to thirty steps ($l = 30$) which is equivalent to a window length of 234 ms. This is the amount of delay in filtering operation, which is near real-time.

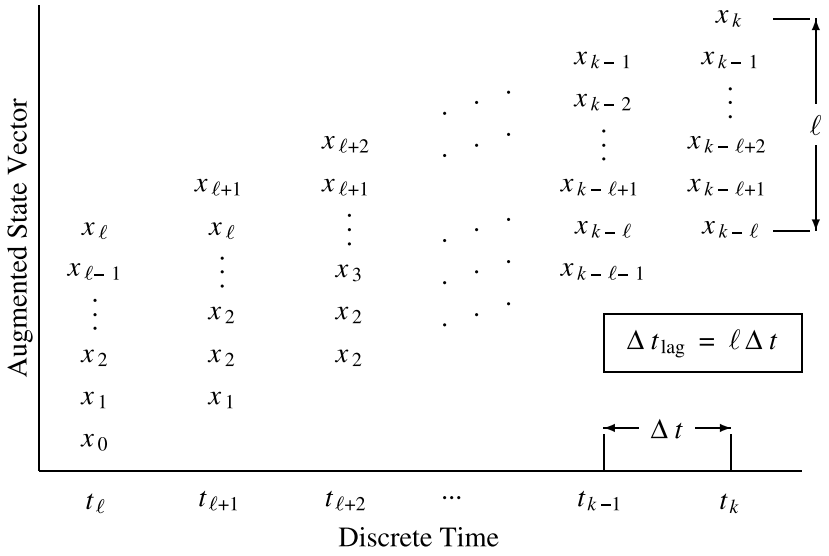

Figure 5.6: Miswas-Mahalanabis augmented state vector where $l\Delta t$ is the amount of the time lag and l is the number of lagged steps [9].

The implementation of the fixed-interval smoother implements the Rauch-Tung-Striebel two-pass smoother, which is the fastest fixed-interval smoother in terms of computation [9]. All the implementations are coded in Matlab on a 2.6 GHz Intel Core i7 computer with 16 GB RAM. The running time of the algorithm is not studied in the thesis, although it is essential this be addressed for online applications.

5.4.1 Noise Generation

White noise is mathematically defined to have a flat power spectral density over all frequencies. Noise from the ECG is usually not white noise and have non-flat spectral densities that decrease in power at higher frequencies, which makes the noise "colour" in the frequency spectrum. Coloured noise is a signal with a frequency spectrum such that the power spectral density decreases monotonically with frequency[31]:

$$S(f) \propto \frac{1}{f^{\beta}} \tag{5.4}$$

where f is the frequency of the signal and β determines the noise colour. The spectrum corresponds to white noise when $\beta = 0$, and corresponds to pink noise when $\beta = 1$. The generation of the noise uses the noise generation function provided in the OSET toolbox [29].

5.5 Results and Discussion

In Figure 5.7(a) and Figure 5.7(b) results of EFK-filtering based on ECG17 and ECG2 are illustrated. ECG2 and ECG17 remove most of the noise with mean SNR improvement of 9.28 dB and 9.78 dB, respectively. The ECG17 model gives better filtering than ECG2 around the transition from the end of T wave to the beginning of the next P wave. In addition, the ECG17 model tracks the ECG segment with less overshoot around the QRS complex than ECG2. To better appreciate the slight improvement of the ECG17 model over the ECG2 model, Figure 5.8 shows the SNR improvement for both mean and standard deviation in SNR improvement of ECG17 and ECG2 over various input noise variances in decibels using EKF. ECG17 outperforms ECG2 in terms of the mean SNR improvement as well as the standard deviation in SNR improvements. In other words, ECG17 is more robust to data variations in patients.

As previously mentioned, four types of filters are implemented (EKF, UKF, fixed-interval smoother and fixed-lag smoother) and compared in terms of SNR improvement (See Figure 5.9). Among the four Bayesian filters, fixed-interval smoother has the best performance and EKF has the worst performance. As mentioned in Section 3.2.4, the UKF is expected to outperform the EKF because it does not require the calculation of Jacobian matrices, which is clear in Figure 5.11. From Figure 5.11 one sees that the UKF performed better around the sharp turning points because the calculations of the Jacobian matrices for EKF at rapidly changing regions, assuming the sampling rate is low, may cause an increase in the values of the covariance matrix $\hat{P}_{k+1}^{-}$. With increasing value in $\hat{P}_{k+1}^{-}$, the EKF relies less on the dynamics of the system and tends to follow the noisy measurement signal. Since the dynamics of ECG2 and ECG17 are quite nonlinear around QRS, this suggests that UKF is more robust than EKF. The sampling rate is an important factor for the EKF around rapidly changing regions. If the sampling rate is sufficiently high, the dynamics of the system behave in a quasi-linear fashion because the time step between samples is sufficiently small. As a result, the Taylor series approximate error is significantly reduced.

The fixed-interval smoother and the fixed-lag smoother have similar performance, where the lines of fixed-interval smoother and fixed-lag smoother in Figure 5.9 overlap. The fixed-

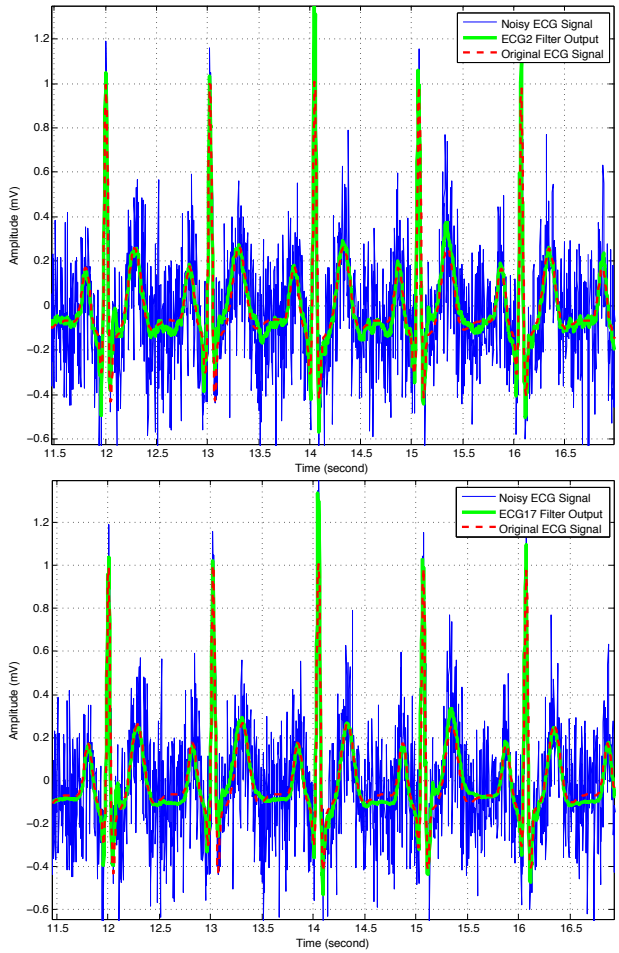

Figure 5.7: (a) The result of the de-noising filter using the ECG2 model with EKF. (b) The result of the de-noising filter using the ECG17 model with the EKF. Both results use ECG recordings from DB1 with 0dB white Gaussian noise.

interval smoother, however, performed somewhat better than fixed-lag smoother, which is to be expected. The fixed-interval smoother provides estimates by considering all past and future estimates, whereas the fixed-lag smoother considers all estimates within the fixed-sized window. If the size of the window is extended to infinity, the fixed-lag smoother is expected to give the same results as the fixed-interval smoother. Figure 5.12, demonstrates this result where the mean SNR improvement converges to an upper bound. A lag window of thirty steps ($l = 30$) gives approximately 95% of the optimal results.

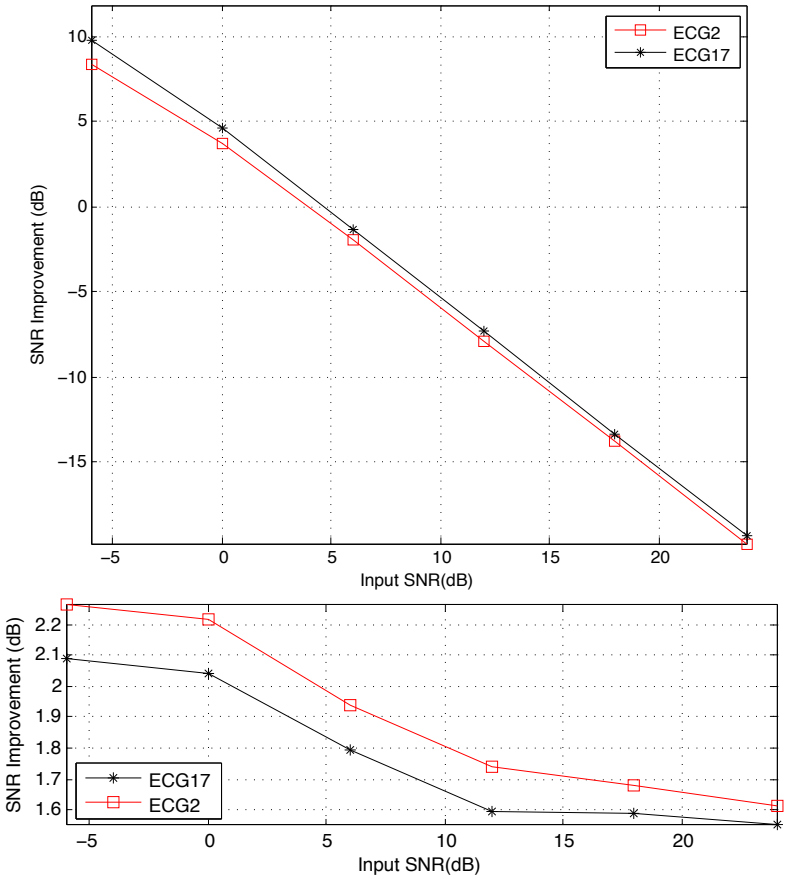

Figure 5.8: Mean and standard deviation in SNR improvements compared between the ECG2 and the ECG17 over various input SNRs with white Gaussian noise using EKF

One of the main concerns for the fixed-lag smoother is the phenomenon that arises when the dimension of the augmented state vector becomes high-dimensional. The augmented state vector for the fixed-lag smoother is of length $n(l+1)$, with $l+1$ n-dimensional sub-vectors $\mathbf{x}_k$, $\mathbf{x}_{k-1}$, $\mathbf{x}_{k-2}$,...$\mathbf{x}_{k-l}$, as shown in Figure 5.6. Using the ECG17 model with $l = 10$ introduces an augmented state vector of length 170. When dealing with matrix computations, such as matrix inversion and matrix multiplication, this high dimension become a definite burden for real-time applications. This phenomenon is often known as the curse of dimensionality. Comparing the fixed-lag smoother performance between ECG2 and ECG17 shows ECG17 has no advantage over ECG2, which implies ECG2 is the more appropriate choice for fixed-lag smoothing since its significantly lower dimension means

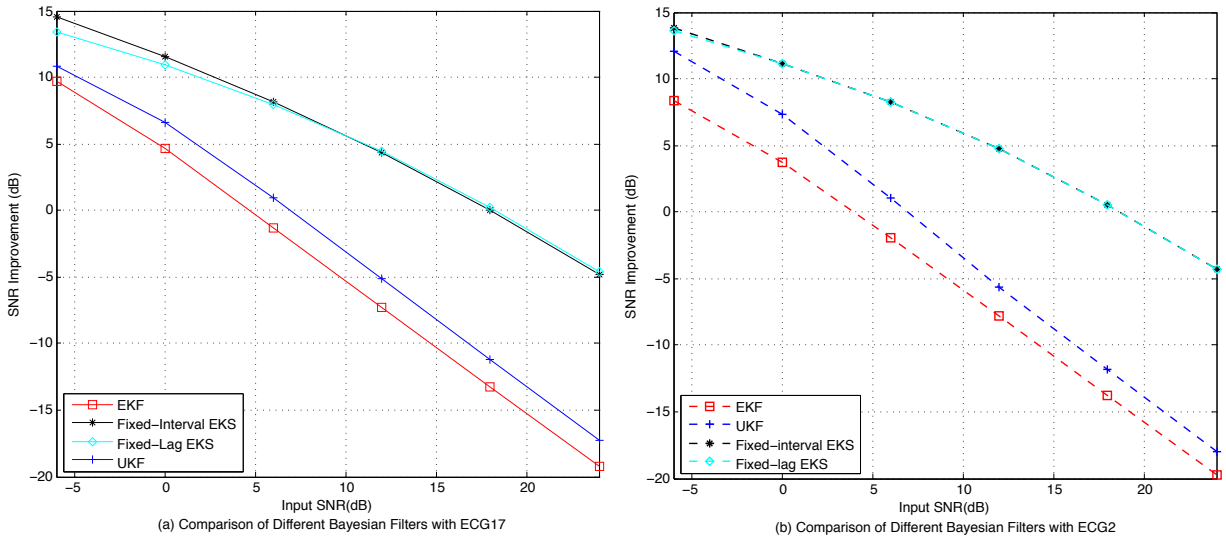

Figure 5.9: Mean SNR improvement of ECG2 and ECG17 with EKF, UKF, fixed-interval smoother and fixed-lag smoother. (a) ECG17 (b) ECG2

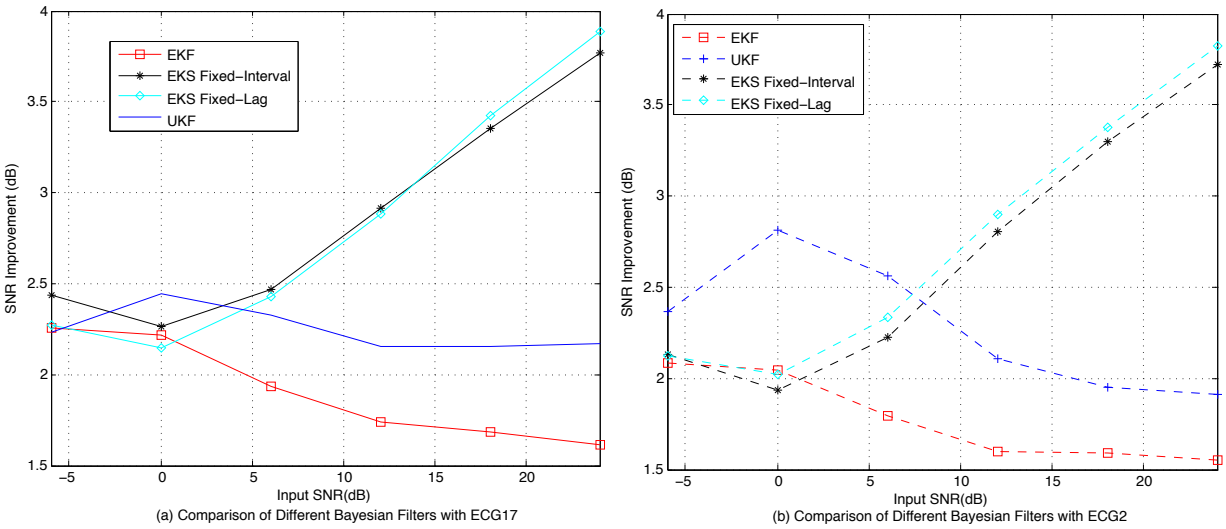

Figure 5.10: Standard Deviation in SNR improvement of ECG2 and ECG17 with EKF, UKF, fixed-interval smoother and fixed-lag smoother. (a) ECG17 (b) ECG2

lower computational cost. There are two reasons for this. First, using ECG2 reduces the dimension of the augmented state vector from 170 to 20 (assuming $l = 10$). Second, the

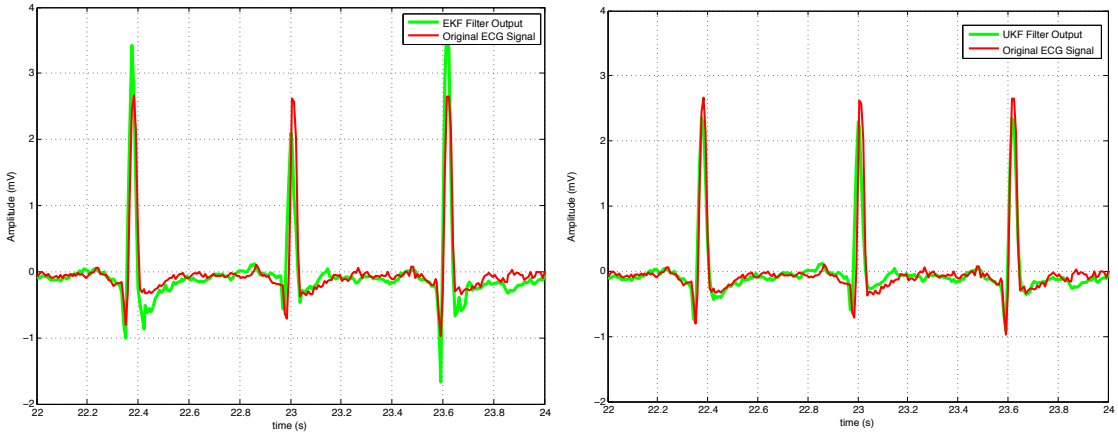

Figure 5.11: Typical filter output between EKF (left) and UKF (right) for an input signal of 0 dB from patent 16265 in DB1 with ECG17

run-time complexity of the fixed-lag smoother is reduced, because there are less multiplications and additions in dealing with matrices. Despite these improvements of ECG2 over ECG17, the dimension of the augmented state vector may still be high-dimensional if the width l of the lag window is very large. The dimension of the augmented state vector can however be substantially reduced without appreciable loss in performance by finding a suboptimal state vector. This is discussed in Chapter 6.

Even though the fixed-interval smoother has the highest SNR-performance among the four filters, there is a price to be paid for this in that the fixed-interval smoother can actually smooth out some clinically important features and information from the ECGs. On the other hand, use of the fixed-lag smoother enables one to avoid such excessive smoothing by controlling the window length of the filter, and therefore controlling the amount of smoothing applied to ECGs (shown in Figure 5.13).

Figure 5.14 illustrates the mean SNR performance of the ECG2 and the ECG17 models under white noise, pink noise, and muscle artifacts with the EKF. The performance of the filter degrades with pink noise and muscle artifacts (MA). Denoising pink noise and MA is a much more challenging problem than denoising white noise for any filtering method. Both pink noise and MA greatly change the morphologies of clean signals.
For example, noisy signals have been totally shifted up or down around the QRS complex in the yellow circle in Figure 5.15. The Kalman Filter tends to follow the dynamical model rather than the measurement to achieve optimal performance. In this situation, it is impossible to achieve good performance for any denoising method. The most difficult

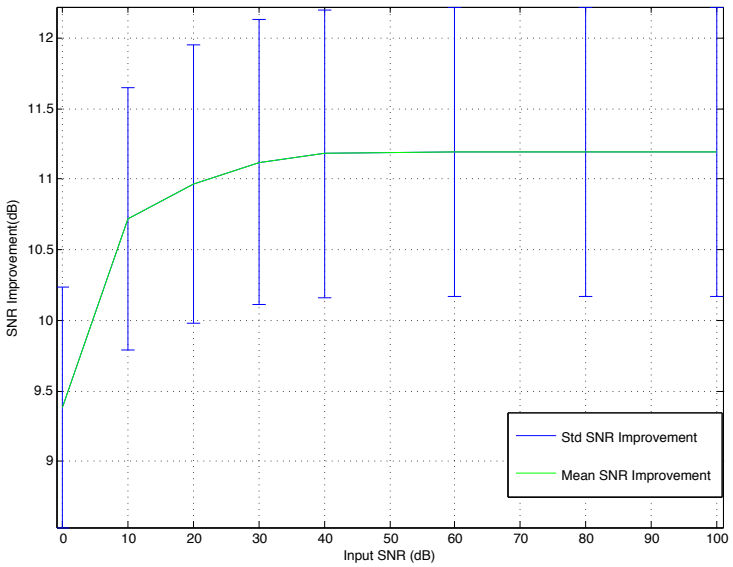

Figure 5.12: Mean and Standard Deviation in SNR improvements for fixed-lag smoother with ECG17 over various lag windows; the results are generated using patient data from DB1

noise is the MA, which shown to have no improvements in SNR with EKF. Furthermore, the SNR improvement for the MA has the largest deviation ranges from $\pm 5dB$ to $\pm 7dB$. Consequently, the EKF is inadequate in dealing with MA. It should be also noted that the ECG17 has better SNR improvements in the presence of white noise; however, ECG2 outperformed ECG17 in the presence of coloured noise and the MA. In real situations, coloured noise and MA are blended in with ECGs; thus, the ECG2 model is the better dynamical model in this case.

With the use of a fixed-interval smoother instead of EKF, the mean SNR performance of filtering with white noise or pink noise or MA greatly improves (Figure 5.16). If the input SNR is higher greater than 10 dB, that noisy signal has little difference with clean signal, the denoising process actually has little denoising effects. Therefore, the calculation of SNR improvement for input SNR above 10 dB has less meaning. The EKF therefore represents the lower bound and the fixed-interval smoother represents the upper bound of SNR performance with various types of Bayesian filters. The fixed-interval smoother provides the best overall SNR improvement in the presence of various types of noise. For real-time applications, a fixed-lag smoother with an appropriate lag value gives the best SNR improvement in the presence of noise in comparison to EKF and UKF.

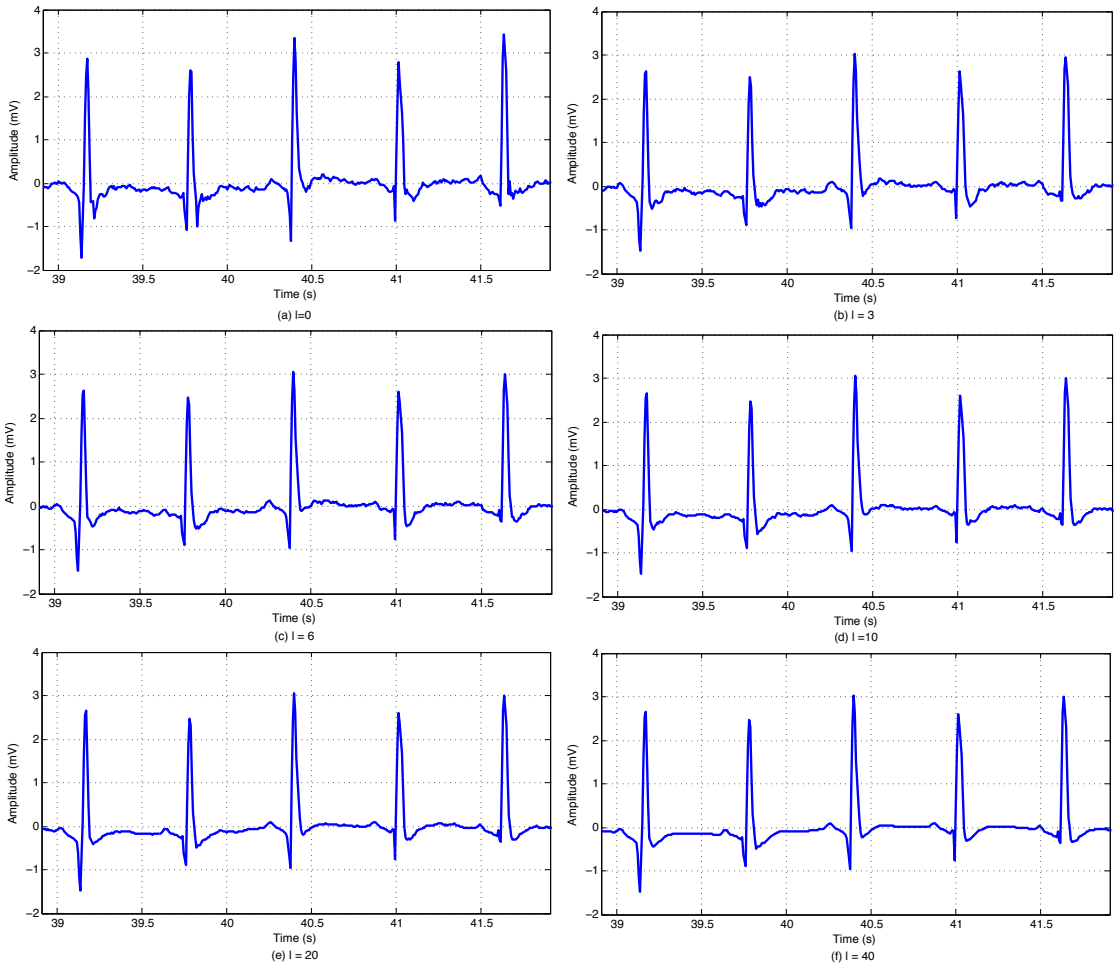

Figure 5.13: Typical output results for a fixed-lag smoother with different lag values: (a) $l = 0$, (b) $l = 3$, (c) $l = 6$, (d) $l = 10$, (e) $l = 20$, and (f) $l = 40$. The fixed-lag smoother controls the amount of smoothing.

In the derivation of the Bayesian filter, assumptions are made about the process and measurement noise for mathematical simplicity. Both the process and measurement noise are assumed to be stationary, Gaussian and uncorrelated. These assumption might limit the performance of the filter. For one, these assumptions do not hold when MA or electrode motion artifacts (EM) affect the ECGs. Both MA and EM are non-stationary and non-Gaussian measurement noise, contary to these assumtions. As a result, the variance of the measurement noise changes with time. In these circumstances the use of a constant

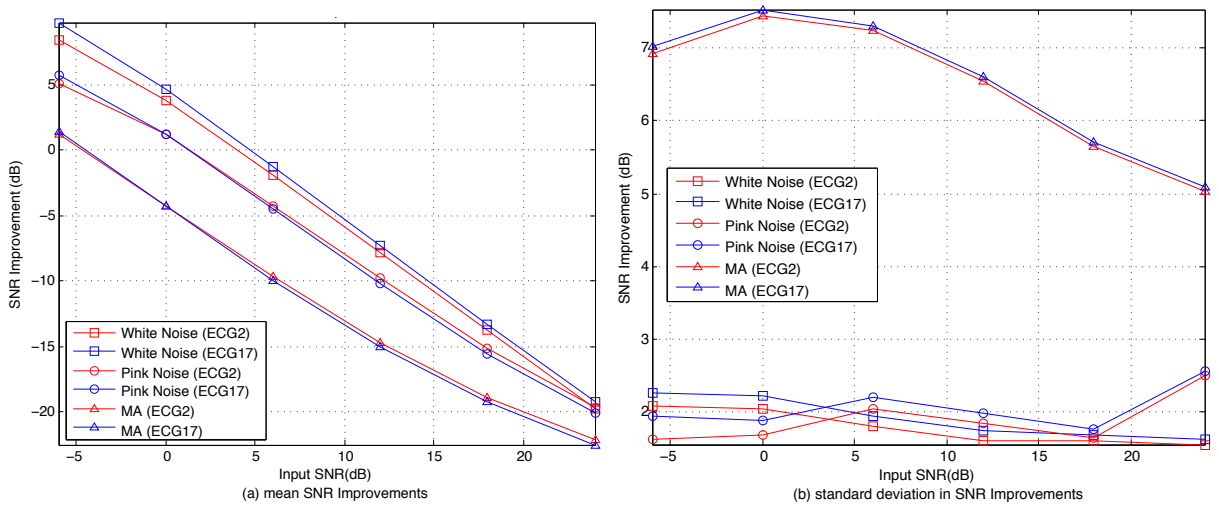

Figure 5.14: Mean (left) and Standard Deviation (right) of the SNR improvements of ECG2 and ECG17 with EKF versus different input SNRs. In these curves various types of noise are applied: white noise, pink noise and muscle artifacts.

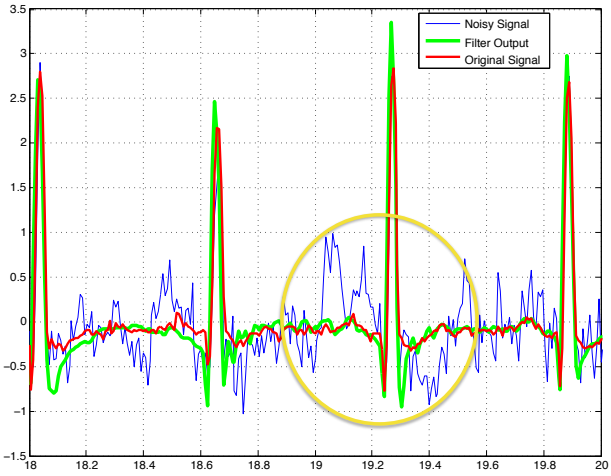

Figure 5.15: Typical EKF filter output result for noisy ECG signal with muscle artifacts. The yellow circle demonstrates the EKF following the ECG dynamical model when approaching sudden upward or downward shift in measurments.

measurement covariance matrix $\mathbf{R}_k$ for the whole duration of the filtering process is not a particularly good model. To alleviate this, one can treat $\mathbf{R}_k$ as a parameter which is

adapted to the variances of innovation process of the filter. Sameni *et al.* [31] suggest a method to monitor the covariance matrix of the innovation signal during filtering and to update the values of $\mathbf{Q}_k$ and $\mathbf{R}_k$ accordingly. We do not address this problem in the present thesis.

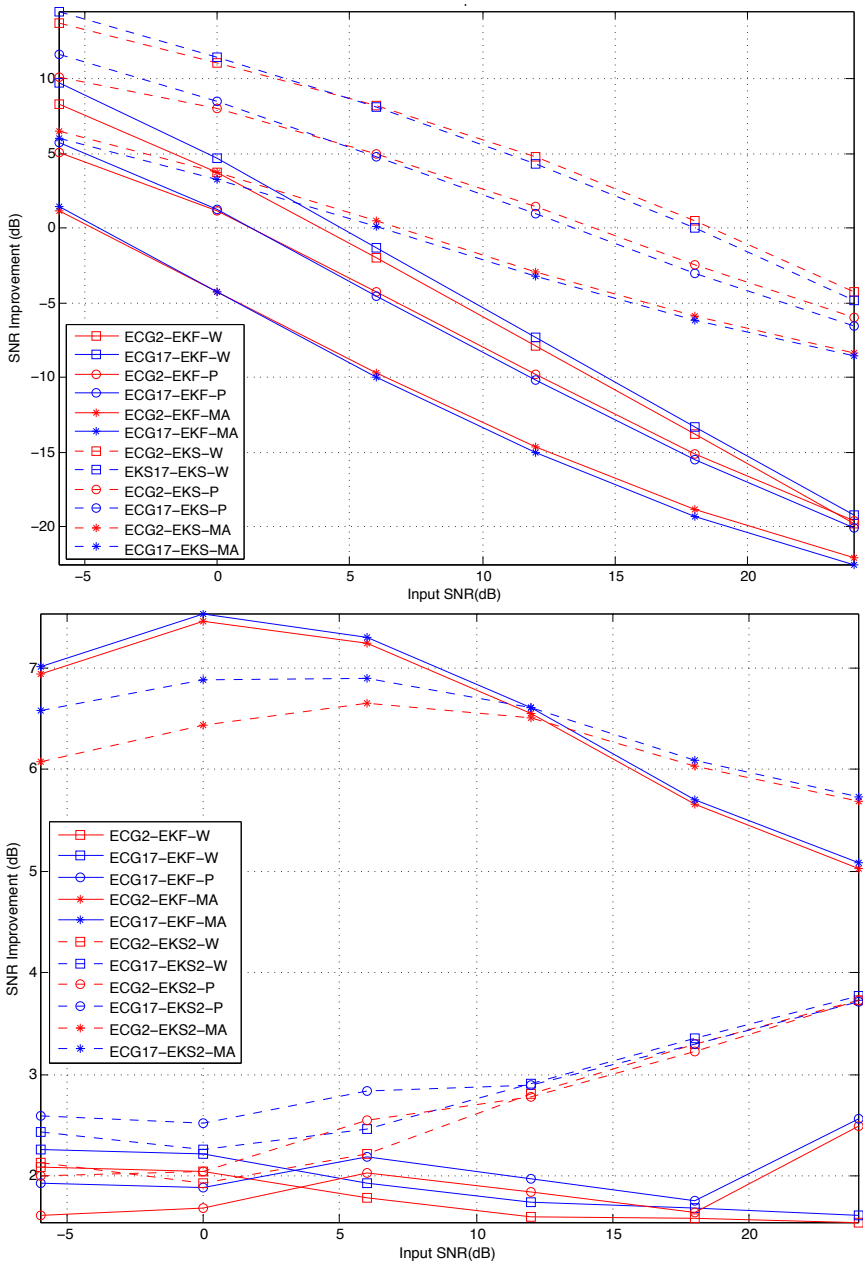

Figure 5.16: Comparison of SNR Mean Improvement between EKF and fixed-interval EKS with three types of noise: white Gaussian noise (W), pink Gaussian noise (P) and muscle artifacts (MA).

Chapter 6

Sub-optimal Fixed-Lag Smoother

6.1 Introduction

In Chapter 5 it is seen that a fixed-lag smoother with a lag of thirty-steps has a performance close to a fixed-interval smoother. Since the goal of the project is to build an online ECG noise filter, the fixed-lag smoother is an obvious choice since it can be implemented online, in contrast to the fixed-interval smoother which can only be implemented offline. However, a significant problem with this fixed-lag smoother is the size of the state vector. Thus, a fixed-lag smoother based on the ECG2 model with a lag of thirty steps has a state vector of dimension sixty-two. Inverse matrix calculations of dimension sixty-two become problematic. The aim of this chapter is to propose a sub-optimal fixed-lag smoother which reduces the computational burden arising from large state vectors. The Schmidt-Kalman Suboptimal filter described in [9] provides a method for reducing the processing and memory requirements of Kalman filters by decoupling unessential states. We first review the dynamics of the Biswas-Mahalanabis Fixed-lag smoother for the ECG2 model. We focus on this model since it was concluded in Section 5.5 that there are no genuine advantages in using ECG17 instead of ECG2 for fixed-lag smoothers, because the de-noising performance from ECG2 and ECG17 are practically the same.

6.2 Dynamics of Fixed-Lag Smoother with ECG2

The Biswas-Mahalanabis Fixed-Lag Smoother (BMFLS) is essentially a Kalman filter that uses an augmented state vector to track successive values of the original state vector over

a discrete time window of fixed width[9]. In order to distinguish between the Kalman filter state vector and the BMFLS state vector, we will use the following notations in this chapter:

- $\mathbf{x}_{k,KF}$ denotes the true state value of the Kalman filter state vector at kth time step.
- $\hat{\mathbf{x}}_{k,KF}$ denotes the estimated state value of the Kalman filter state vector at kth time step.
- $\mathbf{x}_{k,BMFLS}$ denotes the true state value of the BMFLS state vector at kth time step.
- $\hat{\mathbf{x}}_{k,BMFLS}$ denotes the estimated state value of the BMFLS state vector at kth time step.

A BMFLS with l lagged time steps keeps $\mathbf{x}_{k,KF}$, $\mathbf{x}_{k-1,KF}$,..., $\mathbf{x}_{k-l+1,KF}$ stacked into the BMFLS's state vector. In other words, the BMFLS saves the current state $\mathbf{x}_{k,KF}$ as well as $l-1$ past steps in memory. The augmented state vector for BMFLS with l lagged time steps can be constructed as:

$$\mathbf{x}_{k,BMFLS} = \begin{bmatrix} \mathbf{x}_{k,KF} \\ \mathbf{x}_{k-1,KF} \\ \mathbf{x}_{k-2,KF} \\ \vdots \\ \mathbf{x}_{k-l+1,KF} \end{bmatrix} \tag{6.1}$$

The BMFLS constructs this augmented state vector which is then used in a conventional two-step Kalman filter algorithm. During each measurement-update step, the current measurement and all past measurements are used to provide smoothed estimates for $\mathbf{x}_{k-1,KF}$, $\mathbf{x}_{k-2,KF}$,...,$\mathbf{x}_{k-l+1,KF}$. The estimated state vector of BMFLS is equivalent to

$$\hat{\mathbf{x}}_{k,BMFLS} = \begin{bmatrix} \hat{\mathbf{x}}_{k|k,KF} \\ \hat{\mathbf{x}}_{k-1|k,KF} \\ \hat{\mathbf{x}}_{k-2|k,KF} \\ \vdots \\ \hat{\mathbf{x}}_{k-l|k,KF} \end{bmatrix} \tag{6.2}$$

where $\hat{\mathbf{x}}_{k-l|k,KF}$ is the smoothed estimate of $\mathbf{x}_{k-l,KF}$ given all the measurements from past up to $\mathbf{z}_k$. This idea is similar to the fixed-interval smoother. The fixed-interval smoother uses all measurements in the past and the future to derive the smoothed estimates, whereas

the BMFLS uses all past measurements and a fixed number of future measurements to provide the smoothed estimates.

The state transition matrix for BMFLS is then

$$\begin{aligned}
\hat{\mathbf{x}}_{k+1,BMFLS} &= F_{Aug}\left(\hat{\mathbf{x}}_{k,BMFLS}, \mathbf{w}_k, k\right) \\
\begin{bmatrix} \hat{\mathbf{x}}_{k+1,KF} \\ \hat{\mathbf{x}}_{k,KF} \\ \hat{\mathbf{x}}_{k-1,KF} \\ \vdots \\ \hat{\mathbf{x}}_{k-l+1,KF} \end{bmatrix} &= \begin{bmatrix} F\left(\hat{\mathbf{x}}_{k,KF}, \mathbf{w}_k, k\right) \\ \hat{\mathbf{x}}_{k-1,KF} \\ \hat{\mathbf{x}}_{k-2,KF} \\ \vdots \\ \hat{\mathbf{x}}_{k-l,KF} \end{bmatrix}
\end{aligned} \tag{6.3}$$

Here $F(\mathbf{.})$ is the state transition matrix of ECG2 in (4.7) . If $l = 30$, then the size of $\mathbf{x}_{k,BMFLS}$ has 62 states. From Equation (6.3), the first row of the system equation implements the dynamic system in (4.7), while the remaining rows implement successive time delays.

The corresponding process noise covariance matrix, observation matrix, and measurement noise covariance matrix for BMFLS are of course

$$\mathbf{Q}_{k,BMFLS} = \begin{bmatrix} \mathbf{Q}_{k,KF} & \mathbf{0} & \dots & \mathbf{0} \\ \mathbf{0} & \mathbf{0} & \dots & \mathbf{0} \\ \vdots & \vdots & \ddots & \vdots \\ \mathbf{0} & \mathbf{0} & \dots & \mathbf{0} \end{bmatrix} \tag{6.4}$$

$$\mathbf{H}_{k,BMFLS} = \begin{bmatrix} \mathbf{H}_{k,KF} & \mathbf{0} & \dots & \mathbf{0} \end{bmatrix} \tag{6.5}$$

$$\mathbf{R}_{k,BMFLS} = \mathbf{R}_{k,KF} \tag{6.6}$$

6.3 Sub-optimal Filtering

All the required components to run BMFLS with a conventional Kalman filter structure have been defined in Section 6.2, and reducing the number of states of $\mathbf{x}_{k,BMFLS}$ will then resolve the curse of dimesionality. The Schmidt-Kalman filter is a sub-optimal filter from which unnecessary states have been removed [9]. This filter was proposed by Stanley F. Schmidt for reducing the processing and memory requirements of Kalman filters with predictable and slight performance degradation. It has been used in GPS navigation applications as a means of eliminating additional variables. With a predictable loss of estimated performance as the price for improved computational performance, the method enables Kalman filters to be approximated so that they can be implemented in real time.

6.3.1 State Vector Partitioning

The Schmidt-Kalman filter partitions the state vector into essential variables, designated by the subscript e, and unessential variables, designated by the subscript u. Thus the BMFLS state vector $\mathbf{x}_{k,BMFLS}$ is partitioned into the vector of essential states $\mathbf{x}_{e,k}$ and the vector of unessential states $\mathbf{x}_{u,k}$:

$$\mathbf{x}_{k,BMFLS} = \begin{bmatrix} \mathbf{x}_{e,k} \\ \mathbf{x}_{u,k} \end{bmatrix} \tag{6.7}$$

where $\mathbf{x}_{e,k}$ is the $n_e \times 1$ subvector of essential states to be estimated, $\mathbf{x}_{u,k}$ is the $n_u \times 1$ subvector that is not be estimated, and

$$n_e + n_u = n \tag{6.8}$$

is the total number of state variables in $\mathbf{x}_{k,BMFLS}$.

To find the essential and unessential states, we first express the augumented state vector of $\mathbf{x}_{k,BMFLS}$ in terms of θ_k and z_k:

$$\mathbf{x}_{k,BMFLS} = \begin{bmatrix} \theta_{k,KF} \\ z_{k,KF} \\ \theta_{k-1,KF} \\ z_{k-1,KF} \\ \theta_{k-2,KF} \\ z_{k-2,KF} \\ \vdots \\ \theta_{k-l,KF} \\ z_{k-l,KF} \end{bmatrix} \tag{6.9}$$

Here $\theta_{k,KF}$ is the angular state variable that indicates the angular location on the circular limit cycle. The propagation of the angular location is governed by the additive term $\omega\delta$ in the dynamics for θ_k, which describes the angular velocity along the limit cycle. The change in angular velocity depends on the heart rate variability of the subject. In hospital settings patients are usually stationary with little movement, which results in slow-varying heart rates. Thus, the process noise of θ_k is small. Furthermore, the θ_k undergoes phase synchronization using the phase assignment technique, which results in accurate estimation of $\hat{\theta}_k$. Since the estimation error for $\hat{\theta}_k$ is trivial, the BMFLS applies limited correction on estimates. Thus, $\theta_{k-j}, j = 2, ..., l$ are the unessential states in $\mathbf{x}_{k,BMFLS}$. Reducing

the unessential states from the augmented state vector results in following the suboptimal state vector for BMFLS:

$$\mathbf{x}_{e,k} = \begin{bmatrix} \theta_{k,KF} \\ z_{k,KF} \\ z_{k-1,KF} \\ z_{k-2,KF} \\ \vdots \\ z_{k-l,KF} \end{bmatrix} \tag{6.10}$$

$$\mathbf{x}_{u,k} = \begin{bmatrix} \theta_{k-1,KF} \\ \theta_{k-2,KF} \\ \vdots \\ \theta_{k-l,KF} \end{bmatrix} \tag{6.11}$$

The unessential state vector $\mathbf{x}_{u,k}$ is removed from the state vector and is not estimated by the Kalman filter. After removing these unessential states the state transition matrix of the BMFLS reduces to

$$\begin{aligned} \hat{\mathbf{x}}_{e,k+1} &= F_e\left(\hat{\mathbf{x}}_{e,k}, \mathbf{w}_k, k\right) \\ \begin{bmatrix} \hat{\mathbf{x}}_{k+1,KF} \\ \hat{z}_{k,KF} \\ \hat{z}_{k-1,KF} \\ \vdots \\ \hat{z}_{k-l+1,KF} \end{bmatrix} &= \begin{bmatrix} F\left(\hat{\mathbf{x}}_{k,KF}, \mathbf{w}_k, k\right) \\ \hat{z}_{k-1,KF} \\ \hat{z}_{k-2,KF} \\ \vdots \\ \hat{z}_{k-l,KF} \end{bmatrix} \end{aligned} \tag{6.12}$$

The process noise covariance matrix, observation matrix, and measurement noise covariance matrix for suboptimal BMFLS are now

$$\mathbf{Q}_{ee,k} = \begin{bmatrix} \mathbf{Q}_{k,KF} & 0 & \dots & 0 \\ 0 & 0 & \dots & 0 \\ \vdots & \vdots & \ddots & \vdots \\ 0 & 0 & \dots & 0 \end{bmatrix} \tag{6.13}$$

$$\mathbf{H}_{e,k} = \begin{bmatrix} \mathbf{H}_{k,KF} & \mathbf{0} \end{bmatrix} \tag{6.14}$$

$$\mathbf{H}_{u,k} = \mathbf{0} \tag{6.15}$$

$$\mathbf{R}_{e,k} = \mathbf{R}_{k,KF} \tag{6.16}$$

6.3.2 Covariance Matrix Partition

The covariance matrix of the Schmidt-Kalman filter is correspondingly partitioned as

$$\mathbf{P}_{k,BMFLS} = \begin{bmatrix} \mathbf{P}_{ee,k} & \mathbf{P}_{eu,k} \\ \mathbf{P}_{ue,k} & \mathbf{P}_{uu,k} \end{bmatrix} \tag{6.17}$$

where $\mathbf{P}_{ee,k}$ is a $n_e \times n_e$ matrix, $\mathbf{P}_{eu,k}$ is a $n_e \times n_u$ matrix, $\mathbf{P}_{ue,k}$ is a $n_u \times n_e$ matrix and $\mathbf{P}_{uu,k}$ is a $n_u \times n_u$ matrix. Additionally, $\mathbf{P}_{eu,k} = \mathbf{P}_{ue,k}^T$.

When implementing the Schmidt-Kalman filter, the covariance matrix $\mathbf{P}_{ee,k}$ takes into account the effect of the unessential states. Therefore, the Schmidt-Kalman filter calculates the covariance matrix of uncertainty in the unestimated state variables $\mathbf{P}_{uu,k}$ as the cross-covariance matrix between the essential sub-vector and unessential sub-vector $\mathbf{P}_{ue,k}$. $\mathbf{P}_{ee,k}$, $\mathbf{P}_{uu,k}$ and $\mathbf{P}_{ue,k}$ are then used in the calculation of the Schmidt-Kalman gain [9]. Just like the Kalman filter, the Schmidt-Kalman Filter has two distinct phases: the observation update phase and the time update phase. The two-step recursive algorithm of the Schmidt-Kalman Filter is in Appendix C.

6.3.3 Initialize the Suboptimal BMFLS States

The initialization of the essential state $\mathbf{x}_{e,k}$, and the estimation covariance matrix $\mathbf{P}_{ee,k}$, are somewhat problematic. Naively, one could run the standard conventional KF with no augmentation states until the desired fixed lag to formed the augmented states. This approach produces the correct estimates of $\mathbf{x}_{e,k}$ and the correct Schemdt-Kalman gain $\mathbf{K}_{SK,k}$, where $k = 0, ..., l$. However, the initialization of the augmented state vector with $\mathbf{x}_{e,k}$ does not have the correct conditioning. This approach also does not provide the correct conditioning between different state delays.

A successful approach for initializing the filter is to increase the size of the augmented state vector until it has built up the complete augmented states. During start-up, the augmented state vector $\mathbf{x}_{e,k}$ must proceed through a transition from a state vector with no augmentation ($l = 0$) to augmentation with an increase in the number of states, until the state vector reaches its desired fixed lag. At the initial time step, $k = 0$, the BMFLS starts with a single estimate $\hat{\mathbf{x}}_{e,0}$ of the system state vector and a single value for the estimation covariance matrix $\mathbf{P}_{ee,0}$. Initially, the augmented state vector has dimension of 2×1 and the covariance matrix has dimension of 2×2. At the KF update-step, the smoother incrementally builds up its augmented state vector until the augmented state

vector becomes a matrix dimension of $(l+2) \times 1$. Throughout the smoothing process, the topmost two states are always the current estimates of the system. The states from the third state to the last state are previous estimates of z_k.

Another simpler approach is to initialize the states $\theta_{0,KF}$ and $z_{0,KF}$ to the best estimates in $\mathbf{x}_{e,0}$. All the remaining delayed components of the augmented state vectors are put equal to zero. The covariance matrix is initialized in the similar way, where all the delayed components are again put equal to zero. With this approach, the augmented state components and augmented covariance components attain their true values only when $k > l$, where l is the length of the smoothing window. This is the approach that we use in the initialization of the BMFLS.

6.4 Results and Discussion

The approach for testing the performance of the suboptimal BMFLS is very similar to the experiment described in 5.4. In the experiment, artificial white noise, artificial pink noise, and MA with different variances are generated and added to the clean ECG segments from eighteen different subjects in the DB1. The generated noisy ECG segments are presented to the proposed suboptimal BMFLS to measure its SNR improvement against other types of filter.

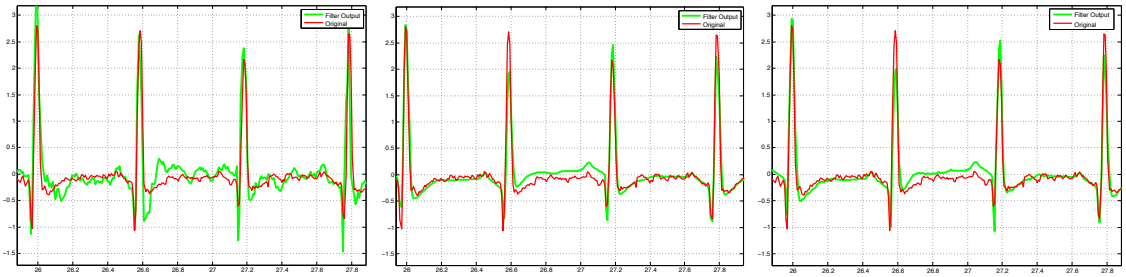

Figure 6.1: Filter output from EKF (left), suboptimal BMFLS (middle) and fixed-interval smoother (right).

In Figure 6.1, typical results of the proposed BMFLS with $l = 30$, EKF and fixed-interval smoother are presented for a white Gaussian input of -6 dB. When visually comparing theses results, the proposed BMFLS performs closely to the fixed-interval smoother. The EKF has difficulty filtering out noise and tracking the model around the S wave. The BMFLS and the fixed-interval smoother are able to properly filter noise around the S wave.

This shows superiority of the BMFLS and the fixed-interval smoother, both of which use future measurements to correct estimates.

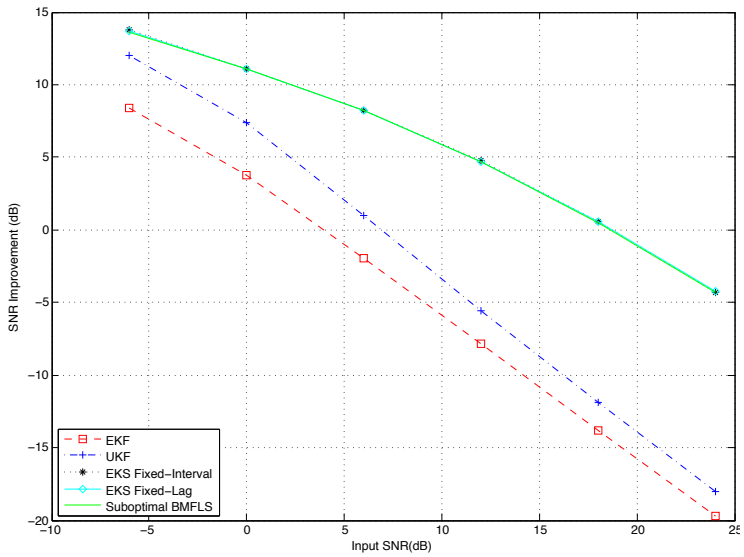

Figure 6.2: Mean SNR Improvement between different Bayesian filters. The supoptimal BMFLS reduced the dimension of the state vector with little loss in performance.

In a detailed quantitative comparison of suboptimal BMFLS against other types of filters, the mean and standard deviation of SNR improvement versus different input SNRs are illustrated in Figure 6.2. The result in Figure 6.2 uses white Gaussian noise with various input SNR. The suboptimal BMFLS, fixed-interval smoother and the fixed-lag smoother have almost the same mean SNR performance. As one would expect, the fixed-interval smoother has the best performance, but nevertheless outperforms the suboptimal BMFLS and fixed-lag smoother by less than 4% (see Table 6.1 and 6.2). The similarity in mean SNR performance between these three filters remains consistent even when the noisy ECG segments are injected with pink noise or MA. This shows that one can use the suboptimal BMFLS (which is implementable online) to achieve essentially the same performance as the fixed-interval smoother (which is only implementable offline). Tables 6.1 and 6.2 show the SNR improvements of input ECG signals with white noise having the SNR values of -6, 0 and 6 db. These tables demonstrate the similarity in performance between the fixed-interval smoother and the suboptimal BMFLS.

Table 6.1: Performance Evaluation between the Fixed-Lag Smoothing and the Sup-optimal BMFLS with input SNR of 6 dB and 0 dB

Patient Number	6dB						0dB					
	White Noise		Pink Noise		MA		White Noise		Pink Noise		MA	
	Fixed-Interval	BMFLS	Fixed-Interval	BMFLS	Fixed-Interval	BMFLS	Fixed-Interval	BMFLS	Fixed-Interval	BMFLS	Fixed-Interval	BMFLS
16265m	10.1639	10.5529	7.8312	7.9213	2.0191	2.5381	12.6435	12.9239	8.5470	8.5579	4.3152	4.8468
16272m	6.5538	6.5954	1.7032	1.7491	-0.5782	-0.5631	9.9347	9.9486	7.2338	7.1090	2.5669	2.6111
16723m	9.6337	9.5527	6.3568	6.0976	1.5836	1.3844	12.2199	12.2503	8.9868	8.8483	5.0065	4.9643
16420m	9.8256	9.6061	7.0543	6.6595	3.1892	2.8540	11.4819	11.3871	9.6126	9.2436	6.4455	6.1099
16483m	8.7568	8.9343	5.2588	5.6456	0.3887	0.9665	11.2197	11.7721	7.2417	7.6941	2.9029	3.8227
16539m	7.2734	7.0029	4.8119	4.5772	-0.4300	-0.6362	9.6596	9.5311	7.4213	7.2814	3.6132	3.4145
16773m	8.2030	8.3986	3.9984	4.0428	1.0111	1.1535	10.8695	10.8549	7.8661	7.6487	3.8047	3.9033
16786m	9.8496	9.9912	7.1255	7.0639	3.6687	3.8122	12.3322	12.3098	9.8707	9.6810	6.1532	6.4423
16795m	4.7295	4.3910	1.0268	0.7233	-2.4408	-2.7388	8.9654	8.5951	6.5504	6.1900	1.3633	1.0139
17052m	8.2915	8.2527	4.7490	4.5964	0.7560	0.7241	11.1730	11.1824	8.7845	8.6081	4.2324	4.2633
17453m	9.0919	9.0014	5.8367	5.7844	0.9955	0.9118	11.9214	11.9226	9.1155	8.7893	4.3218	3.8515
18177m	6.8823	6.2689	3.2782	2.8389	-2.1853	-2.7189	10.4454	10.0032	6.3810	5.8974	2.0430	1.6558
18184m	8.9825	9.0634	5.6446	5.6145	1.0945	1.2292	11.5992	11.5979	8.4330	8.3754	4.5398	4.6865
19088m	7.4085	7.5423	3.7115	3.7965	-1.3637	-1.2432	10.6826	10.5438	7.1260	7.0501	1.9524	1.9371
19090m	7.3290	7.2353	4.6246	4.4836	-1.1621	-1.3277	11.1860	10.9133	7.1808	6.8368	2.9132	2.4814
19093m	7.5077	7.6756	4.5209	4.6411	1.0298	1.2155	10.3543	10.5224	7.1057	6.9721	3.3946	3.4532
19140m	7.3452	7.4173	3.8042	3.8129	-1.3363	-1.3381	10.5883	10.5451	7.9977	7.7481	2.7094	2.4314
19830m	10.1391	10.4623	7.4115	7.5092	3.5788	3.4654	12.2950	12.6068	10.354	10.4846	6.0648	6.5968
Mean SNR	8.22039	8.21913	4.9305	4.86432	0.5455	0.5383	11.0873	11.07836	8.1005	7.94533	3.7968	3.8048
Std SNR	1.41827	1.54765	1.8053	1.83554	1.6971	1.82	0.9811	1.103093	1.0569	1.07315	1.3901	1.4774
Difference (%)		0.02%		1.34%		1.32%		0.08%		1.92%		0.21%

Table 6.2: Performance Evaluation between the Fixed-Lag Smoothing and the Sup-optimal BMFLS with input SNR of -6 dB

Patient Number	-6dB					
	White Noise		Pink Noise		MA	
	Fixed-Interval	BMFLS	Fixed-Interval	BMFLS	Fixed-Interval	BMFLS
16265m	14.9452	14.9924	11.1362	10.758	6.8057	6.9910
16272m	12.5852	12.4864	10.5125	10.09	5.6655	5.7703
16723m	14.9533	14.7743	11.1368	10.596	7.8701	7.8125
16420m	13.4775	13.3236	10.5757	10.07	8.5780	8.2975
16483m	13.3294	13.7219	9.7016	9.6950	5.0957	5.9805
16539m	12.0067	11.8493	9.4748	9.1549	7.0923	6.8193
16773m	13.8527	13.6836	10.4562	10.141	6.6218	6.6205
16786m	14.6354	14.5638	10.8312	10.48	8.3558	8.67
16795m	12.7126	12.2970	9.2951	8.8313	4.9874	4.6594
17052m	14.2268	14.0953	10.4561	10.053	6.9960	6.8482
17453m	14.5999	14.3843	10.5457	10.166	7.0590	6.3338
18177m	13.8120	13.4629	9.3250	8.9381	5.5311	5.2350
18184m	13.6003	13.6361	10.6749	10.275	7.2185	7.1291
19088m	13.3932	13.2929	9.7495	9.5172	5.0646	4.8688
19090m	13.9045	13.5658	9.4287	8.9296	6.0859	5.4468
19093m	12.4276	12.3587	9.1460	8.9794	6.1081	6.1828
19140m	14.5026	14.1213	9.3550	8.9483	5.9508	5.5646
19830m	14.1164	14.2505	11.3488	11.248	7.5930	8.0886
Mean SNR	13.7267	13.6033	10.175	9.8261	6.5933	6.5177
Std SNR	0.87042	0.89399	0.66613	0.6289	1.1004	1.1241
Difference (%)	0.90%		3.43%		1.15%	

Chapter 7

Conclusions and Future Work

7.1 Conclusions

In this thesis two modifications of an ECG dynamical model due to Sameni *et al.* [31] are proposed for filtering noise from contaminated ECG recordings. The first modification extends the the system state space from two states to seventeen states to incorporates changes in the Gaussian functions; however, the results show a general lack of clear improvement over the two-state model. The second modification is to introduce a suboptimal BMFLS fixed-lag smoother, which is derived from the optimal BMFLS filter by the removal of unessential states from the dynamical model. The EKF is applied to the suboptimal BMFLS and the simulation results demonstrate that the proposed model can serve as a novel dynamical model for achieving similar performance results as fixed-interval smoothing, but with the significant advantage of being implementable online, while fixed interval smoothing is only implementable offline. The proposed model is applied on the model-based Bayesian framework for online filtering, which is usable for applications such as real-time detection of cardiac arrhythmia.

7.2 Future Work

As discussed in Section 6.4, the proposed BMFLS has the ability to control the amount of smoothing on estimates by controlling the size of the lag window. If one chooses a window of excessive width, the fixed-interval smoother could however over-smooth the state estimates, which could in term lead to the removal of clinically important features

from the ECG. It remains to investigate appropriate lag window sizes for the proposed suboptimal BMFLS to obtain filtering without excessive smoothing.

The experiments in the thesis involves only normal ECG signals from patients and the main focus has been on denoising. In future work abnormal ECG signals arising from emergency situations such as cardiac arrythmia should also be addressed. The Bayesian filtering theory allows the detection of anomalous measurement data, which monitors the information matrix of the innovations. With the monitoring of anomalous measurement data, the detection of abnormal activities is possible in ECG traces. This idea could be incorporated into the filtering framework for online arrhythmia detection.

APPENDICES

Appendix A

Recursive Algorithm of the Unscented Kalman Filter

The two-step recursive algorithm considers the same nonlinear system discussed in Section 3.2.1.

$$\mathbf{x}_{k+1} = f(\mathbf{x}_k, \mathbf{w}_k, k) \tag{A.1}$$

$$\mathbf{z}_k = g(\mathbf{x}_k, \mathbf{v}_k, k) \tag{A.2}$$

where $\mathbf{w}_k$ and $\mathbf{v}_k$ are white Gaussian random noise processes with the same statistics as the EKF.

$$\mathrm{E}\{\mathbf{w}_k\} = 0, \mathrm{E}\{\mathbf{w}_k\mathbf{w}_k^T\} = \mathbf{Q}_k, \tag{A.3}$$

$$\mathrm{E}\{\mathbf{v}_k\} = 0, \mathrm{E}\{\mathbf{v}_k\mathbf{v}_k^T\} = \mathbf{R}_k, \tag{A.4}$$

The following summary of the UKF equations adheres closely to the presentation of Haykin[11]. The UKF recursive algorithm starts with the following initial conditions:

$$\mathbf{x}_0 = \mathrm{E}[\mathbf{x}_0] \tag{A.5}$$

$$\mathbf{P}_0 = \mathrm{E}[(\mathbf{x}_0 - \hat{\mathbf{x}}_0)(\mathbf{x}_0 - \hat{\mathbf{x}}_0)^T] \tag{A.6}$$

$$\hat{\mathbf{x}}_0^a = \mathrm{E}[\mathbf{x}_0^a] = \begin{bmatrix}\hat{\mathbf{x}}_0^T & \mathbf{0} & \mathbf{0}\end{bmatrix} \tag{A.7}$$

$$\mathbf{P}_0^a = \mathrm{E}[(\mathbf{x}_0^a - \hat{\mathbf{x}}_0^a)(\mathbf{x}_0^a - \hat{\mathbf{x}}_0^a)^T] = \begin{bmatrix}\mathbf{P}_0 & \mathbf{0} & \mathbf{0} \\ \mathbf{0} & \mathbf{R}_0 & \mathbf{0} \\ \mathbf{0} & \mathbf{0} & \mathbf{Q}_0\end{bmatrix} \tag{A.8}$$

The augmented state variable $\mathbf{x}_k^a$ contains the original state and noise variables, $\mathbf{x}_k^a = \begin{bmatrix}\mathbf{x}_k^T & \mathbf{w}_k^T & \mathbf{v}_k^T\end{bmatrix}^T$. The augmented covariance matrix $\mathbf{P}_k^a$ is also a concatenation of the original state and the noise variables. For every time-step $k = 1, 2, \ldots$ the recursive algorithm is defined by the following two-step procedure:

Set Selection of Sigma Points

Let $\boldsymbol{\mathcal{X}}_k^a$ be the set of $2L + 1$ points defined as follows

$$\begin{aligned}\boldsymbol{\mathcal{X}}_k^a &= \begin{bmatrix}\hat{\mathbf{x}}_k^a & \hat{\mathbf{x}}_k^a + \gamma\sqrt{\mathbf{P}_k^a} & \hat{\mathbf{x}}_k^a - \gamma\sqrt{\mathbf{P}_k^a}\end{bmatrix} &\text{(A.9)}\\ &= \begin{bmatrix}(\boldsymbol{\mathcal{X}}_k^x) & (\boldsymbol{\mathcal{X}}_k^w) & (\boldsymbol{\mathcal{X}}_k^v)\end{bmatrix} &\text{(A.10)}\end{aligned}$$

with $\gamma = \sqrt{L + \lambda}$. Here λ is the composite scaling parameter, and L is the dimension of the augmented state.

The Time-Update Equations

The sigma points are propagated through the nonlinear system

$$\boldsymbol{\mathcal{X}}_{k+1}^x = f(\boldsymbol{\mathcal{X}}_k^x, \boldsymbol{\mathcal{X}}_k^w, k) \tag{A.11}$$

The posteriori mean, $\hat{\mathbf{x}}_k^-$, and covariance, $\mathbf{P}_k^-$, are determined from the statistics of the propagated sigma points as follows:

$$\begin{aligned}\hat{\mathbf{x}}_k^- &= \sum_{i=0}^{2L} W_i^m \boldsymbol{\mathcal{X}}_{\boldsymbol{i,k}}^{\boldsymbol{a}} &\text{(A.12)}\\ \mathbf{P}_k^- &= \sum_{i=0}^{2L} W_i^c \left(\boldsymbol{\mathcal{X}}_{i,k} - \hat{\mathbf{x}}_k^-\right)\left(\boldsymbol{\mathcal{X}}_{i,k} - \hat{\mathbf{x}}_k^-\right)^T &\text{(A.13)}\end{aligned}$$

The weights, W_i^c and W_i^m, are calculated using

$$\begin{aligned}W_0^m &= \frac{\lambda}{L+\lambda} &\text{(A.14)}\\ W_0^c &= \frac{\lambda}{L+\lambda} + 1 - \alpha^2 + \beta &\text{(A.15)}\\ W_i^c &= W_i^m = \frac{\lambda}{2(L+\lambda)} &\text{(A.16)}\end{aligned}$$

The Measurement-Update Equations

The estimated measurement matrix $\boldsymbol{\mathcal{Z}}_k$ is calculated by transforming the sigma points using the nonlinear measurement model

$$\boldsymbol{\mathcal{Z}}_k = g(\boldsymbol{\mathcal{X}}^{\boldsymbol{x}}_{\boldsymbol{i,k}}, \boldsymbol{\mathcal{X}}^{\boldsymbol{v}}_{\boldsymbol{i,k}}) \tag{A.17}$$

The estimated measurement $\hat{\mathbf{z}}_k$ can be determined by

$$\hat{\mathbf{z}}_k = \sum_{i=0}^{2L} W_i^m \boldsymbol{\mathcal{Z}}_{i,k} \tag{A.18}$$

The measurement covariance $\mathbf{P}_{y_k y_k}$ is calculated based on the statistics of the transformed sigma points.

$$\mathbf{P}_{y_k y_k} = \sum_{i=0}^{2L} W_i^c \left(\boldsymbol{\mathcal{Z}}_{i,k} - \hat{\mathbf{z}}_k\right) \left(\boldsymbol{\mathcal{Z}}_{i,k} - \hat{\mathbf{z}}_k\right)^T + \mathbf{R}_k \tag{A.19}$$

The cross-correlation covariance, $\mathbf{P}_{x_k y_k}$ is then calculated using

$$\mathbf{P}_{x_k y_k} = \sum_{i=0}^{2L} W_i^c \left(\boldsymbol{\mathcal{X}}_{i,k} - \hat{\mathbf{x}}_k^-\right) \left(\boldsymbol{\mathcal{Z}}_{i,k} - \hat{\mathbf{z}}_k\right)^T \tag{A.20}$$

Then the Kalman gain $\mathbf{K}_k$ is approximated from $\mathbf{P}_{y_k y_k}$ and $\mathbf{P}_{x_k y_k}$ as follows

$$\mathbf{K}_k = \mathbf{P}_{x_k y_k} \mathbf{P}^{-1}_{y_k y_k} \tag{A.21}$$

Now $\mathbf{K}_k$ is used to update the *a priori* estimate and covariance of the states as follows

$$\hat{\mathbf{x}}_k^+ = \hat{\mathbf{x}}_k^- + \mathbf{K}_k \left(\mathbf{z}_k - \hat{\mathbf{z}}_k\right) \tag{A.22}$$

$$\mathbf{P}_k = \mathbf{P}_k^- - \mathbf{K}_k \mathbf{P}_{y_k y_k} \mathbf{K}_k^T \tag{A.23}$$

Appendix B

Recursive Algorithm of the Rauch-Tung-Striebel Two-Pass Smoother

The Rauch-Tung-Striebel two-pass filter (RTS) is the fastest fixed-interval smoother [9], which uses two filters: a forward filter and a backward filter. The forward filter uses a standard EKF to compute all state estimates pertained to the past measurements, whereas the backward filter reduces the inherent bias in the EKF estimates. The two-step recursive algorithm considers the same nonlinear system discussed in Section 3.2.1.

$$\mathbf{x}_{k+1} = f(\mathbf{x}_k, \mathbf{w}_k, k) \tag{B.1}$$

$$\mathbf{z}_k = g(\mathbf{x}_k, \mathbf{v}_k, k) \tag{B.2}$$

where $\mathbf{w}_k$ and $\mathbf{v}_k$ are white Gaussian random noise processes with the same statistics as the EKF.

$$\mathrm{E}\{\mathbf{w}_k\} = 0, \mathrm{E}\{\mathbf{w}_k \mathbf{w}_k^T\} = \mathbf{Q}_k, \tag{B.3}$$

$$\mathrm{E}\{\mathbf{v}_k\} = 0, \mathrm{E}\{\mathbf{v}_k \mathbf{v}_k^T\} = \mathbf{R}_k, \tag{B.4}$$

The following summary of the RTS equations adheres closely to the presented in [11].

Forward Filter

The RTS first runs the forward filter forward in time using the standard EKF algorithm discussed in Section 3.2.1. The forward filter starts with the following initial conditions at

$k = 0$:

$$\hat{\mathbf{x}}_0 = \mathrm{E}[\mathbf{x}_0] \tag{B.5}$$

$$\mathbf{P}_0 = \mathrm{E}[(\mathbf{x}_0 - \hat{\mathbf{x}}_0)(\mathbf{x}_0 - \hat{\mathbf{x}}_0)^T] \tag{B.6}$$

The two-step recursive computes the estimates for the forward filter $\hat{\mathbf{x}}_k^f$ using the time update step and the measurement time update step in Section 3.2.1 . The following equations are reproduced from Equations (3.30)- (3.31) and (3.32) - (3.35):

$$\begin{aligned}
\hat{\mathbf{x}}_{k+1}^- &= f(\hat{\mathbf{x}}_k^f, \bar{\mathbf{w}}_k, k) && \text{(B.7)}\\
\mathbf{P}_{k+1}^- &= \mathbf{A}_k \mathbf{P}_k^f \mathbf{A}_k^T + \mathbf{F}_k \mathbf{Q}_k \mathbf{F}_k^T && \text{(B.8)}\\
\mathbf{K}_k &= \mathbf{P}_k^- - \mathbf{C}_k^T \left[\mathbf{C}_k \mathbf{P}_k^- \mathbf{C}_k^T + \mathbf{R}_k\right]^{-1} && \text{(B.9)}\\
\mathbf{r}_k &= \mathbf{z}_k - g(\hat{\mathbf{x}}_k^-, \bar{\mathbf{v}}_k, k) && \text{(B.10)}\\
\hat{\mathbf{x}}_k^f &= \hat{\mathbf{x}}_k^- + \mathbf{K}_k \mathbf{r}_k && \text{(B.11)}\\
\mathbf{P}_k^f &= \mathbf{P}_k^- - \mathbf{K_k} \mathbf{C}_k \mathbf{P}_k^- && \text{(B.12)}
\end{aligned}$$

Backward Filter

The backward filter begins with the following initial conditions at $k = N$:

$$\hat{\mathbf{x}}_N = \hat{\mathbf{x}}_N^f, \tag{B.13}$$

$$\mathbf{P}_N = \mathbf{P}_k^f. \tag{B.14}$$

The following equations are computed to determine the smoothed estimates $\hat{\mathbf{x}}_k$ in reverse time (i.e., $k = N-1, N-2, N-3, ..., 1$):

$$\begin{aligned}
\mathbf{B}_k &= \mathbf{P}_k^f \mathbf{A}_{k+1}^T [\mathbf{P}_{k+1}^-]^{-1}, && \text{(B.15)}\\
\mathbf{P}_k &= \mathbf{P}_k^f - \mathbf{B}_k \left(\mathbf{P}_{k+1}^- - \mathbf{P}_{k+1}\right) \mathbf{B}_k^T, && \text{(B.16)}\\
\hat{\mathbf{x}}_k &= \hat{\mathbf{x}}_k^f + \mathbf{B}_k \left(\hat{\mathbf{x}}_{k+1} - \hat{\mathbf{x}}_{k+1}^-\right). && \text{(B.17)}
\end{aligned}$$

where $\mathbf{B}_k$ is the gain matrix for the backward filter.

Appendix C

Recursive Algorithm of the Schmidt-Kalman Filter

The implementation equations of the Schmidt-Kalman Filter follow the summary table found in [9]. Just like the Kalman filter, the Schmidt-Kalman filter has two distinct phases: the observation update phase and the time update phase as follows:

Observation Update Phase

$$
\begin{aligned}
\mathbf{C} &= \mathbf{H}_{e,k}\left[\mathbf{P}^{-}_{ee,k}\mathbf{H}^{T}_{e,k} + \mathbf{P}^{-}_{eu,k}\mathbf{H}^{T}_{u,k}\right] \\
&\quad + \mathbf{H}_{u,k}\left[\mathbf{P}^{-}_{ue,k}\mathbf{H}^{T}_{e,k} + \mathbf{P}^{-}_{uu,k}\mathbf{H}^{T}_{u,k}\right] && \text{(C.1)} \\
\mathbf{K}_{SK,k} &= \left[\mathbf{P}^{-}_{ee,k}\mathbf{H}^{T}_{e,k} + \mathbf{P}^{-}_{eu,k}\mathbf{H}^{T}_{u,k}\right]\mathbf{C} && \text{(C.2)} \\
\hat{\mathbf{x}}^{+}_{e,k} &= \hat{\mathbf{x}}^{-}_{e_k} + \mathbf{K}_{SK,k}\left[\mathbf{z}_k - \mathbf{H}_{e,k}\mathbf{x}^{-}_{e,k}\right] && \text{(C.3)} \\
\mathbf{A} &= \mathbf{I}_{n_e} - \mathbf{K}_{SK,k}\mathbf{H}_{e,k} && \text{(C.4)} \\
\mathbf{B} &= \mathbf{A}\mathbf{P}^{-}_{eu,k}\mathbf{H}^{T}_{u,k}\mathbf{K}^{T}_{SK,k} && \text{(C.5)} \\
\mathbf{P}^{+}_{ee,k} &= \mathbf{A}\mathbf{P}^{-}_{ee,k} - \mathbf{A}^{T} - \mathbf{B} - \mathbf{B}^{T} \\
&\quad + \mathbf{K}_{SK,k}\left[\mathbf{H}_{u,k}\mathbf{P}_{uu,k} - \mathbf{H}^{T}_{u,k} + \mathbf{R}_k\right]\mathbf{K}^{T}_{SK,k} && \text{(C.6)} \\
\mathbf{P}^{+}_{eu,k} &= \mathbf{A}\mathbf{P}^{-}_{eu,k} - \mathbf{K}_{SK,k}\mathbf{H}_{u,k}\mathbf{P}^{-}_{uu,k} && \text{(C.7)} \\
\mathbf{P}^{+}_{ue,k} &= \mathbf{P}^{T+}_{eu,k} && \text{(C.8)} \\
\mathbf{P}^{+}_{uu,k} &= \mathbf{P}^{-}_{uu,k} && \text{(C.9)}
\end{aligned}
$$

Time Update Phase

$$\hat{\mathbf{x}}^{-}_{e,k+1} = F_e(\hat{\mathbf{x}}_{e,k}, k) \tag{C.10}$$

$$\mathbf{P}^{-}_{ee,k+1} = \Phi_{e,k}\mathbf{P}^{+}_{ee,k}\Phi^{T}_{e,k} + \mathbf{Q}_{ee,k} \tag{C.11}$$

$$\mathbf{P}^{-}_{eu,k+1} = \Phi_{e,k}\mathbf{P}^{+}_{eu,k}\Phi^{T}_{u,k} \tag{C.12}$$

$$\mathbf{P}^{-}_{ue,k+1} = \mathbf{P}^{T-}_{eu,k+1} \tag{C.13}$$

$$\mathbf{P}^{-}_{uu,k+1} = \Phi_{u,k}\mathbf{P}^{+}_{uu,k}\Phi^{T}_{u,k} + \mathbf{Q}_{uu,k} \tag{C.14}$$

Appendix D

Glossary

ECG	electrocardiogram, page 4
EMG	electromyography, page 4
PL	power line interference, page 12
BW	respiration baseline wandering, page 13
EM	electrode motion artifact, page 13
MA	muscle artifact, page 13
DB1	MIT-BIH normal sinus rhythm database, page 49
DB2	MIT-BIH noise stress test database, page 49
EKF	extended Kalman Filter, page 17
UKF	unscented Kalman Filter, page 24
BMFLS	Biswas-Mahalanabis Fixed-Lag Smoother, page 61
EKF	extended Kalman Filter, page 17
ECG2	two states ECG dynamical model, page 34
ECG17	proposed seventeen states ECG dynamical model, page 34

$\mathbf{x}_k$ unobserved system state vector at time instant k, page 17

$\mathbf{z_k}$ measurement vector at time instant k, page 17

$f(\cdot)$ state differential function, page 17

$g(\cdot)$ observation function, page 17

$\mathbf{x}_0$ true initial state vector, page 17

$\hat{\mathbf{x}}_k$ estimated state vector at time instant k, page 17

$\mathbf{P}_l$ estimation covariance matrix at time instant k, page 17

$\mathbf{R}_k$ process noise covariance matrix, page 17

$\mathbf{Q}_k$ measurement noise covariance matrix, page 17

$\hat{\mathbf{x}}_k^+$ *a posteriori* state estimate , page 18

$\hat{\mathbf{x}}_k^-$ *a priori* state estimate , page 18

$\mathbf{P}_k^+$ *a posteriori* estimation covariance matrix , page 21

$\mathbf{P}_k^-$ *a priori* estimation covariance matrix , page 21

θ_k the angular position of the trajectory on the circular limit cycle, page 33

z_k ECG measurement at time instant k, page 33

θ_i the angular position of the Gaussian function for $i \in \{P, Q, R, S, T\}$, page 31

a_i the peak of the Gaussian function for $i \in \{P, Q, R, S, T\}$, page 31

b_i the variance of the Gaussian function for $i \in \{P, Q, R, S, T\}$, page 31

α_i the peak of the Gaussian function in millivolts for $i \in \{P, Q, R, S, T\}$, page 32

ω the sampling frequency of the ECG measurements in Hz, page 32

$\Delta\theta_i$ The angular difference between the angular position of the trajectory and the angular position of the Gaussian for $i \in \{P, Q, R, S, T\}$, page 30

$\overline{ECG}(\theta)$ the mean ECG waveform function, page 44

$\sigma_{ECG}(\theta)$ the variance of the ECG waveform function, page 44

l the amount of lagged time steps of the BMFLS, page, page 62

$\mathbf{x}_{e,k}$ the true state value of the suboptimal BMFLS state vector at kth time step, page 65

$\hat{\mathbf{x}}_{e,k}$ the estimated state value of the suboptimal BMFLS state vector at kth time step, page 65

References

[1] P. M. Agante and J.P.M. de Sa. ECG noise filtering using wavelets with soft-thresholding methods. In *Computers in Cardiology, 1999*, pages 535–538, 1999.

[2] M.P.S. Chawla. PCA and ICA processing methods for removal of artifacts and noise in electrocardiograms: A survey and comparison. *Applied Soft Computing*, 11(2):2216 – 2226, 2011.

[3] Y. Chen, Z. Yan, and W. He. Detection of qrs-wave in electrocardiogram: Based on kalman and wavelets. In *Engineering in Medicine and Biology Society, 2005. IEEE-EMBS 2005. 27th Annual International Conference*, pages 2758–2760, 2005.

[4] G.D. Clifford, A. Shoeb, P.E. McSharry, and B.A. Janz. Model-based filtering, compression and classification of the ECG. In *Bioelectromagnetism and 5th International Symposium on Noninvasive Functional Source Imaging within the Human Brain and Heart*, 2005.

[5] G. M. Friesen, T. C. Jannett, M. A. Jadallah, S. L. Yates, S. R. Quint, and H. T. Nagle. A comparison of the noise sensitivity of nine QRS detection algorithms. *IEEE Transactions on Biomedical Engineering*, 37:85–98, 1990.

[6] A. Gelb. *Applied Optimal Estimation*. MIT Press, 1974.

[7] D. B. Geselowitz. On the theory of the electrocardiogram. *Proceedings of the IEEE on*, 77(6):857–876, 1989.

[8] A. L. Goldberger, L. A. N. Amaral, L. Glass, J. M. Hausdorff, P. Ch. Ivanov, R. G. Mark, J. E. Mietus, G. B. Moody, C.-K. Peng, and H. E. Stanley. PhysioBank, PhysioToolkit, and PhysioNet: Components of a New Research Resource for Complex Physiologic Signals. *Circulation*, 101(23):e215–e220.

[9] M.S. Grewal and A.P. Andrews. *Kalman Filtering: Theory and Practice Using MATLAB*. Wiley, 2011.

[10] J. Hartikainen and S. Särkkä. *Optimal filtering with Kalman filters and smoothers a Manual for Matlab toolbox EKF/UKF*. Department of Biomedical Engineering and Computational Science, Helsinki University of Technology, February 2008.

[11] S. Haykin. *Kalman Filtering and Neural Networks*. Adaptive and Learning Systems for Signal Processing, Communications and Control Series. Wiley, 2004.

[12] T. He, G. Clifford, and L. Tarassenko. Application of independent component analysis in removing artefacts from the electrocardiogram. *Neural Computing and Applications*, 15:105–116, 2005.

[13] I.G. Khan. *Rapid ECG Interpretation*. Contemporary Cardiology. Humana Press, 2008.

[14] P. Laguna, R. Jane, O. Meste, P.W. Poon, P. Caminal, H. Rix, and N.V. Thakor. Adaptive filter for event-related bioelectric signals using an impulse correlated reference input: comparison with signal averaging techniques. *Biomedical Engineering, IEEE Transactions on*, 39(10):1032–1044, 1992.

[15] M. Malik and A. J. Camm. Heart rate variability. *Clinical Cardiology*, 13(8):570–576, August 1990.

[16] V. R. Mankar and A. A. Ghatol. Design of Adaptive Filter Using Jordan/Elman Neural Network in a Typical EMG Signal Noise Removal. *Advances in Artificial Neural Systems*, 2009:1–9, 2009.

[17] P.S. Maybeck. *Stochastic Models, Estimation, and Control*. Mathematics in Science and Engineering. Elsevier Science, 1982.

[18] J. McNames and M. Aboy. Statistical modeling of cardiovascular signals and parameter estimation based on the extended kalman filter. *Biomedical Engineering, IEEE Transactions on*, 55(1):119–129, 2008.

[19] P.E. McSharry, G.D. Clifford, L. Tarassenko, and L.A. Smith. A dynamical model for generating synthetic electrocardiogram signals. *Biomedical Engineering, IEEE Transactions on*, 50(3):289–294, 2003.

[20] Geeky Medics. How to read an ecg. http://geekymedics.com/2011/02/28/how--to--read--an--e, February 2013. [Online; Accessed June, 2013].

[21] C.R. Meyer and H.N. Keiser. Electrocardiogram baseline noise estimation and removal using cubic splines and state-space computation techniques. *Computers and Biomedical Research*, 10(5):459 – 470, 1977.

[22] G.B. Moody, W.E. Muldrow, and R.G. Mark. The MIT-BIH Noise Stress Test Database. http://www.physionet.org/physiobank/database/nstdb/. [Online; Accessed December, 2012].

[23] G.B. Moody, W.E. Muldrow, and R.G. Mark. The MIT-BIH Normal Sinus Rhythm Database. http://www.physionet.org/physiobank/database/nstdb/. [Online; Accessed December, 2012].

[24] J. Pan and W.J. Tompkins. A real-time qrs detection algorithm. *Biomedical Engineering, IEEE Transactions on*, BME-32(3):230–236, 1985.

[25] S. Poungponsri and X. Yu. Electrocardiogram (ECG) signal modeling and noise reduction using wavelet neural networks. *2009 IEEE International Conference on Automation and Logistics*, pages 394–398, 2009.

[26] H. Rauch. Solutions to the linear smoothing problem. *IEEE Transactions on Automatic Control*, 8(4):371–372, October 1963.

[27] M.I. Riberio. Kalman and extended Kalman filters: concepts, derivation and properties. Technical report, Institute for Systems and Robotics, Lisboa, 2004.

[28] R. Sameni. *Extraction of fetal cardiac signals from an array of maternal abdominal recordings*. PhD thesis, 2008.

[29] R. Sameni. The Open-Source Electrophiological Toolbox. http://www.oset.ir/index.html, 2010. [Online; accessed January, 2013].

[30] R. Sameni, M.-B. Shamsollahi, C. Jutten, and M. Babaie-Zadeh. Filtering noisy ecg signals using the extended kalman filter based on a modified dynamic ecg model. In *Computers in Cardiology, 2005*, pages 1017–1020, 2005.

[31] R. Sameni, M.B. Shamsollahi, C. Jutten, and G.D. Clifford. A Nonlinear Bayesian Filtering Framework for ECG Denoising. *IEEE Transactions on Biomedical Engineering*, 54, 2007.

[32] O. Sayadi and M.-B. Shamsollahi. ECG Denoising and Compression Using a Modified Extended Kalman Filter Structure. *Biomedical Engineering, IEEE Transactions on*, 55(9):2240–2248, 2008.

[33] O. Sayadi, M.-B. Shamsollahi, and G.D. Clifford. Robust detection of premature ventricular contractions using a wave-based bayesian framework. *Biomedical Engineering, IEEE Transactions on*, 57(2):353–362, 2010.

[34] P. E. Tikkanen. Nonlinear wavelet and wavelet packet denoising of electrocardiogram signal. *Biological Cybernetics*, 80:259–267, 1999.

[35] R. Vullings, Bert De Vries, and J. W M Bergmans. An adaptive kalman filter for ecg signal enhancement. *Biomedical Engineering, IEEE Transactions on*, 58(4):1094–1103, 2011.

[36] D. J. Wagner. Pitfalls and artifacts in electrocardiography. *Journal Iowa State Medical Society*, 43:412–415, 1953.

[37] J. Yan, Y. Lu, J. Liu, X. Wu, and Y. Xu. Self-adaptive model-based ECG denoising using features extracted by mean shift algorithm. *Biomedical Signal Processing and Control*, 5(2):103 – 113, 2010.

[38] J. M. ski and N. Henzel. ECG baseline wander and powerline interference reduction using nonlinear filter bank. *Signal Processing*, 85(4):781–793, 2005.